COMPARATIVE TESTS OF JOINT SURFACE ROUGHNESS OF ROCKS FROM THE McMURDO SOUND AREA, ANTARCTICA

A thesis

submitted in partial fulfillment

of the requirements for the Degree

of

Master of Science

in Earth Sciences

at the

University of Waikato

by

WILLIAM RICHARD DOOLIN

1986

ABSTRACT

Barton and co-workers (Barton, 1973, 1976; Barton and Choubey, 1977; Barton and Bandis, 1980; Bandis *et al.*, 1981) have developed an empirical relationship to estimate the peak frictional resistance of a joint, which considers both the joint wall compressive strength and a joint surface roughness coefficient (JRC). Estimation of JRC can be achieved by comparing joint surface profiles with standard profiles of known JRC values. Alternatively, Barton proposes two simple index tests, tilt and pull (or push) tests, suitable for use in the field, from which JRC values can be back-calculated.

Results from tests using these methods, conducted on 67 joints from six Antarctic lithologies, were statistically compared to results obtained from a numerical characterisation technique, involving computer digitisation, developed by Tse and Cruden (1979). While tilt and pull tests correlate well together, neither performs as reliably against the numerical technique as the profile comparison method.

The Schmidt test hammer can be used to estimate compressive strength by quantitative relationships established with point load strength or uniaxial compressive strength. Its usefulness lies in its ability to test the narrow zone of influence of a joint wall. Basic friction angles can be simply estimated by a modified method of Stimpson (1981), involving the tilting of three cylindrical cores arranged as an elongated pyramid.

Time series analysis of 125 joint surface profiles, using autocorrelation and spectral density functions, suggests that a majority of joint surfaces from all tested lithologies show a high amplitude periodic roughness with a wavelength of between 100 and 150 mm, upon which is superimposed one or more secondary, lower amplitude, periodic roughnesses, with a wavelength dependent on the degree of joint roughness, but most often around 12 mm.

ACKNOWLEDGEMENTS

Firstly I would like to thank Professor M. Selby for the opportunity to participate in his research programme, and for his guidance and supervision in this project. Field work was financed by a UGC research grant to Professor Selby.

The co-operation of the Ross Dependency Research Committee, and the assistance of many personnel of the Antarctic Division, DSIR, is acknowledged. Thanks are also due to the University of Waikato Antarctic Research Unit, and its field assistants Mr D. Bailey and Mr L. Gaylor.

In addition, I would like to thank the following:

Dr R. Briggs for his petrographic assistance;
Dr K. Black and Mr P. Scadden for their help in FORTRAN programming, and discussion of time series analysis;
Dr A. Sneyd and the late Dr R. Osborne for their discussion on the core tilting method of calculating basic friction angles;
Mr S. Edbrooke for the use of his geological map of the upper Wright Valley;
Dr E. Bardsley and Ms M. Hunt for their statistical advice;
Mr T. Major for his tutoring in the use of the SAS statistical package;
Mr Yeo Chun Cheng for the use of his program DIGIT, and for an introduction to the digitiser;
Mr P. Augustinus for the contribution of some scarce Antarctic rock, and for his participation in the profile comparison exercise, as well as countless discussions on Antarctic geology;
Mr K. Hind for his kind donation of several kilograms of ignimbrite;
The Earth Science Department secretaries and technical staff for their cheerful assistance;
My friends and colleagues, particularly Mr D. Fergusson and Mr P. McCabe, for challenging debate, joviality, and my sanity.

Finally, I would like to thank Laurie, my wife, for her careful typing, provocative discussion, and for her endless support and encouragement.

TABLE OF CONTENTS

LIST OF FIGURES

LIST OF TABLES

CHAPTER ONE

INTRODUCTION

CHAPTER 1: INTRODUCTION

1.1 Background

The term *joint*, when applied to rock, is used to describe the mechanical discontinuities of geological origin, that intersect rock masses. Joints showing differential movement parallel to their surface are best described as *faults*. Joints discussed in this study are assumed to be *unfilled*, that is the rock walls of the joint are in direct contact. *Filled* joints, containing soft plastic materials such as clay, constitute a class of joint requiring special consideration. Generally, joints will tend to have irregular surfaces as a result of local changes in lithology and, on a smaller scale, changes in the strength of the constituent minerals. The undulating surface of a rock joint is described as its *roughness*. Thus, the surface roughness of rock joints depends on their mode of origin, and on the mineralogy of the rock. The roughest joints will be those formed by tensile brittle failure, often in intrusive rocks. Joints associated with plastic deformation such as shear joints, often tectonic or metamorphic in origin, will be among the smoothest (Barton, 1973).

Most rock masses have sufficient intact strength to support vertical slopes of considerable height. It is the frictional resistance to sliding along joints which controls the stability of most slopes formed on exposed rock (Selby, 1982). An important controlling factor on the shear strength, or frictional resistance, along a rock joint is the magnitude of the effective normal stress acting across the joint. Even considering the effective normal stress levels generally operating in most rock engineering problems, there is still a wide variation in the shear strength of rock joints. This is due to the influence of variable rock strength, and more importantly,

to the influence of surface roughness (Barton, 1973, 1976).

Given that irregularities or roughness along failure surfaces play an important role in the shear strength of rock joints, it seems pertinent to examine joint roughness more closely. Barton (1973) derives an empirical equation for the estimation of peak shear strength which considers both the compressive strength of the joint walls and their roughness. He defines the roughness parameter as the *joint roughness coefficient* (JRC). Barton and Choubey (1977) and Barton and Bandis (1980) describe methods for the field estimation of this roughness coefficient. Tse and Cruden (1979) propose a numerical technique for the characterisation of surface roughness using computer digitisation. With this method they are able to accurately determine the JRC of joint surface profiles. Testing of these methods on natural joints in field conditions would provide a measure of their applicability and reliability.

A number of authors (Wu and Ali, 1978; Krahn and Morgenstern, 1979; Dight and Chiu, 1981) have examined the surface profiles of rock joints statistically, in an attempt to characterise joint roughness and to determine whether the joint surface is composed of randomly occurring irregularities, or can be attributed to some underlying regular pattern. The latter type of attempts have generally met with mixed results. If a regular joint surface waveform can be found in specific rock types interesting relationships can be proposed between joint roughness and joint lithology.

The rocks of the McMurdo Dry Valley region, South Victoria Land, Antarctica, provide an excellent opportunity to study geological processes dominated by physical factors. Because of the dry climatic conditions, chemical weathering plays a subordinate role to mechanical

weathering, and joint surfaces are comparatively free of clay products. The geomorphology of the exposed rock in the Taylor Valley and Olympus and Asgard Ranges, provides joints suitable for study in a natural situation removed from the complicating influence of man. In addition, the geology of this area promotes the study of a wide range of intrusive and metamorphic rocks within a relatively localised area, a situation not easily accessible in New Zealand.

1.2 Research Objectives

The purpose of this study is to evaluate existing methods of studying surface roughness, on joints formed in a number of Antarctic lithologies, thereby improving our understanding of roughness so that engineering design and studies of slope stability have a more reliable data base.

This study has three primary objectives:

(a) to characterise six Antarctic lithologies with regard to their petrography and certain geotechnical properties,

(b) to compare the reliability and performance of three recommended field techniques for the estimation of joint roughness coefficient with a numerically based laboratory technique, for natural joints,

(c) to explore the concept of time series analysis with regard to natural joint surfaces.

The achievement of these objectives involves a number of secondary methodologies:

(1) petrographically characterise the rocks used and place them in the stratigraphic context of the McMurdo Sound area;

(2) review the joint roughness coefficient, and the field techniques

recommended by Barton and co-workers for estimating it - theory and procedure;

(3) conduct a programme of field and laboratory testing to obtain a database enabling the comparison of methods for estimating the joint roughness coefficient;

(4) discuss and develop suitable secondary techniques for the determination of component elements within the main techniques used to estimate the joint roughness coefficient;

(5) develop for more general application a numerical technique which characterises joint roughness;

(6) statistically compare the joint roughness coefficients obtained from the field techniques against numerically calculated values, in order to predict the reliability of each technique;

(7) determine whether individual lithologies can be characterised by a mean joint roughness coefficient;

(8) characterise each lithology used on the basis of unit weight, basic friction angle, Schmidt rebound hardness, point load strength index, compressive strength, and typical joint roughness coefficient;

(9) review suitable techniques for the time series analysis of profiles;

(10) develop computer software to accomplish such an analysis;

(11) analyse joint surface profiles from different lithologies and joint roughness ranges, in order to isolate characteristic regular wavelengths;

1.3 Study Area

The Taylor Valley is one of several east-west trending ice-free valleys located west of McMurdo Sound, South Victoria Land, Antarctica (Figure 1.1). Lying between the Asgard Range to the north, and the Kukri Hills to the south, the main valley can be divided naturally into three sections (Haskell *et al.*, 1965). The upper Taylor Valley lies above the fork of the Taylor and Ferrar Glaciers. The narrow middle section extends from the fork to the Nussbaum Riegel, which almost crosses the valley in the vicinity of the Suess Glacier. The lower Taylor Valley is broader and flatter, being 6.5 km across at its widest point. Lakes, permanently frozen except for marginal summer melting, occur throughout the middle and lower Taylor Valley, and alpine glaciers flow into the valley from the surrounding ranges. The Taylor Valley was cut by eastward flowing ice from the inland Polar Plateau. A number of Ross Sea ice advances and retreats from the west are also recorded in the lower valley. The present 'interglacial' has caused recession of the Taylor and alpine glaciers leaving the deglacierised terrain of today.

The Asgard and Olympus Ranges, flanking the Wright Valley which lies immediately to the north of the Taylor Valley, are transverse units of the Transantarctic Mountain chain in Victoria Land (Bull *et al.*, 1962). They extend roughly 60 km eastward from the edge of the Polar Plateau to the coastal piedmont. The westward parts of these ranges contain peaks reaching 2000 to 2400 m, separated by passes at around 1500 m. The alpine glaciers which cut the dividing passes are absent, represented only by relict névé fields which once fed them. To the east, peaks reach 1500 m and alpine glaciers fall to the floors of bordering valleys.

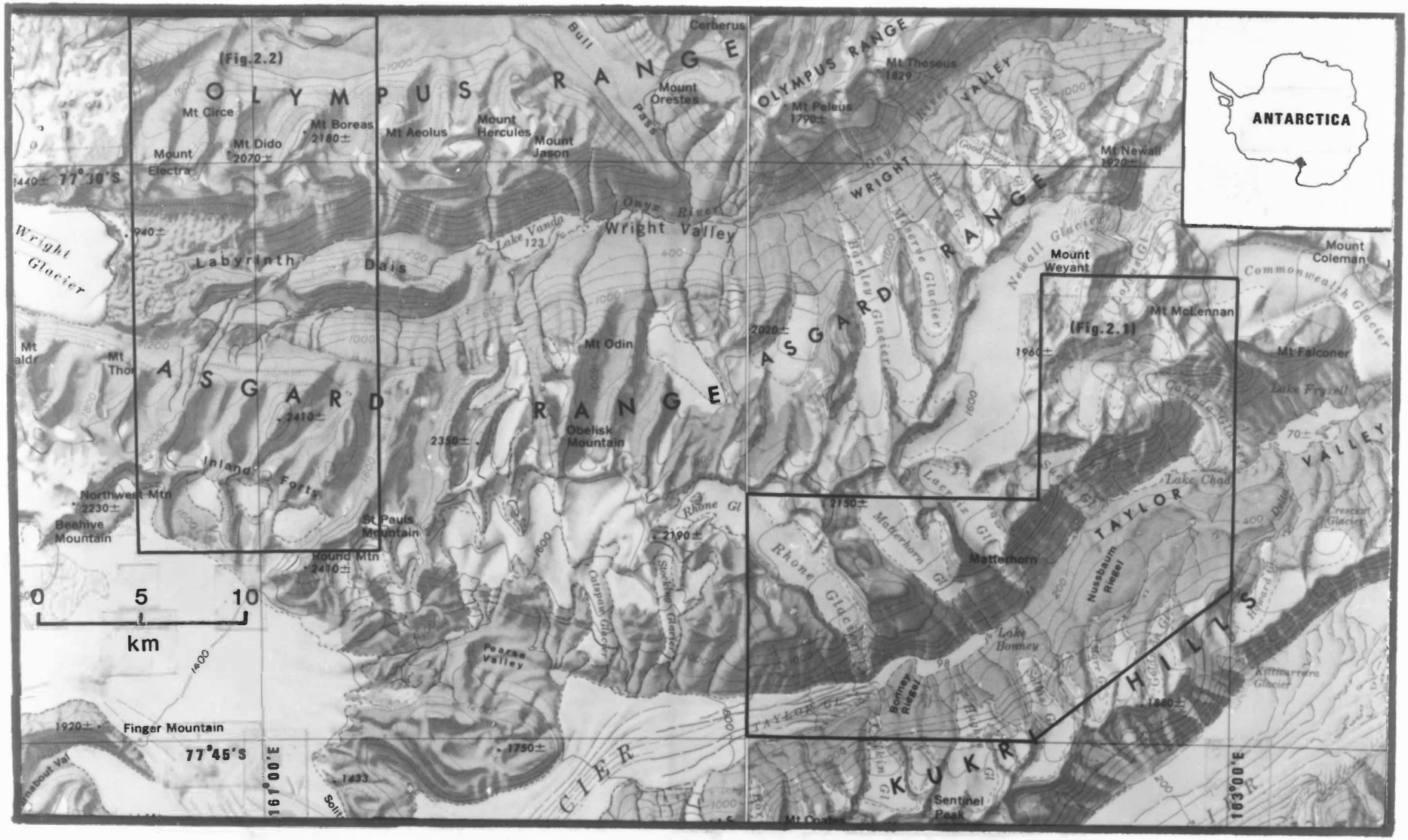

FIGURE 1.1 Location map (U.S. Geological Survey, 1962,1970)

CHAPTER TWO

PETROLOGY

CHAPTER 2: PETROLOGY

2.1 Stratigraphy

The stratigraphic geology of the middle Taylor Valley, and the Asgard and Olympus Ranges on either side of the upper Wright Valley is summarised in Table 2.1 . The basement complex consists of tightly folded, steeply dipping metamorphosed sediments (Koettlitz Group) and a variety of igneous rocks (Granite Harbour Intrusives) of early Paleozoic age. The Koettlitz Group metasediments are bounded east and west by the Olympus Granite-gneiss. The generally gradational contact is thought to be intrusive since metasediment inclusions occur within the Olympus Granite-gneiss in the contact zone (Jones and Faure, 1967). The relationship between the Olympus Granite-gneiss and the Larsen Granodiorite which flanks it is unclear, although Palmer *et al.* (1967) interpret the Olympus Granite-gneiss as a border facies of the Larsen Granodiorite due to their similarity in composition and the gradational contact between them. Localised tabular bodies and veins of the Theseus Granodiorite intrude the Koettlitz Group metasediments, Olympus Granite-gneiss and Larsen Granodiorite. The latter two lithologies are intruded by dykes and sills of the Irizar Granite. All the basement rocks are cut by swarms of lamprophyre and porphyry dykes.

The basement rocks were later uplifted and eroded to form the Kukri erosion surface, upon which a thick sedimentary sequence, the Beacon Supergroup (Taylor Group, Victoria Group), was deposited unconformably during the Devonian to the Triassic. The early Taylor Group records a marine transgression during which tidally influenced sediments (New Mountain Subgroup, Altar Mountain Formation) progressively buried the Kukri erosion surface. A slow regression

TABLE 2.1 Stratigraphic units of the Asgard and Olympus Ranges, and Taylor Valley, Antarctica.
Terminology after Haskell *et al.* (1965), McKelvey *et al.* (1970), Kyle and Cole (1974), McKelvey *et al.* (1977), Plume (1978), and Findlay *et al.* (1984).

AGE	GROUP		FORMATION
Quaternary			Surficial glacial deposits
- Tertiary	McMurdo Volcanic Gp		Basic volcanics
Jurassic	Ferrar Group		Ferrar Dolerite
Triassic	Beacon Supergp	Victoria Group	Lashly Formation
Trias.- Perm.			Feather Conglomerate
Permian			Weller Coal Measures
			PYRAMID EROSION SURFACE
Carboniferous			Metschel Tillite
			MAYA EROSION SURFACE
Upper Devonian		Taylor Group	Aztec Siltstone
			Beacon Heights Orthoquartzite
			Arena Sandstone
Mid-Lower Devonian			Altar Mountain Formation
			HEIMDALL EROSION SURFACE
		New Mtn Subgp	New Mountain Sandstone
			Terra Cotta Siltstone
			Windy Gully Sandstone
			KUKRI EROSION SURFACE
			Lamprophyre and porphyry dykes
Ordovician - Cambrian	Granite Harbour Intrusives		Irizar Granite
			Theseus Granodiorite
			Larsen Granodiorite
			Olympus Granite-gneiss
Cambrian - Vendian	Koettlitz Group		Hobbs Formation
			Salmon Marble
			Marshall Formation

followed during the later Taylor Group deposition (Arena Sandstone, Beacon Heights Orthoquartzite) with fluviatile conditions established by the late Devonian (Aztec Siltstone) (Bradshaw, 1981). The lowest Victoria Group formation is a diamictite (Metschel Tillite) bounded unconformably between the Maya erosion surface and the younger Pyramid erosion surface, indicating a glacial environment for the late Carboniferous (Barrett, 1981). The later Victoria Group comprises a Permian-Triassic sequence involving generally fluvial environments (Weller Coal Measures, Feather Conglomerate, Lashly Formation). Both the basement complex and the Beacon Supergroup were intruded during the early Jurassic by dolerite dykes and sills of the Ferrar Group. Lastly, volcanic activity in the late Cenozoic was accompanied by alkali olivine basalt extrusions of the McMurdo Volcanic Group (Armstrong, 1978).

The distribution of the stratigraphy in the area studied is shown in Figures 2.1 and 2.2 . In the middle Taylor Valley (Figure 2.1) bedrock exposures are confined to the valley walls. Glacial debris mantles the basement rocks of the valley floor. With the exception of the Ferrar Dolerite, which disrupts the basement sequence on the northern valley wall, the geology here is restricted to lithologies of the basement complex - metasediments, metavolcanics, and plutonics of the Granite Harbour Intrusives and the Koettlitz Group. The Beacon Supergroup is absent in this section of the Taylor Valley, probably due to a shallow regional westward dip of about 4°, and greater erosion to the east. Irregularly shaped mounds and cones of scoriaceous basalt belonging to the McMurdo Volcanic Group are scattered along the valley shoulders on both sides.

GEOLOGICAL MAP OF THE MIDDLE TAYLOR VALLEY

1 : 100 000

Compiled from Haskell *et al.*(1965) and field observations.

	Ice, glaciers, lakes		
cm	Moraine		Upper
cb	Basic volcanics	McMurdo Volc. Gp	Cenozoic
mf	Ferrar Dolerite	Ferrar Group	Jurassic
		Victoria Group	Trias.- Carb.
		Taylor Group	Devonian
—	Undifferentiated dykes		
pi	Irizar Granite	Granite	Ordivician
pt	Theseus Granodiorite	Harbour	- Cambrian
pl	Larsen Granodiorite	Intrusives	
po	Olympus Granite-gneiss		
ps	Undiff. metasediments	Koettlitz Group	Cam.- Vendian

(1) Sampling localities

× 123 Spot heights (m)

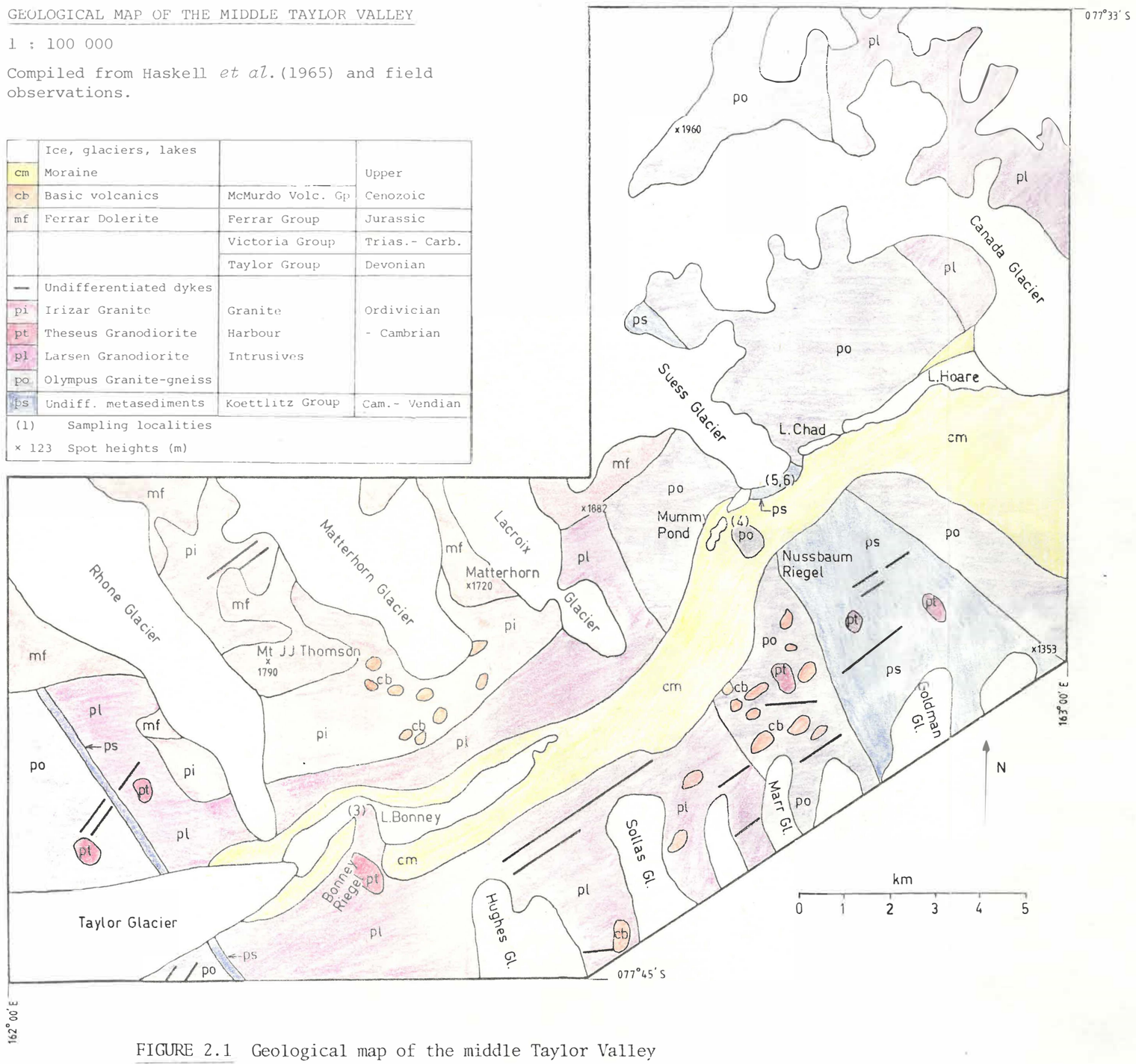

FIGURE 2.1 Geological map of the middle Taylor Valley

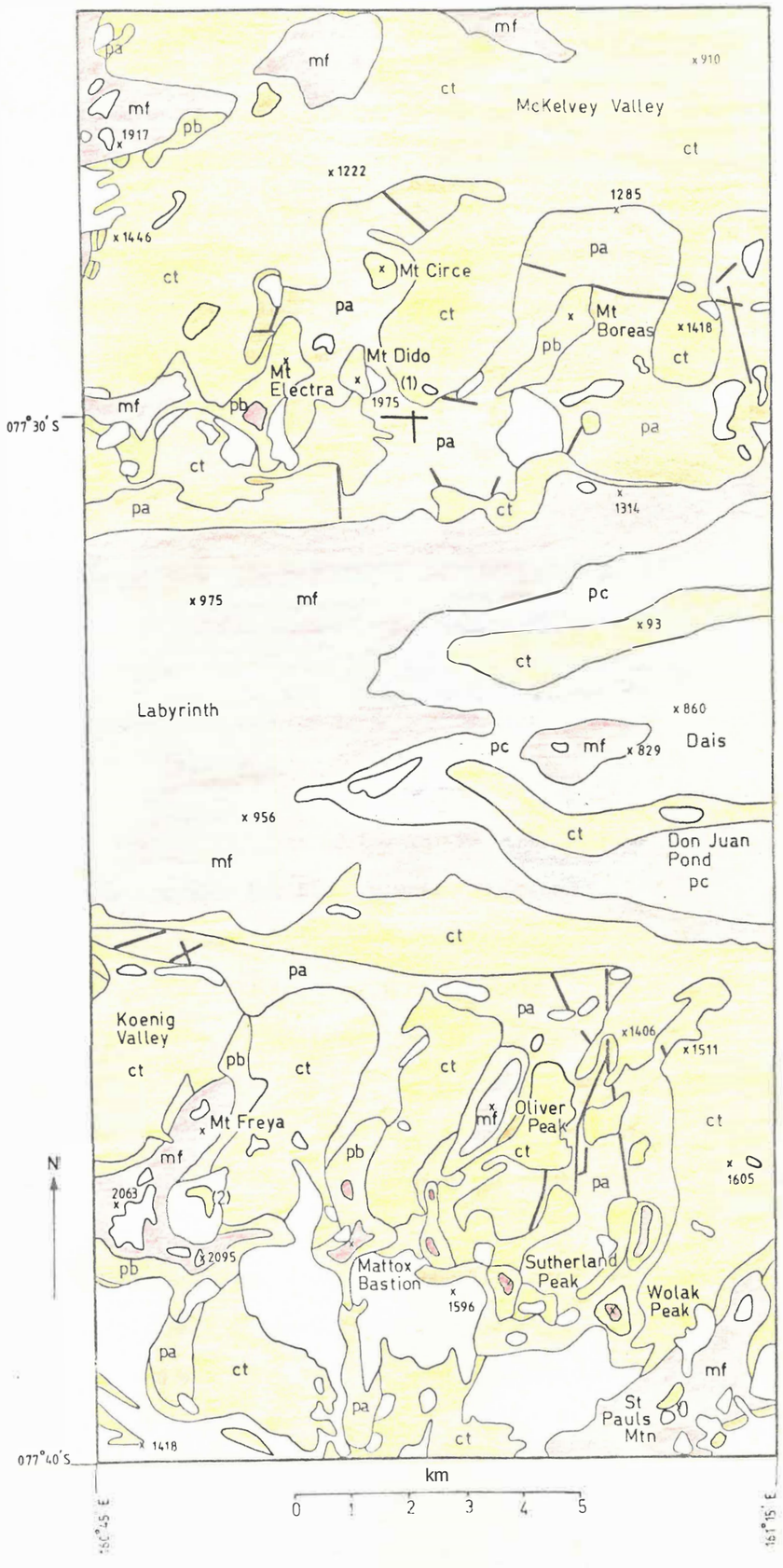

GEOLOGICAL MAP OF THE UPPER WRIGHT VALLEY

1 : 100 000

Compiled from McKelvey and Webb (1962), and Bryan *et al.* (1983).

	Ice, permanent snow		Upper
ct	Talus, moraine		Cenozoic
mf	Ferrar Dolerite	Ferrar Group	Jurassic
		Victoria Group	Trias.- Carb.
	Aztec Siltstone		Upper
pb	Beacon Heights Orthoquartzite		Devonian
	Arena Sandstone	Taylor Group	Mid-Lower
pa	Altar Mountain Fm		Devonian
	New Mountain Subgroup		
—	Undifferentiated dykes	Granite	Lower
pc	Basement complex	Harbour	Paleozoic
	(metavolcanics and plutonics)	Intrusives	
(1)	Sampling localities		
× 123	Spot heights (m)		

FIGURE 2.2 Geological map of the upper Wright Valley

In contrast, the more westward location of the Asgard and Olympus Ranges (Figure 2.2) produces a thick sequence of the Taylor Group, although in the area studied the Victoria Group is limited to a very small outcrop of Weller Coal Measures on the top of Mt. Electra (Bryan *et al.*, 1983). Extensive sills of Ferrar Dolerite intrude the sequences in both ranges, with occasional rafts of Beacon Supergroup rocks floating in the larger sills. Rocks of the basement complex are confined to the Wright Valley floor, in the area of the Dais.

2.2 Sample Petrography

Altogether, six lithologies at six sampling sites (Figures 2.1, 2.2) were used in this study - one sedimentary rock, three rocks from intrusive environments, and two rocks of metamorphic origin. Each site was chosen for the presence of a large number of accessible joints of common origin and similar form.

(a) Site 1 sampled quartz arenite, and was situated in the Olympus Range, in a basin formed between Mts Dido, Circe, and Boreas.

(b) Site 2 sampled dolerite, and was located on the eastern flanks of Mt Freya, near the Inland Forts of the Asgard Range.

(c) Site 3 sampled granite, and was situated at the Bonney Riegel, at the narrowest part of Lake Bonney in the middle Taylor Valley.

(d) Site 4, also in the middle Taylor Valley, sampled gneissic granite, and was located at the easternmost point of Nussbaum Riegel, at Mummy Pond.

(e) Site 5 sampled schist, and was situated opposite the Suess Glacier, in the narrowest part of the Taylor Valley.

(f) Site 6 sampled marble, and was also located opposite the Suess Glacier.

Sample thin sections were cut from each lithology, and viewed under a petrological microscope in order to determine their mineralogy. A point counting exercise was carried out on each thin section. Point counts were performed using 4 traverses of each slide. Components were counted at 0.2 mm intervals along each line, resulting in 500 counts per slide. The estimated percentage of the section occupied by a specific mineral is given in brackets in the following descriptions (<1% refers to percentages from between 1% and 0%; tr refers to minerals seen but not counted).

2.2.1 Quartz arenite (Site 1, Olympus Range; WT25101; Figure 2.3)

A number of very large blocks of quartz arenite lying at the base of the near-vertical eastern face of Mt Dido were examined. These blocks contained numerous joints, running parallel to bedding planes and cut by cross joints, forming joint pairs of consistent size, orientation, and origin. Because of the difficulty in testing joints from the cliff face itself, the large fall blocks were used as a source of jointed quartz arenite.

In thin section, quartz (95%) dominates this rock, the grains showing evidence of annealing. That is, the once sharp boundaries are approaching triple point junctions. This indicates the possibility of some diagenetic or low grade metamorphic influence. Any gaps remaining are filled with a mixture of sericite and quartz cement (4%). Accessory minerals are biotite (<1%), zircon (tr), tourmaline (tr), and opaques (<1%). This rock is part of the cliff-forming Beacon Heights Orthoquartzite (McKelvey *et al.*, 1970, 1977; Bradshaw, 1981), which is characterised by having a quartz cement. It can be distinguished by its field relations and petrography from the underlying Arena Sandstone (McKelvey *et al.*, 1970, 1977; Bradshaw,

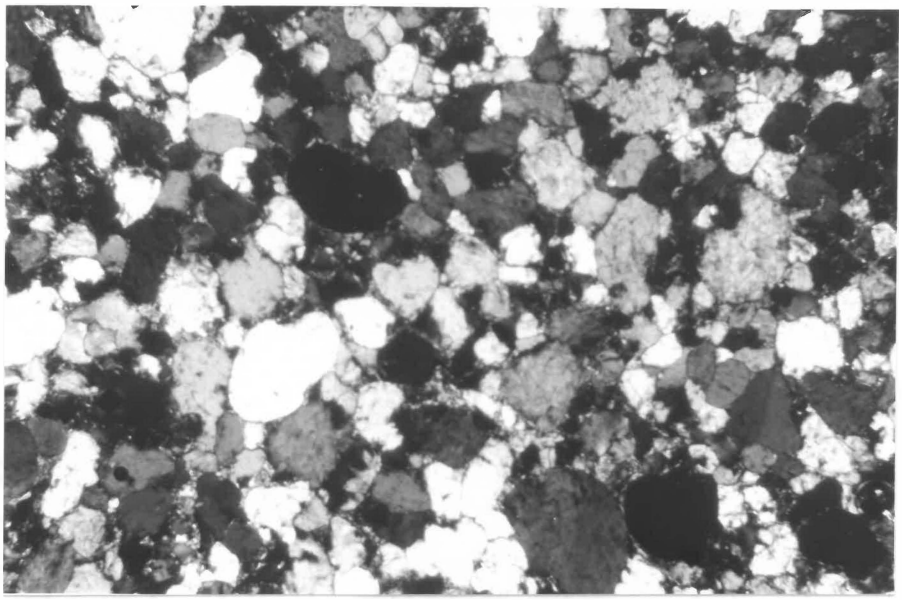

FIGURE 2.3 Quartz arenite; mosaic intergrowth of quartz grains, with minor sericite infilling.

25 X ; crossed nicols; ⊢——— 1mm ———⊣

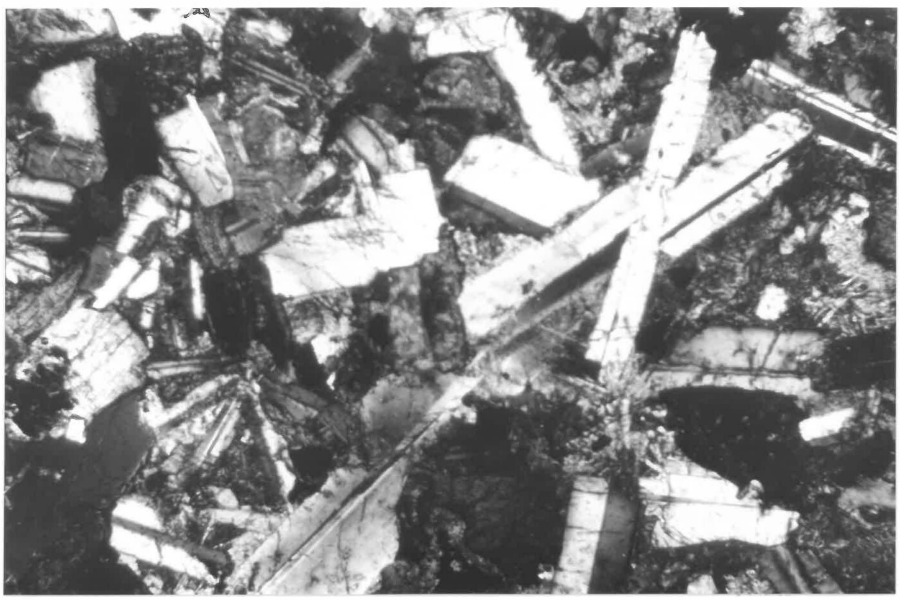

FIGURE 2.4 Dolerite; intergrown plagioclase and pyroxenes, with myrmekitic intergrowths.

25 X ; crossed nicols; ⊢——— 1mm ———⊣

1981), whose arenites are slope-forming and have a clay cement.

2.2.2 Dolerite (Site 2, Asgard Range; WT25102; Figure 2.4)

Dolerite of the Ferrar Group (Gunn and Warren, 1962; McKelvey and Webb, 1962; Burgess *et al.*, 1981) is abundant in the upper Taylor and Wright Valleys. At least three major sills can be recognised along with numerous smaller dykes and sills. The dolerite often outcrops as columnar jointed blocks. At the head of a side valley on the eastern side of Mt Freya a moraine type feature has formed, composed of blocks derived from the dolerite sill which outcrops above it. As before, due to the inaccessibility of the outcrop, large blocks, containing dolerite cooling joints, were used for testing.

In thin section this rock shows a doleritic texture of intergrown plagioclase (probably labradorite) (45%), and pyroxene (augite and pigeonite) (38%). The augite is occasionally twinned and is often uralitised. Quartz (14%) is the other major mineral, with opaques (3%) being a minor constituent. Apatite (tr) is accessory. Interstices are filled with myrmekitic (quartz-plagioclase) intergrowths. The petrography of this section is typical of the Ferrar Dolerite.

2.2.3 Granite (Site 3, Bonney Riegel; WT25103; Figure 2.5)

On the steep northern face of Bonney Riegel the surficial glacial deposits which surround Lake Bonney are absent, exposing the granite which forms the Riegel. Here sheeting joints, a result of unloading stresses, dip out of the face providing numerous examples of joints formed in granite.

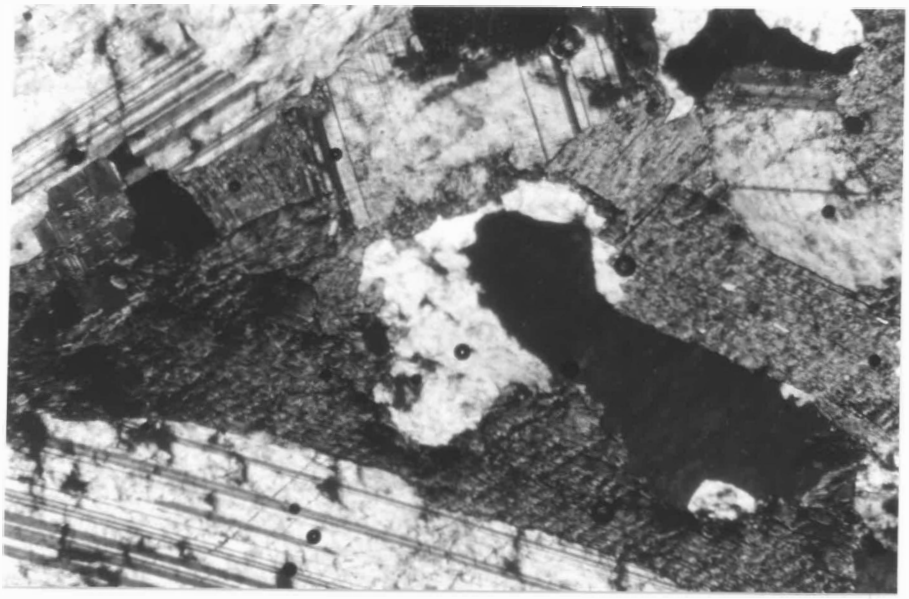

FIGURE 2.5 Granite; sericitised orthoclase crystals, twinned plagioclase, and hornblende.
25 X ; crossed nicols; ⊢——— 1mm ———⊣

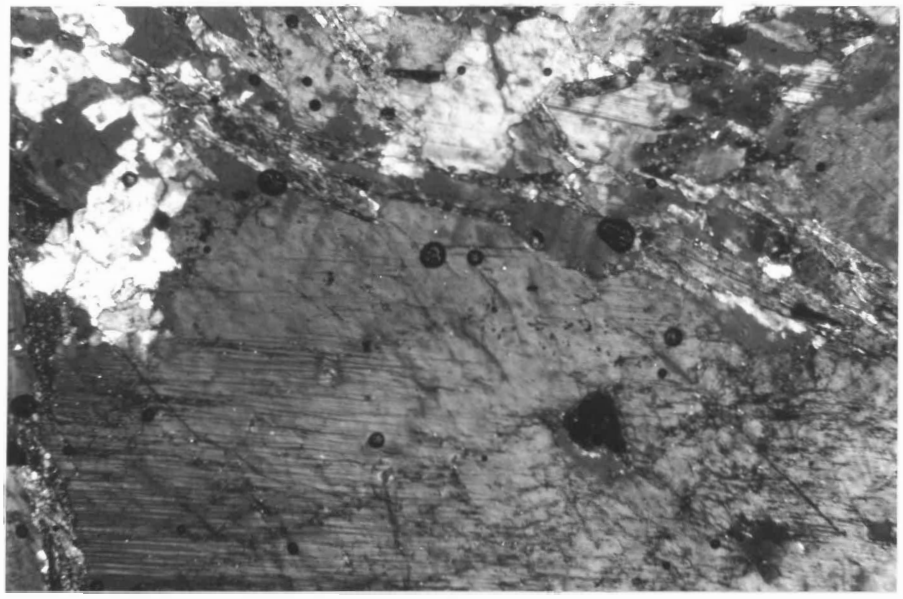

FIGURE 2.6 Gneissic granite; large plagioclase augens, with intervening crudely aligned biotite, hornblende, and quartz grains.
25 X ; crossed nicols; ⊢——— 1mm ———⊣

In thin section this rock shows the typical hypidiomorphic granular texture of a granite. Quartz (17%), plagioclase (32%), and orthoclase (20%) dominate the mineralogy. Hornblende (17%) with occasional sodic rims, and biotite (13%), in places altering to chlorite (<1%), complete the major minerals. Accessory minerals are sericite (<1%), which replaces orthoclase, sphene (<1%), apatite (tr), and opaques (tr). Some foliation occurs due to the alignment of feldspar phenocrysts and biotite flakes. This rock is a granite, as determined from a ternary classification involving ratios of quartz, alkali feldspar, and plagioclase (Streckeisen, 1976). Its field relations and petrography are consistent with the Larsen Granodiorite (Gunn and Warren, 1962; Haskell *et al.*, 1965; Palmer *et al.*, 1967; Burgess *et al.*, 1981).

2.2.4 Gneissic granite (Site 4, Nussbaum Riegel; WT25104; Figure 2.6)

Nussbaum Riegel consists of interlayered marbles and schists with large exposures of gneissic granite. One such exposure forms the flank of a large roche moutonnée located on the southern side of Mummy Pond (Figure 2.7). The asymmetry of such features, best developed on well-jointed granites, has been related to ice action (Sugden and John, 1976). In this case, the northern side of the hill has been steepened to form a craggy bluff, parallel to ice movement along the Taylor Valley. Some 40-50 metres above the valley floor an outcrop provided sheeting joints suitable for testing.

In thin section the texture of this rock is generally hypidiomorphic granular. In hand specimen it shows crude gneissic foliations and augens of plagioclase up to 40 mm in diameter. Major minerals are quartz (17%), plagioclase (42%), orthoclase (23%), biotite (8%), and hornblende (8%). Accessory minerals are microcline

FIGURE 2.7 Roche moutonnée features in the vicinity of Mummy Pond, Taylor Valley, Antarctica.

(tr), sericite (<1%), chlorite (<1%), apatite (tr), zircon (<1%), sphene (<1%), and opaques (tr). Graphic (quartz-orthoclase) intergrowths are also present. On the ternary classification of Streckeisen (1976), this rock plots as a granite. Field relations and petrographic description suggest it belongs to the Olympus Granite-gneiss (McKelvey and Webb, 1962; Haskell *et al.*, 1965).

2.2.5 Schist (Site 5, Suess Glacier; WT25105; Figure 2.9)

In the vicinity of the Suess Glacier, the Nussbaum Riegel consists of a steeply dipping sequence of well-bedded crystalline marbles, and biotite-schists (Figure 2.8). The near-vertical layering trends northwest and is deformed locally by small folds (Williams *et al.*, 1971). Layers of dark, foliated schist occur at a site two-thirds along the snout of the Suess Glacier from the western end. Jointing is well-developed along planes parallel to the schistosity of the rock.

In thin section, this rock is dominated by plagioclase (22%), orthoclase (46%), and quartz (16%), the former two often occurring as porphyroblasts. The orthoclase is commonly sericitised, and some of the alkali feldspar porphyroblasts are microcline (<1%). The other major mineral is biotite (15%). Accessory minerals are hornblende (<1%), opaques (<1%), apatite (tr), and sphene (tr). Graphic intergrowths of quartz and orthoclase were observed. Foliation is a result of interbedded laminae of feldspar and quartz, and biotite. This rock is grouped with the biotite-schists of the Koettlitz Group metasediments (Gunn and Warren, 1962; McKelvey and Webb, 1962; Haskell *et al.*, 1965; Findlay *et al.*, 1984).

FIGURE 2.8 Schists and marbles of the Koettlitz Group metasediments, Suess Glacier, Taylor Valley, Antarctica.

FIGURE 2.9 Schist; interlaminated quartz grains and biotite lathes, surrounding feldspar porphyroblasts.
25 X ; crossed nicols; ⊢——— 1mm ———⊣

FIGURE 2.10 Marble; interlocking twinned calcite grains, with high relief anhedral forsterite surrounded by fibrous antigorite.
25 X ; crossed nicols; ⊢——— 1mm ———⊣

2.2.6 Marble (Site 6, Suess Glacier; WT25106; Figure 2.10)

Outcropping marble forms part of the sequence opposite the Suess Glacier described previously. The marble is well-jointed, in planes defined by layering in the marble and cut by cross joints.

Petrographically, the major constituents of this rock are calcite (82%) and rounded forsterite (12%). Minor constituents are antigorite (4%), which surrounds the forsterite grains, and the mica phlogopite (2%). Accessory minerals are the calcic garnet, grossularite (<1%), epidote (<1%), granular opaques, probably magnetite (<1%), and tremolite (tr). A fine layering, composed of accessory minerals and mica, is often present. Triple point junctions, evidence of recrystallisation, confirm the metamorphic nature of this rock, which belongs to the Salmon Marble Formation of the Koettlitz Group. (Gunn and Warren, 1962; McKelvey and Webb, 1962; Haskell *et al.*, 1965; Findlay *et al.*, 1984).

CHAPTER THREE

DETERMINATION OF JOINT SURFACE ROUGHNESS

CHAPTER 3: DETERMINATION OF JOINT SURFACE ROUGHNESS

3.1 Introduction

The resistance to shearing along rock surfaces, i.e. the frictional strength of rock joints, is the result of two components:

(1) the basic friction angle, ϕ_b, dependent on the strength of the rock and its mineralogy, is effectively the frictional resistance which arises when two flat rock surfaces slide against each other;

(2) the effective roughness angle, i, is dependent on the geometric irregularities or asperities on the rock surface, and the degree of contact between the two surfaces offered by the asperities.

The basic equation used in the prediction of the peak shear strength of rock surfaces, that is, the frictional resistance at the point of shearing, was first described by Patton (1966) and later elaborated by Barton (1973). In its simplest form the relationship is,

$$\tau = \sigma_n \tan\phi_j \qquad (3.1)$$

where τ is the peak shear strength, σ_n is the effective normal stress and ϕ_j is the joint friction angle. Thus, zero shear strength of an irregular rock surface at zero normal stress produces a curved peak shear strength envelope. This represents an improvement over earlier attempts to fit the Coulomb relationship and a linear envelope,

$$\tau = c + \sigma_n \tan\phi \qquad (3.2)$$

(where c is an effective cohesion parameter), to rock discontinuities. The basic relationship in equation (3.1) can be expanded to include the two parameters outlined previously,

$$\tau = \sigma_n \tan(\phi_b + i) \qquad (3.3)$$

Barton (1973) derives an empirical relationship in which the effective roughness angle, i, is equal to,

$$JRC \log_{10}(JCS/\sigma_n)$$

where JCS is the joint wall compressive strength, and JRC is the joint roughness coefficient. Thus, in its most complex form equation (3.1) becomes,

$$\tau = \sigma_n \tan[\phi_b + JRC \log_{10}(JCS/\sigma_n)] \qquad (3.4)$$

If the joint is completely unweathered then JCS will equal the unconfined compressive strength of the unweathered rock (σ_c). Generally however, the rock joint walls are weathered to some extent and JCS will be lower than σ_c, possibly as low as 0.25 σ_c. A Schmidt hammer is applied directly to the exposed joint wall, and the rebound value converted to the relevant estimate of compressive strength, (the method is described fully later). JRC is a geometric coefficient generated on a roughness scale from 0 to 20. The higher is JRC, the higher is the degree of roughness. It is the joint roughness coefficient which is the most difficult quantity to accurately estimate in equation (3.4).

3.2 Estimation of JRC

A number of methods have been evolved to enable estimation of the joint roughness coefficient. Of these, three provide simple field techniques, and a fourth, mathematical, technique provides a useful check on values of JRC generated from less precise methods.

1. Comparison of joint surface roughness profiles with ten standard

roughness profiles yields a value of JRC between 0 and 20 (Barton and Choubey, 1977).

2. Tilting of a joint pair, and measurement of the tilt angle at which sliding occurs, followed by back-calculation to estimate JRC (Barton and Bandis, 1980).
3. Measurement of the force required to pull the upper block of a joint pair along the lower block. JRC is back-calculated similarly to the previous method (Barton and Bandis, 1980).
4. Numerical characterisation of surface roughness taken from surface profiles measured in the field, using a number of statistical parameters (Tse and Cruden, 1979).

3.2.1 Profile comparison

Barton and Choubey (1977) present ten standard surface roughness profiles, typical of JRC groupings, based on a number of joint specimens. JRC was back-calculated from shear box tests conducted on each joint, These standard profiles are shown in Figure 3.1 . Comparison of joint surface profiles sampled in the field with the standard profiles gives a preliminary estimation of JRC. However, small errors in the assignment of JRC lead to somewhat larger errors in the estimated peak shear strength. Rougher surfaces lead to greater percentage differences (Tse and Cruden, 1979). For this reason a more precise method is recommended.

A variety of methods exist for the profiling of joint surfaces. Optical techniques are exact but time consuming and cover only a small range of depths. The most reliable method is linear profile measurement by a stylus instrument. However, common stylus instruments are not suitable for surface profiling of rock joints because of the comparatively large depth of roughness involved.

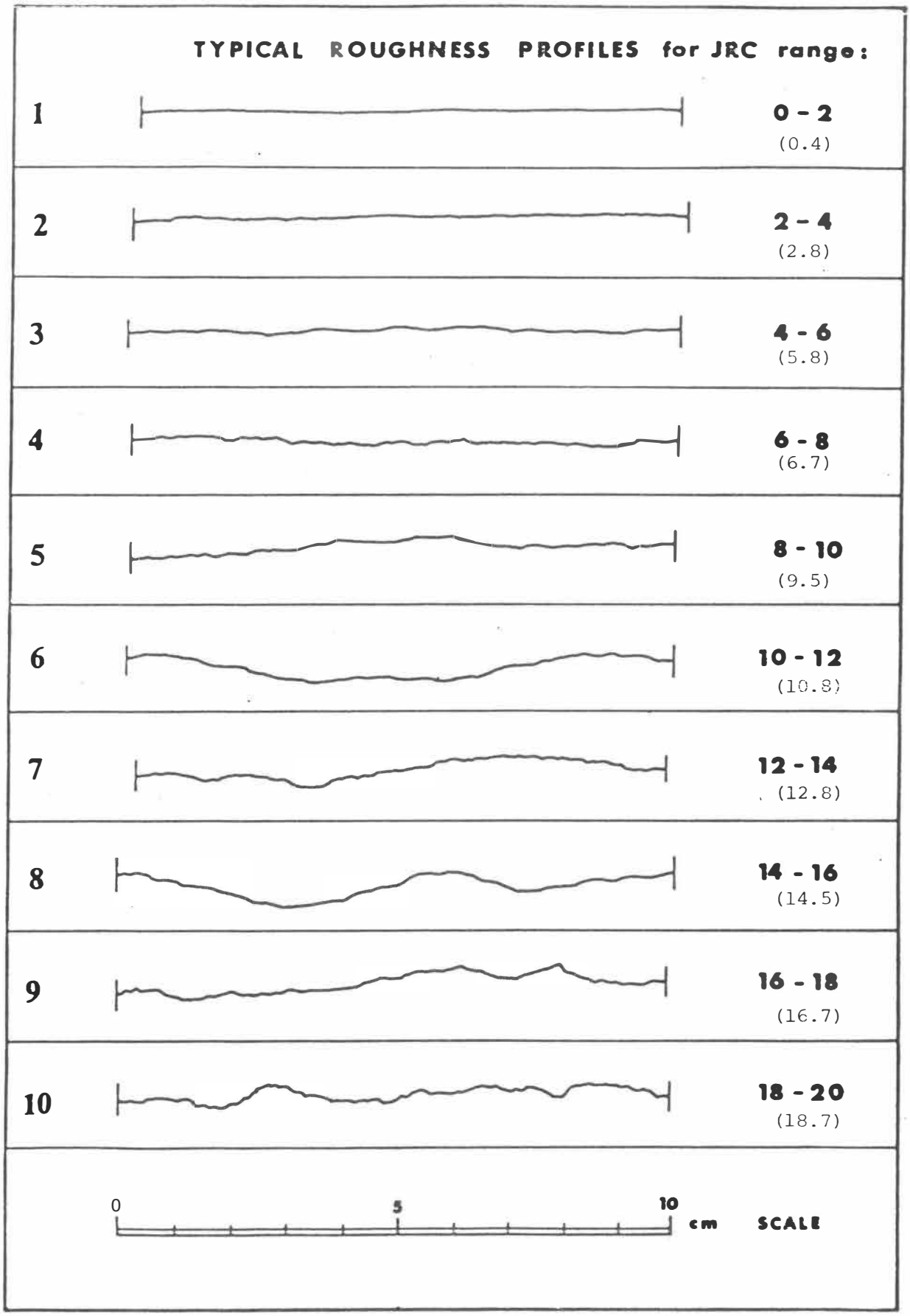

FIGURE 3.1 Standard roughness profiles and JRC ranges. Actual back-calculated JRC values for each joint are shown in brackets. (Barton and Choubey, 1977).

Stylus instruments which are suitable for high amplitude profiles generally fail because continuous horizontal movement is prohibited by deep, steep roughness troughs. Enlarging the radius of the stylus tip or attaching a small roller disc overcomes this problem but reduces the accuracy of the measurement. Weissbach (1978) describes an instrument in which the horizontal movement of the stylus is not continuous but in steps, contact between the needle and the rock existing only at intermittent periods of rest. Horizontal movement is matched with vertical movement of the stylus, thus preventing sticking. Peek (1981) outlines a technique which samples the roughness of an area on a joint surface, by measuring the area of shadow cast by asperities when the joint is illuminated by unidirectional light at a particular oblique angle. Almost all the techniques described are limited to laboratory conditions. For profile sampling in the field, an adjustable template, similar to that used by Barton and Choubey (1977), may be employed.

3.2.2 Tilt testing

The choice of an appropriate joint test size for shear strength determinations is usually based on economic and technical considerations. High cost, conventional large scale shear tests are often replaced with cheaper laboratory testing of small joint samples. However, scale effects on joint shear strength exist. Barton and Bandis (1980) find that generally JRC is only a constant for a fixed joint length. Longer profiles of the same joint have lower JRC values, and therefore lower peak shear strength. This scale effect on peak shear strength implies that there is a minimum joint test size which should be technically acceptable. Barton and Choubey (1977) suggest that the natural block size as controlled by the spacing of

cross joints might be the most correct test size. A cheap solution for obtaining a scale-free estimate of JRC is to conduct simple tilt, pull, or push tests on naturally occurring blocks using only the self-weight of the overlying block as the source of normal stress (Bandis *et al.*, 1981).

Mated rock blocks intersected by a joint can be slowly tilted until sliding occurs down the joint plane (Bandis *et al.*, 1981). The tilt angle is measured, and individual JRC values can be back-calculated from each test using the equation,

$$JRC = \frac{\alpha - \phi_r}{\log_{10}(JCS/\sigma_{no})} \qquad (3.5)$$

where $\alpha°$ is the tilt angle, JCS is the joint wall compressive strength (MN/m^2), σ_{no} is the normal stress induced by self weight of the sliding block (MN/m^2), and $\phi_r°$ is the residual friction angle. The normal stress when sliding occurs, σ_{no}, can be derived from,

$$\sigma_{no} = \gamma\ h\ \cos^2\alpha \qquad (3.6)$$

where γ is the unit weight of the rock (MN/m^3), and h is the thickness of the upper block (m).

3.2.3 Pull testing

In the case of the pull test (Bandis *et al.*, 1981), the upper block is pulled parallel to the horizontal or inclined joint plane. Values of JRC for each test can be calculated by,

$$JRC = \frac{\tan^{-1}[(T_1+T_2)/N] - \phi_r}{\log_{10}(JCS\ A/N)} \qquad (3.7)$$

where A is the joint area (m^2), JCS is the joint compressive strength

(MN/m^2), N is the normal component of the block weight (MN), T_1 is the tangential component of the self-weight of the upper block (MN), T_2 is the external pulling force (MN), and $\phi_r°$ is the residual friction angle of the joint.

From Figure 3.2,

$$T_1 = W \sin\beta \tag{3.8}$$

$$N = W \cos\beta \tag{3.9}$$

where W is the weight of the upper block (MN), and $\beta°$ is the inclination of the joint plane.

3.2.4 Numerical calculation

Small errors in estimating JRC can result in serious errors in estimating the peak shear strength from equation (3.4). Tse and Cruden (1979) recommend a more precise estimation of surface roughness by detailed profiling and numerical characterisation of the roughness utilising a number of statistical parameters. By digitising the ten standard joint roughness profiles of Barton and Choubey (1977), Tse and Cruden (1979) investigated the relationship between the appropriate JRC values and eight parameters used to characterise surface roughness in mechanical engineering. Values of one of the parameters, Z_2, were strongly correlated with values of JRC. The Z_2 function (Myers, 1962), is the root mean square of the first derivative of the profile. The regression equations developed by Tse and Cruden (1979) avoid the subjectivity of cruder estimates of JRC, such as profile comparison. This method has been used by Pearson (1981), and studies involving the Z_2 parameter by Krahn and Morgenstern (1979) have produced a similar correlation.

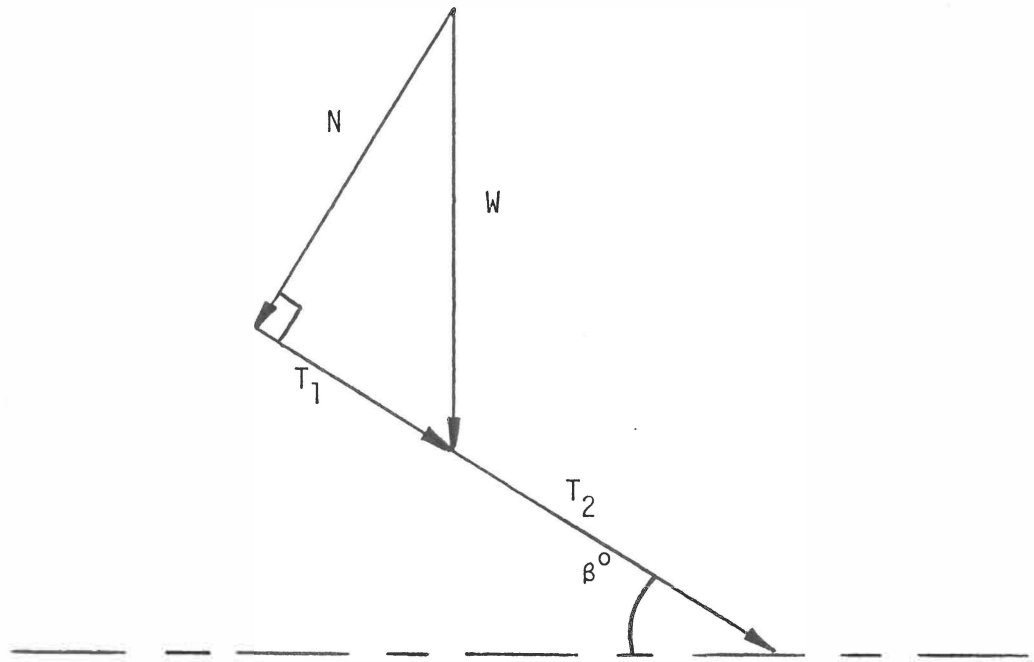

FIGURE 3.2 Distribution of forces on an inclined joint block during a pull test.

Unfortunately, the equations presented by Tse and Cruden (1979) apply only to profiles digitised at an interval of 1.27 mm. Significant variation in the density of the profile sampling will result in changes of the value of Z_2 (Section 5.4). The derivation of alternative relationships between Z_2 and JRC, for more standard sampling intervals, is treated in Section 5.5 . The relationship used in this study is for a sampling interval of 1.0 mm,

$$JRC = 32.29 + 33.84 \log Z_2 \qquad (3.10)$$

3.3 Sampling Programme

A 7 week field season was spent in the McMurdo Sound area, Antarctica, during November and December of 1983, with Event 11 of the New Zealand Antarctic Research Programme. The sampling programme (Doolin and Selby, 1984) involved 3 major types of testing - pull tests, tilt tests, and profile recording. Pull tests and tilt tests were repeated ten times per joint sample to obtain a representative result. Because the stresses across the joint are low there is no appreciable damage, enabling the tests to be repeated on the same joint sample. Approximately ten joint samples from each lithology were used per test type. Tests were conducted on the following lithologies,

quartz arenite (Olympus Range)

dolerite (Asgard Range)

granite (Bonney Riegel)

gneissic granite (Nussbaum Riegel)

schist (Suess Glacier)

marble (Suess Glacier)

Pull tests were conducted on all lithologies except for the quartz arenite. Tilt tests were conducted on the quartz arenite, schist, and

marble.

The procedure for each test was:

(a) Selection of a joint (that is, a mated pair of joint blocks). Some degree of standardisation within each lithology was achieved by selecting joints from the same joint set and mode of formation. An effort was made to avoid excessive effects of scale on the determination of JRC, by sampling joints which were of the natural block size for each site (Barton and Choubey, 1977; Barton and Bandis, 1980; Bandis *et al.*, 1981).

(b) Three representative surface sections of one of the joint blocks, (usually the upper mobile block), were profiled. This was done using a "Maco" adjustable template similar to that used by Barton and Choubey (1977). The adjustable template is a series of thin metal rods which can move freely, moulding themselves to a surface. When clamped in place they retain the image of the surface, enabling a line to be traced and recorded in a field notebook (Figure 3.3).

(c) (i) Pull test - the upper block was pulled over the lower block by means of a tape loop, placed as close to the joint as possible to avoid moments, and connected to a Salter suspended spring balance (Model 235), used in this case as a stress gauge, recording the applied force at the point of movement (Figure 3.4).

(ii) Tilt test - the mated pair of blocks was tilted and the tilt angle at which the upper block slid was measured (Figures 3.5,3.6).

(d) Measurement of the area and weight of the upper joint block, and the slope angle, for the pull test. Measurement of the thickness of the upper block for the tilt test. Area estimates were obtained by summing measured component areas. Weight was measured

FIGURE 3.3 Joint surface roughness profiling.

FIGURE 3.4 Pull testing a joint pair.

using the Salter suspended balance (Figure 3.7). Angle measurements were taken using an Abney level or Brunton type structural compass (Seiwa S40D).

(e) Measurement of the hardness of the joint surface using a N-type Schmidt hammer (N-34 101755) - an instrument which simply records the rebound of a spring-loaded plunger after its impact with the joint surface (Figure 3.8).

(f) Collection of samples of each lithology for unit weight measurements and thin-sectioning (mineralogical description) in New Zealand.

(g) Collection of large block samples of each lithology for coring and subsequent measurement of the basic friction angle (ϕ_b), and unweathered Schmidt hardness, in New Zealand.

The surface roughness profiles obtained were used for comparison with standard profiles, in the numerical characterisation technique of estimating JRC, and for time series analysis of joint profiles. The remaining data collected were applied to the two equations for the derivation of JRC from the tilt test and the pull test (equations 3.5 and 3.7, respectively). It was originally intended to attempt recovery of small diameter cores taken through joints using hand drills, for testing in a laboratory rock shear box and determination of the joint friction angle. As will be discussed later, this part of the project was abandoned and any drilling was postponed until the return to New Zealand.

All the equipment used, (with the exception of the rock drills), performed satisfactorily in the Antarctic conditions that were experienced. Large metal components in some of the equipment used (e.g. crowbars, adjustable template), meant that they became extremely cold, leading to considerable discomfort when used in the

FIGURE 3.5 Tilt testing a joint pair.

FIGURE 3.6 Measurement of tilt angle.

FIGURE 3.7 Weight measurement of a joint block.

FIGURE 3.8 Measurement of surface hardness with a Schmidt hammer.

cold conditions generally prevalent in the Olympus and Asgard Ranges. This, as would be expected, slowed work down, time being required to rewarm extremities. It was originally intended to attempt drilling of rock samples using small motorised hand drills, with ethanol as the coolant. Due to a number of problems, both inherent in the drills themselves and produced by the cold conditions, adequate performance was not achieved. It was then decided to abandon that section of the programme, and to postpone any drilling until the return to New Zealand. This allowed expansion of the earlier and major part of the project. It is the opinion of the author that despite the problems encountered, such drilling, although difficult, is possible in the locations visited. Supplying the large quantities of coolant required for the drills used is an important limitation.

A considerable amount of time and effort was spent by the author developing a rock shear box within the Department of Earth Science, University of Waikato. Unfortunately, due to a lack of departmental finance and suitable recording equipment, the project was postponed beyond the time scale of a M.Sc. thesis. An alternative option, numerical characterisation of joint surface profiles, was used as a laboratory standard for comparative purposes. An attempt was also made to modify a soil direct shear box for the testing of rock cores, to determine basic friction angle. However, the high normal loads necessary for testing rock surfaces could not be applied satisfactorily. Once again, this part of the project had to be abandoned. Instead, the tilting of cores to determine basic friction angle was investigated.

CHAPTER FOUR

DETERMINATION OF COMPONENT PARAMETERS

CHAPTER 4: DETERMINATION OF COMPONENT PARAMETERS

4.1 Introduction

Within each of the two major field methods for estimation of JRC, namely tilt and pull tests, four component parameters need to be derived indirectly rather than directly measured. These four are the unit weight (γ), the basic friction angle (ϕ_b), the joint residual friction angle (ϕ_r), and the joint wall compressive strength (JCS). The former two can be determined from cored samples, and the latter two can be estimated from relationships involving Schmidt hammer rebound hardness. The general applicability of the tilt and pull tests relies to some degree on the ease of measurement of these component parameters. The development of techniques which satisfactorily achieve this merits discussion.

4.2 Unit Weight

Unit weight is defined as mass density multiplied by gravitational acceleration,

$$\gamma = \rho \, g \tag{4.1}$$

Mass density or bulk density is the density of the dry rock with its pore spaces filled with air. This was determined by a buoyancy technique using Archimedes principle (Battey, 1975; Brown, 1981). Gravitational acceleration is a standard 9.807 m/s^2 at sea level.

The mass density (ρ) of a rock sample is simply,

$$\rho = \frac{w_1}{w_1 - w_2} \tag{4.2}$$

where w_1 (g) is the mass measured in air, and w_2 (g) is the mass of the sample suspended in water. The mass of water displaced ($w_1 - w_2$) gives the volume of the sample. This mass should be corrected to a mass at a standard temperature of 4°C. A table of correction factors for the density of water at various temperatures is provided by Battey (1975). Density determinations were conducted for each lithology. The results are tabulated in Table 4.1 .

TABLE 4.1 Mass density and unit weight by lithology

	Quartz arenite	Dolerite	Granite	Gneissic granite	Schist	Marble
ρ (Mg/m^3)	2.45 2.46	2.86 2.88	2.74 2.73	2.73 2.71	2.69 2.68	2.91 2.81 2.85
Mean	2.46	2.87	2.74	2.72	2.69	2.86
γ (kN/m^3)	24.1	28.1	26.9	26.7	26.4	28.0

4.3 Basic Friction Angle

The effective joint friction angle has been previously defined as the result of two components. The first is a basic angle of friction, ϕ_b, related to rock strength and mineralogy. The second is a geometric component, the angle i.

Traditionally, the basic angle of friction has been estimated from shear tests on flat unweathered rock surfaces (Patton, 1966; Coulson, 1972; Barton and Choubey, 1977). The granular texture of the rock should be exposed, but not so as to cause interlocking and dilation. Sand-blasted, flat, rough-sawn surfaces give the most satisfactory results (Stimpson, 1981). Basic friction angles for most

unweathered surfaces lie between 25° and 35°. If necessary, a crude estimation of basic friction angle can be made from tabulated values of ϕ_b such as those presented by Barton (1973), Barton (1976), and Barton and Choubey (1977).

Stimpson (1981) has suggested an alternative method for the determination of the basic friction angle of the rock surfaces. It consists of a simple tilting test which measures the critical angle of sliding of cylindrical core surfaces in contact.

4.3.1 Tilting of cores

A method for estimating basic friction angle involving cores obtained by typical drilling methods (Stimpson, 1981) is advantageous in that the core surfaces are already pre-cut and smooth. Since coring is common in geotechnical investigations, a simple test involving cores has an obvious applicability.

Two lengths of equal diameter core are placed in contact on a horizontal base and restrained from moving. A third piece of core is placed on top of them, in contact with both, and is free to slide. The base is rotated upwards about a horizontal hinge, and the angle at which the upper length of core slides along the lines of contact with the lower cores is measured.

Consider the following system of forces (Figure 4.1) where the base remains horizontal and there is no tilting of the cores. Let W be the weight of the upper core, R be the reaction force at the contact between the upper core and each of the lower cores, f be the lateral frictional forces in the plane perpendicular to the core axis, and $\theta°$ be the angle (measured in the plane normal to the core axis) between the vertical plane through the centre of the upper core and

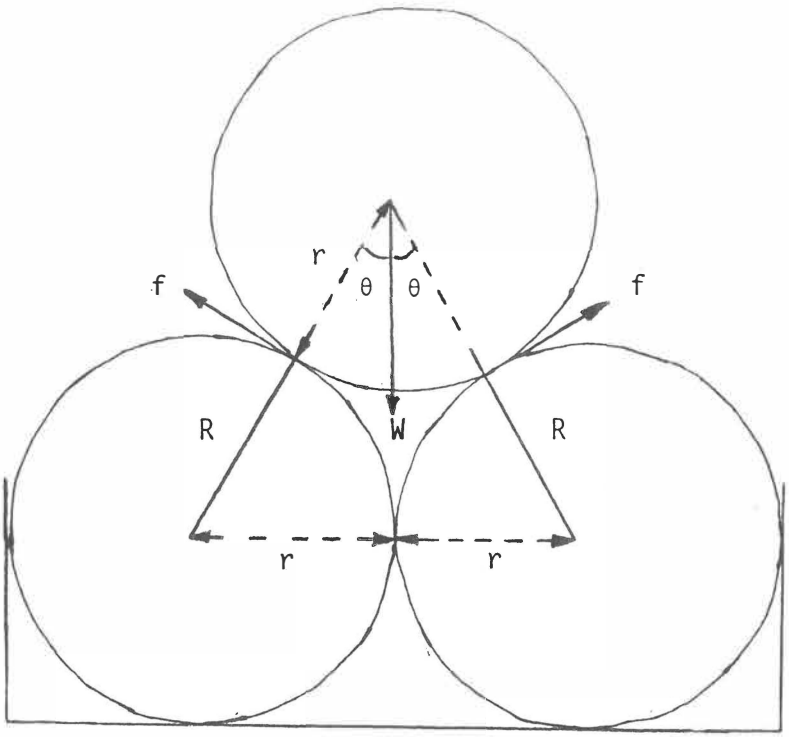

FIGURE 4.1 System of forces for a circular core resting on two identical and laterally restrained cores.

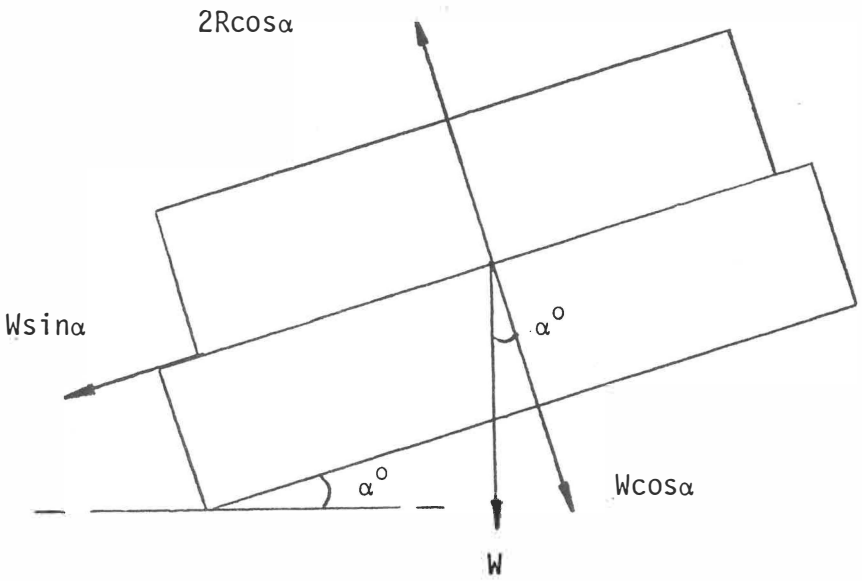

FIGURE 4.2 Distribution of forces on the system of cores when tilted at an angle of α^{o}.

the line connecting the centre of the upper core section to the centre of each lower core. If the lower cores are held fixed, then the frictional forces denoted by f cannot be uniquely determined theoretically. If, however, the upper core is placed gently on the lower cores, then no significant lateral frictional force need occur. Consider for example, if the core surfaces were frictionless. The upper core would still rest on top of the lower cores due to the reaction forces only. In the following theory, the lateral frictional forces are assumed to be zero.

Consider the upper core. Resolving vertically,

$$W = 2\ R\ \cos\theta \tag{4.3}$$

If we introduce to the system a tilt, of angle α° (Figure 4.2), the weight component perpendicular to the core axis becomes,

$$W\ \cos\alpha$$

so that,

$$W\ \cos\alpha = 2\ R\ \cos\theta \tag{4.4}$$

and,

$$R = \frac{W\ \cos\alpha}{2\ \cos\theta} \tag{4.5}$$

By definition, the frictional resistance available at the point of sliding is equal to the reaction force normal to the direction of sliding multiplied by the coefficient of friction. If we assume that the preparation of each core was standard and that the rock is homogeneous, then the coefficient of friction between the upper core and each of the lower cores is equivalent, and equal to $\tan\phi_b$, where

ϕ_b is the basic friction angle. Hence, the total frictional resistance mobilised at the point of sliding is,

$$2 R \tan\phi_b$$

Substituting equation (4.5), the total frictional resistance becomes,

$$\frac{W \cos\alpha \tan\phi_b}{\cos\alpha} \qquad (4.6)$$

Now, at the threshold condition the resisting forces must equal the driving forces, so that,

$$\frac{W \cos\alpha \tan\phi_b}{\cos\theta} = W \sin\alpha \qquad (4.7)$$

Therefore,

$$\tan\phi_b = \cos\theta \tan\alpha \qquad (4.8)$$

From Figure 4.1, $\theta = 30°$, so that,

$$\cos\theta = 0.866$$

Hence,

$$\tan\phi_b = 0.866 \tan\alpha$$

or,

$$\phi_b = \tan^{-1}(0.866 \tan\alpha) \qquad (4.9)$$

It should be noted that the derivation presented here differs from that of Stimpson (1981). Stimpson (1981) quotes, incorrectly, the reaction force, R, as,

$$R = \frac{W \cos\theta \cos\alpha}{2}$$

instead of equation (4.5),

$$R = \frac{W \cos\alpha}{2 \cos\theta}$$

Correspondence has failed to reconcile this discrepancy (B.Stimpson, pers. comm.,1985) and it is recommended that equation (4.9) be used for the calculation of the basic friction angle, and not the one given by Stimpson (1981).

Equation (4.9) was used to estimate the basic friction angle for each Antarctic lithology. Three 56.8 mm diameter cores were recovered from each lithology using a diamond bit in a laboratory drill press. These cores were cut to 100 mm lengths, and tilted according to the method outlined above. Ten tests were carried out for each lithology, using dry cores. After each test the contacts were brushed to remove any fine debris which may have been generated during the test. Tilt angles were measured using a drum inclinometer. The results of the tests are tabulated in Table 4.2 .

The results obtained are consistent with values reported in Barton and Choubey (1977). The low standard deviations involved also improve the general credibility of the data. The core lengths used must be perfectly circular so that sliding occurs along a line and not a plane. Cores must also be perfectly cylindrical, so that there are no ridges running normal to the direction of sliding. So long as these requirements are observed, the tilting of cores provides a useful determination of the basic friction angle.

TABLE 4.2 Results of core tilting tests

	Quartz arenite		Dolerite		Granite		Gneissic granite		Schist		Marble	
Test	$\alpha°$	$\phi_b°$	$\alpha°$	$\phi_b°$	$\alpha°$	$\phi_b°$	$\alpha°$	$\phi_b°$	$\alpha°$	$\phi_b°$	$\alpha°$	$\phi_b°$
1	34.5	30.8	34.8	31.0	38.2	34.3	36.5	32.7	32.1	28.5	36.6	32.7
2	37.6	33.7	38.9	34.9	38.9	34.9	36.2	32.4	33.2	29.5	34.6	30.9
3	35.6	31.8	36.5	32.7	36.2	32.4	34.6	30.9	33.4	29.7	34.9	31.1
4	34.5	30.8	36.6	32.7	36.3	32.5	32.1	28.5	32.4	28.8	33.4	29.7
5	34.7	30.9	32.9	29.3	37.8	33.9	34.8	31.0	30.4	26.9	32.7	29.1
6	37.2	33.3	32.2	28.6	35.5	31.7	33.0	29.4	32.7	29.1	34.3	30.6
7	34.9	31.1	35.3	31.5	36.4	32.6	34.6	30.9	32.1	28.5	34.1	30.4
8	38.5	34.6	33.0	29.4	36.0	32.2	34.0	30.3	32.4	28.8	34.8	31.0
9	38.3	34.4	32.6	29.0	35.9	32.1	35.8	32.0	31.4	27.9	33.1	29.4
10	34.4	30.7	33.5	29.8	34.0	30.3	33.7	30.0	30.0	26.6	35.0	31.2
Mean		32.2		30.9		32.7		30.8		28.4		30.6
Standard Deviation		1.6		2.0		1.3		1.3		1.0		1.0

4.4 Schmidt Hammer Rebound Hardness

The Schmidt hammer, or concrete test hammer, is simply an instrument for recording the rebound of a controlled impact on a rock surface. Since the elastic recovery depends on the surface hardness, which is in turn related to the mechanical strength of the rock surface, the rebound distance yields a relative measure of surface hardness or strength. The advantage of the Schmidt hammer lies in its portability, and its ability to allow rapid, non-destructive, *in situ* testing.

The Proceq type N hammer used in this study has an impact energy of 0.225 kgm, which is imparted by releasing a spring-controlled hammer. The rebound value, indicated by a rider on a scale mounted on the side of the hammer, represents the rebound distance as a percentage of the forward movement of the the hammer mass. The hammer

is calibrated for a horizontal impact direction. When the hammer is inclined upwards, the rebound is assisted by the force of gravity and a negative correction must be applied. The opposite occurs when the hammer is inclined downwards. When used on inclined or horizontal surfaces the rebound value is corrected using the table supplied by the manufacturer (Proceq S.A., 1977).

Use of Schmidt hammer is contentious. Poole and Farmer (1980) list seven recommended sampling techniques for the Schmidt hammer reported in recent literature, none of which apparently, are based on a detailed statistical analysis of a test programme. Poole and Farmer (1980) conducted such an analysis and conclude that:

(1) data distributions of Schmidt hammer rebound values are approximately normal;

(2) rebound values are consistent; variation across the sampling area exceeds that at any one point;

(3) to obtain a repeatable rebound value the peak value from at least five continuous impacts at a point should be used.

This recommendation for a sampling procedure ignores the inaccuracies produced by flaws and fractures in the rock and is distinctly different from the method recommended by the International Society for Rock Mechanics (Brown, 1981) which suggests averaging the upper 50% of at least 20 individual rebound values separated by at least the diameter of the plunger. The ISRM method was used by the author in this study.

4.4.1 Residual friction angle

The Schmidt hammer can be used to estimate the degree of weathering or alteration of a joint surface, and hence allows estimation of a joint residual friction angle (ϕ_r) from an appropriate basic friction angle (ϕ_b). The empirical relationship proposed by Barton and Choubey (1977) is,

$$\phi_r = (\phi_b - 20) + 20\ (r/R) \qquad (4.10)$$

where r is the Schmidt hammer rebound value for the joint surface, and R is the Schmidt rebound for an unweathered rock surface, the ratio of r/R being a estimate of the effect of weathering on the joint surface. This method yields values of ϕ_r within 1° of the value derived by large scale laboratory tests (Selby, 1982). The use of the joint residual friction angle in the calculation of JRC is preferred to the use of the basic friction angle since it allows consideration of weathered rock joints as well as unweathered rock surfaces.

Schmidt hardness testing was conducted on all joints used in this study. The upper 50 % of 10 rebound values from the surface of each joint were averaged. The resultant rebound estimates, r, for each joint (corrected for inclination), together with their appropriate residual friction angles, are tabulated in Sections A2.2 and A2.3 . Rebound values of unweathered rock surfaces, R, were obtained by testing laboratory cores. The upper 50 % of 10 rebound values from an individual core were averaged and corrected for hammer inclination. Three cores were tested in this manner for each lithology. The averages of these values are presented in Table 4.3

TABLE 4.3 Schmidt hardness (Type N hammer) rebound values for unweathered rock by lithology

ROCK	R
Quartz arenite	49
Dolerite	62
Granite	50
Gneissic granite	54
Schist	59
Marble	58

4.4.2 Joint wall compressive strength

So far, discussion of the Schmidt hammer has involved relative measures of surface hardness or strength. It would be convenient to use the Schmidt hammer as an absolute measure of strength. Although the compressive strength of unweathered rock (σ_c) can be estimated from point load testing or uniaxial compressive testing, joints are generally weathered to some extent, and the joint wall compressive strength (JCS) will thus be less than σ_c. The advantage in a Schmidt hammer here is that it can be applied directly to exposed joint walls.

Correlations between the Schmidt rebound number and compressive strength have been presented for the Schmidt type N hammer (Yaalon and Singer, 1974), and for the type L hammer (a lower strength range version of the type N hammer) (Deere and Miller, 1966). Both Yaalon and Singer (1974), and Deere and Miller (1966) found a better correlation was obtained when the logarithm of the compressive strength was used. Day and Goudie (1977) suggest that for each project it would be desirable to produce a calibration curve by testing various rocks in the field area for their Schmidt rebound values and then their compressive strength by standard engineering

procedures. Such an exercise was conducted using five Antarctic lithologies, and a New Zealand ignimbrite to provide the low rebound end of the scale. Due to a general lack of suitable cores uniaxial compressive testing could not be considered, and it was decided to use the point load test to estimate compressive strength.

The point load strength test as recommended by the International Society of Rock Mechanics (1985) involves the application of a concentrated load on a rock sample through a pair of spherically truncated conical platens. The rock samples are prepared in one of four ways - a diametral test (core lengths tested through the core diameters), an axial test (core lengths tested through the core axis), a block test (cut blocks are tested), and an irregular lump test (irregular lumps are tested). Point load strength values are size-corrected to a point load strength index for a 50 mm diameter core (Brook, 1985),

$$I_{s(50)} = F\ (P/D_e^2) \qquad (4.11)$$

$$P = P_0\ (\text{MPa}) \times R_a\ (\text{mm}^2)$$

$$D_e = D\ (\text{mm}) \quad \text{for diametral tests}$$

$$= (4A/\pi)^{0.5} \quad \text{for axial, block, irregular lump tests}$$

$$A = W\ D \quad (\text{mm}^2)$$

$$F = (D_e/50)^{0.45}$$

where P_0 is the failure load, R_a is the ram area (1442.5 mm^2 for the machine used in this study), D_e is the equivalent core diameter, D is the distance between platen contact points, A is the minimum cross-sectional area of a plane through the platen contact points, W is the average width of the sample, and F is the size correction factor. The results of the point load testing are tabulated in Table 4.4 .

TABLE 4.4 Results of the point load testing

ROCK[1]	TEST[2]	L/D[3]	D/W[4]	D_e (mm)	P_0 (MPa)	$I_{s(50)}$ (MPa)
Dolerite[5]	D	1.7	-	56.8	19.0	9.0
	D	1.8	-	56.8	22.0	10.4
	D	1.7	-	56.8	19.5	9.2
	A	-	0.9	60.1	20.0	8.7
	A	-	0.9	60.2	18.5	8.0
	A	-	0.7	48.9	14.5	8.7
	A	-	0.6	50.5	19.0	10.8
	I	-	0.4	55.6	28.0	13.7
	I	-	0.7	46.4	16.0	10.4
	I	-	0.7	41.3	18.5	14.4
	I	-	0.7	54.1	19.5	10.0
Granite[6]	D	1.5	-	56.8	6.9	3.3
	A	-	0.5	42.9	5.0	3.7
	A	-	0.4	41.5	4.0	3.1
	A	-	0.6	45.6	7.0	4.6
	A	-	0.5	44.2	5.5	3.8
	A	-	0.4	37.5	3.0	2.7
	A	-	0.5	43.4	6.0	4.3
Gneissic granite[7]	D	1.0	-	56.8	7.0	3.3
	D	1.0	-	56.8	6.5	3.1
	A	-	0.5	43.8	5.0	3.5
	A	-	0.6	48.4	4.5	2.7
	A	-	0.5	44.8	4.5	3.1
	A	-	0.4	42.6	4.5	3.3
	I	-	0.8	53.6	10.0	5.2
	I	-	0.8	51.0	6.0	3.4
	I	-	0.8	46.4	6.0	3.9
	I	-	0.7	42.7	4.0	2.9
	I	-	0.7	44.7	5.5	3.8

(1) Some axial and irregular lump samples of dolerite, granite, and gneissic granite courtesy of P. Augustinus (pers. comm., 1985) who sampled in the same field areas the following summer season. Ignimbrite samples courtesy of K. Hind (pers. comm., 1985).
(2) D = diametral test; A = axial test; I = irregular lump test.
(3) Diametral test samples must have a L/D (length/diameter) ratio greater than 1.0 .
(4) Axial, block, and irregular lump test samples must have a D/W ratio between 0.3 and 1.0 .
(5) Ferrar Dolerite, Asgard Range, Antarctica.
(6) Larsen Granodiorite, Bonney Riegel, Taylor Valley, Antarctica.
(7) Olympus Granite-gneiss, Nussbaum Riegel, Taylor Valley, Antarctica.

TABLE 4.4 (contd.)

ROCK	TEST	L/D	D/W	De (mm)	Po (MPa)	Is(50) (MPa)
Schist[8]	D	1.7	-	56.8	14.7	7.0
	D	1.8	-	56.8	13.5	6.4
	D	1.8	-	56.8	15.0	7.1
	D	1.0	-	56.8	13.0	6.2
	A	-	0.5	43.8	10.0	7.1
	A	-	0.5	43.1	11.5	8.4
	I	-	0.5	41.7	9.5	7.3
	I	-	0.6	48.2	12.0	7.3
Marble[9]	D	1.3	-	56.8	9.8	4.6
	D	1.4	-	56.8	9.5	4.5
	D	1.5	-	56.8	7.5	3.6
	A	-	0.7	55.1	9.5	4.7
	A	-	0.6	47.7	10.0	6.2
	A	-	0.7	51.7	12.0	6.6
	A	-	0.6	50.3	8.0	4.6
	A	-	0.7	55.1	13.0	6.5
	A	-	0.8	56.2	12.5	6.0
Ignimbrite[10]	D	1.8	-	55.0	4.1	2.0
	D	1.2	-	55.0	3.9	1.9
	D	1.3	-	55.0	3.8	1.9
	D	1.3	-	55.2	3.3	1.6
	A	-	0.6	48.4	2.5	1.5
	A	-	0.6	48.2	2.9	1.8
	A	-	0.6	48.2	3.2	2.0
	A	-	0.6	48.7	2.9	1.7
	A	-	0.5	44.7	2.3	1.6
	A	-	0.6	48.2	3.0	1.8

(8) Koettlitz Group, Suess Glacier, Taylor Valley, Antarctica.
(9) Salmon Marble, Koettlitz Group, Suess Glacier, Taylor Valley, Antarctica.
(10) Waitеariki Ignimbrite, McLaren Falls, Lower Kaimai Range, New Zealand.

ISRM suggests that at least 10 tests per rock type be used, and a mean value calculation performed by removing the two highest and lowest values, and then averaging the remaining values. If less than 10 samples are used, only the highest and the lowest values are removed before averaging. The results of the mean value calculations are shown in Table 4.5 .

A large number of correlations between the point load strength index ($I_{s(50)}$) and uniaxial compressive strength (σ_c) have been reported in the literature (e.g. Brock and Franklin (1972), Bieniawski (1975), Greminger (1982)). On average, compressive strength is 20-25 times point load strength. The following correlation (Brook, 1985) was used to estimate σ_c from the $I_{s(50)}$ mean values (Table 4.5),

$$\sigma_c = 22\ I_{s(50)} \qquad (4.12)$$

TABLE 4.5 Mean $I_{s(50)}$ and appropriate σ_c by lithology

ROCK	No. of Tests	$I_{s(50)}$ (MPa)	σ_c (MPa)	R
Dolerite (AD)	11	9.8	216	62
Granite (BG)	7	3.6	79	50
Gneissic-granite (SG)	11	3.4	75	54
Schist (SS)	8	7.0	154	59
Marble (SM)	9	5.3	117	58
Ignimbrite (MI)	10	1.8	40	37

A regression analysis was conducted to determine the relationships between point load strength (MPa), compressive strength (MPa), and Schmidt rebound hardness. A linear regression of compressive strength against Schmidt rebound number was obtained, with a correlation of $r^2 = 0.713$, which increased to 0.897 when compressive strength was expressed on a log scale (Figure 4.3). No increase in correlation occurred when the Schmidt rebound values were multiplied by the rock unit weight (Deere and Miller, 1966). The appropriate equations are,

$$I_{s(50)} = 0.271\ R - 9.28 \qquad r^2 = 0.714 \qquad (4.13)$$

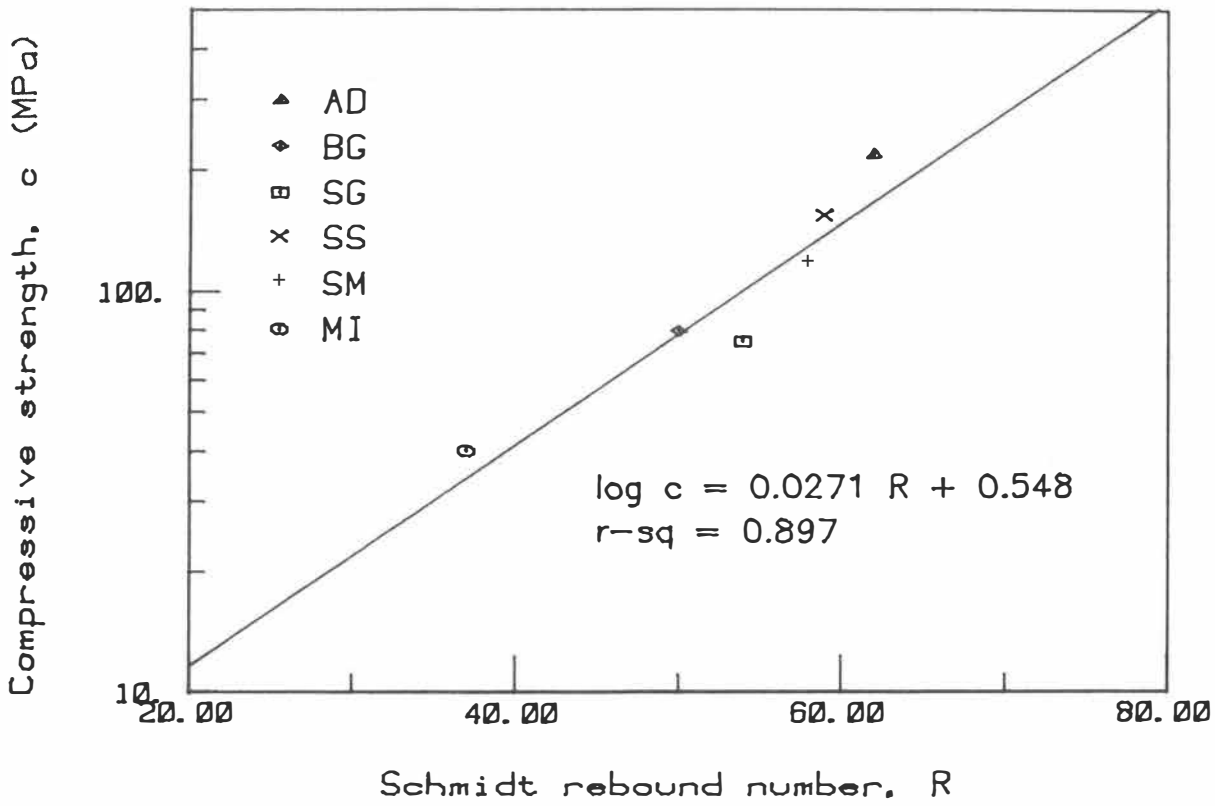

FIGURE 4.3 Calibration curve for compressive strength versus Schmidt rebound number.

$$\log I_{s(50)} = 0.0270\ R - 0.788 \qquad r^2 = 0.886 \qquad (4.14)$$

$$\sigma_c = 5.95\ R - 204 \qquad r^2 = 0.713 \qquad (4.15)$$

$$\log \sigma_c = 0.0271\ R + 0.548 \qquad r^2 = 0.897 \qquad (4.16)$$

Equation (4.16) was used to estimate the joint wall compressive strength (JCS) of joints used in this study, from Schmidt hardness testing conducted during tilt tests and pull tests. Resultant JCS values are tabulated in Sections A2.2 and A2.3

CHAPTER FIVE

NUMERICAL CHARACTERISATION OF SURFACE ROUGHNESS

CHAPTER 5: NUMERICAL CHARACTERISATION OF SURFACE ROUGHNESS

5.1 Introduction

When describing surface roughness it is necessary to define the spatial variation of surface geometry or roughness. That is, the manner in which the height or profile varies with lateral distance or length. Mechanical engineers describing metallic surfaces have used a number of direct mathematical approaches for obtaining numerical values for the main components of surface geometries. Tse and Cruden (1979) analysed several of these numerical characterisation techniques, in an attempt to isolate which best estimated the roughness of ten typical joint profiles presented by Barton and Choubey (1977). By numerically characterising the roughness of a rock surface Tse and Cruden (1979) report that more precise estimates of the roughness of a rock surface can be obtained, than by the comparison of roughness profiles with standard profiles as suggested by Barton and Choubey (1977).

5.2 Definitions of Surface Roughness

Surface roughness is often measured about the centre line. The centre is parallel to the general direction of the profile and is drawn so that the sums of the areas contained between it and the profile on either side of it are equal. A basic roughness characterisation is the centre line average (CLA), defined as (Krahn and Morgenstern, 1979),

$$CLA = \frac{1}{N} \int_0^N |y| \, dx \qquad (5.1)$$

where N is the length of the record, y is the amplitude of the roughness about a mean of zero (the centre line), and dx is the length between successive readings of amplitude.

Another measure of the average deviation is the root mean square (RMS). The RMS is simply the positive square root of the mean square value, which is the average of the squared values of the profile record. The RMS is defined as (Bendat and Piersol, 1971),

$$RMS = \left[\frac{1}{N} \int_0^N y^2 \, dx\right]^{0.5} \tag{5.2}$$

Sayles and Thomas (1977) proposed a structure function (SF) as an alternative means of quantifying variations in surface roughness.

$$SF = \int_0^N \left[h(x) - h(x+R)\right]^2 dx \tag{5.3}$$

where h(x) is the amplitude of the profile at distance x, along length N, and R is a constant distance lag. The SF function is related to the autocorrelation function (ACF) discussed in Section 7.2.

Myers (1962) noted that different surfaces might have the same RMS value, although their geometry differed. By extending the RMS approach Myers (1962) derived three new characteristics for describing surface roughness. Of these, the Z_2 parameter is the RMS of the first derivative of the surface profile, and is defined as,

$$Z_2 = \left[\frac{1}{N} \int_0^N (dy/dx)^2 \, dx\right]^{0.5} \tag{5.4}$$

5.2.1 The Z_2 Parameter

Myers (1962) found that a linear relationship existed between the coefficient of friction and the Z_2 value of metallic surface profiles. A similar result was obtained by Krahn and Morgenstern (1979) for some artificial rock surfaces. Of the surface parameters analysed by Tse and Cruden (1979), the Z_2 parameter yielded the strongest correlation with surface roughness, in this case represented by JRC.

To facilitate characterisation of surface roughness, traced profiles can be converted into a digital form, consisting of discrete measurements of amplitude (y-coordinate) at equal lateral intervals (x-coordinate). In discrete form, Z_2 is calculated (Tse and Cruden, 1979),

$$Z_2 = \left[\frac{1}{Md^2} \sum_{i=1}^{M} (y_{i+1} - y_i)^2\right]^{0.5} \qquad (5.5)$$

That is, for equal intervals, d, Z2 is the sum of the squares of the differences in adjacent y-coordinates over the record length, divided by the the product of the number of intervals, M, and the square of the interval, the square root then being taken.

5.3 Data Preparation

The use of the Z_2 parameter (or other parameters, including the ACF of Section 7.2) places certain constraints on the data used:

(1) the data must be in digital form; that is, a string of x,y coordinates recording profile amplitudes (y) at equal intervals (x);

(2) the data must be equally spaced;

(3) any trend in the mean value of the data must have removed;

(4) the data must fluctuate about a constant mean; that is, the mean of all the amplitudes for a particular profile must be zero.

5.3.1 Digitisation

The digitisation process is achieved using a computer linked digitising table. The table, known as a digitiser, has a free-moving cursor consisting of a lens and crosshairs, or alternatively a pen. As the operator moves the cursor over the table he can depress a button on the cursor, (or the pen "nib" itself), to record the x,y position of the cursor. This is known as point-mode digitising. Alternatively, a timing mechanism can be set to record x,y positions at set time intervals. This is known as stream-mode digitising. The more slowly the operator moves the cursor the more closely spaced points are recorded (Louden et al., 1980). A useful additional feature of the digitiser used in this study (Summagraphics Model ID2-CTR-3648) is the increment function. When this option is used together with stream-mode digitising, a new point is not recorded until the cursor is moved. This prevents the accumulation of identical points as the operator pauses during digitisation.

Software is required to interface between the digitiser and the user. The coordinates recorded by the digitiser need to be converted to a usable form and outputted as x,y coordinates. This is performed by computer program DIGIT (A1.1.3). Some degree of preprocessing is usually required before the digitised data can be used in any actual analysis. In this study, the computor program FILTER (A1.1.4) was run on the digitised data files to remove any errors in the digitising process which produced x-coordinates less than or equal to previous x-coordinates. These problem coordinates were simply the result of a slight backward or upward movement by the operator when digitising was

recommenced after pausing. Such coordinates often cause the failure of subsequent analytical programs. It is easiest to remove them from the data files prior to processing.

5.3.2 Interpolation

Interpolation or equal spacing is the estimation of a particular variable at regularly spaced points from its values at irregular intervals. If a linear relation can be assumed to exist between data points then intermediate values can be estimated by simple linear interpolation, since the difference between two adjacent y-values is a function of the lateral distance separating them (Figure 5.1). The relationship used is (Davis, 1973),

$$y' = \frac{(y_2-y_1)\ (x'-x_1)}{(x_2-x_1)} + y_1 \qquad (5.6)$$

Equal spacing of data by linear interpolation performs satisfactorily provided that the number of equally spaced points is similar to the original number of points, and that the original points are approximately uniformly spaced. Even if the original points are sparse and several intermediate values must be estimated between each pair of original points, the technique will work if the uniformity of the slope between points can be assumed. The routine shown above (equation 5.6) is an integral part of computer programs INTER (A1.1.5), and STAT (A1.1.6).

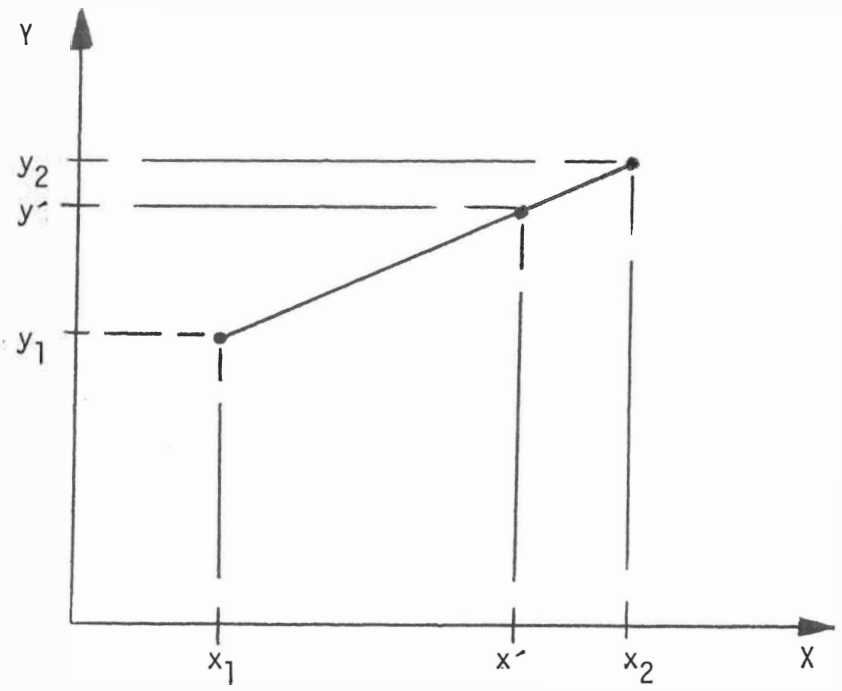

FIGURE 5.1 Linear interpolation between data points along a sequence.

5.3.3 Detrending and normalisation

Often a sequence of data may contain a trend or drift of the mean value of the data. Detrending or removal of this drift is achieved by fitting a linear regression to the data. New y-values are generated by subtracting the regressed line from the original y-values. The computer program subroutine LEASTS uses a linear least squares best fit to obtain the linear regression, and is an important part of programs INTER (A.1.1.5), STAT (A1.1.6), and TEST (A.1.7).

The final step in the data preparation process is to normalise the interpolated y-values so that they have a mean of zero. This task is an inherent part of the subroutine LEASTS.

5.4 Dependence of Z_2 on Data Spacing

The analysis carried out by Tse and Cruden (1979) indicates that the JRC of a rock surface can be confidently predicted by the parameter Z_2. An even stronger correlation can be shown when the logarithm of Z_2 is used. The equation derived by Tse and Cruden (1979) is,

$$JRC = 32.20 + 32.47 \log Z_2 \qquad (5.7)$$

This relationship will hold when the data sampled from the surface profile is spaced at 1.27 mm. Changes in the value of Z_2 could be expected if changes in the density of profile sampling occur.

In order to determine the extent of the effect of data spacing on generated Z_2 values, Barton and Choubey's (1977) standard profile 8 was digitised and its approximate Z2 value was calculated for a progressively increasing sample interval (every 0.1 mm) from 0.2 mm to 3.0 mm. A variant of computer program INTER (A1.1.5) was used. The

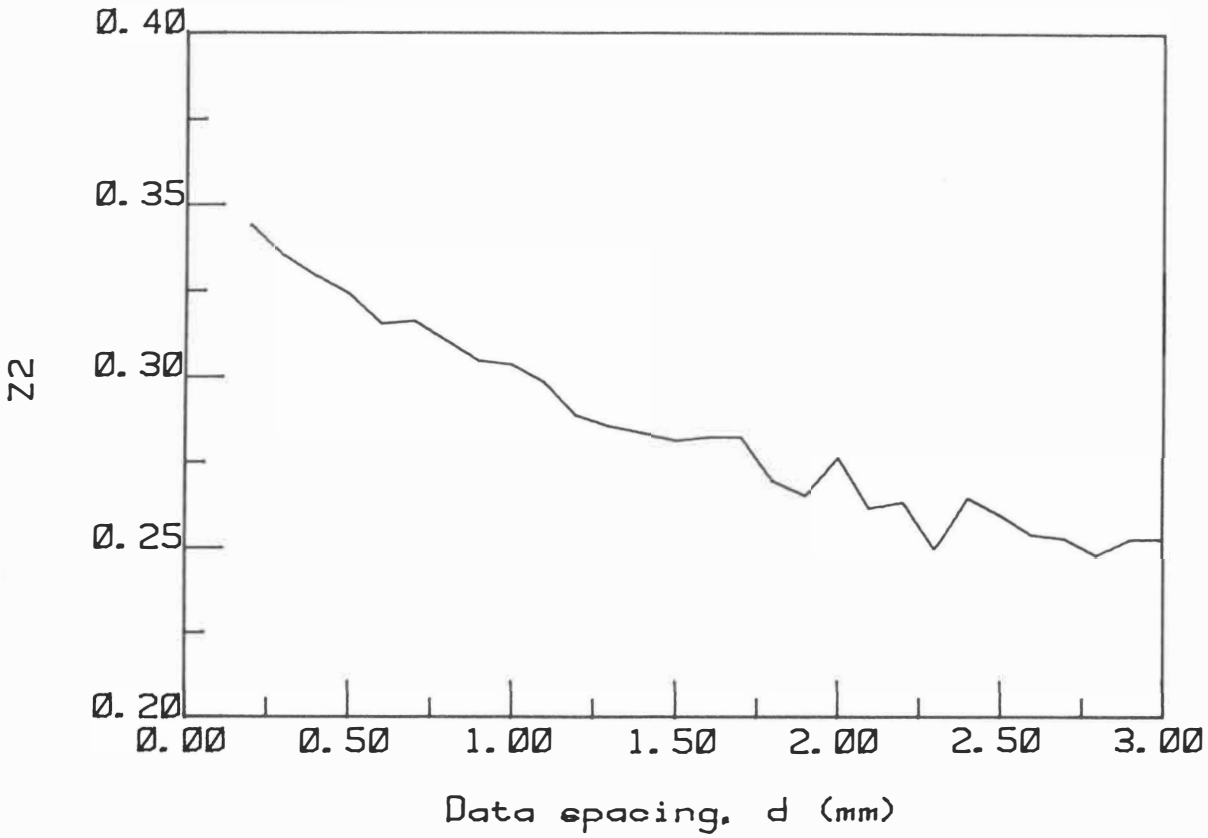

FIGURE 5.2 The effect of data spacing on the Z_2 value for Barton and Choubey's (1977) standard profile 8.

results are plotted in Figure 5.2 . Increasing the size of the sampling interval produced a marked decrease in the Z_2 value generated. The range of the decrease in the Z_2 value corresponds to the range of Z_2 values encountered in natural joints. It follows that since the Z_2 value is not invariant of the density at which the profile is sampled, individual equations must be formulated for different sampling intervals.

5.5 Alternative Correlations Between JRC and Z_2

Tse and Cruden (1979) developed a highly correlated relationship between JRC and the logarithm of Z_2 (Equation 5.7). This was for a specific data spacing or sampling interval of 1.27 mm. It has been shown in the previous section that the value of Z_2 obtained is dependent on the data spacing, d, selected for interpolation. If different data spacings are involved then separate relationships must be formulated for each sampling interval used. It follows that such equations must be compatible with the one previously obtained by Tse and Cruden (1979). To accomplish this, the ten standard profiles of Barton and Choubey (1977) (Figure 3.1) were digitised. The digitised profiles were interpolated at a 1.3 mm interval, and their JRC was estimated from a Z_2 parameter calculated from the relationship established by Tse and Cruden (1979) (equation 5.7) for a sampling interval of 1.27 mm. These profiles were redigitised until their estimated JRC values matched their known values. The Z_2 surface roughness parameter was calculated for each standard profile at data spacings of 0.5 mm, 1.0 mm, 1.3 mm, 1.5 mm, and 2.0 mm, using a variant of program INTER (A1.1.5). For each data spacing the logarithm of the Z2 value for each standard profile was linearly regressed against the appropriate JRC values (Figure 5.3). The

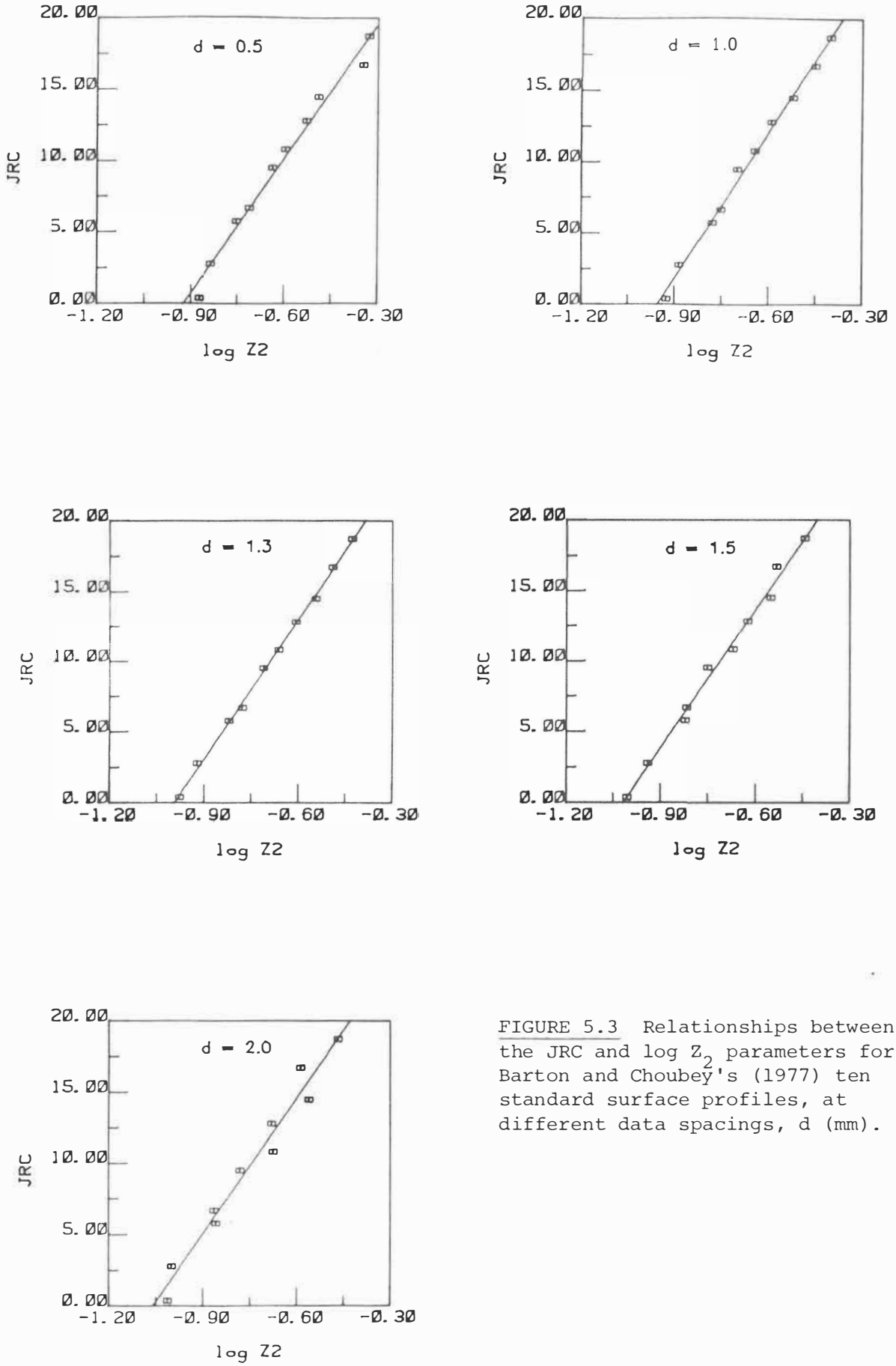

FIGURE 5.3 Relationships between the JRC and log Z_2 parameters for Barton and Choubey's (1977) ten standard surface profiles, at different data spacings, d (mm).

regression equations obtained are shown in Table 5.1 .

Since each digitised profile was corrected until an excellent match was achieved with the profile obtained for a sampling interval of 1.27 mm, the highest correlation obtained was for the relationship with a sampling interval of 1.3 mm. However, any new relationship generated would be compatible with that obtained by Tse and Cruden (1979). Thus, the very high correlations in Table 5.1 are artificial, and reflect a degree of statistical confidence relative to the relationship established by Tse and Cruden (1979). These correlations decrease slightly as the data spacing departs from 1.3 mm. However the departure is small, and the alternative predictor equations for the relationship between JRC and log Z_2 for differing data spacings can be used with confidence. For the estimation of JRC from profiles used in this study it was convenient to use a data spacing of 1.0 mm.

TABLE 5.1 Results of regression analysis of Barton and Choubey's (1977) ten standard surface profiles with the Z_2 surface parameter, for different data spacings (d).

d (mm)	Regression equation	r^2
0.5	JRC = 28.97 + 31.37 log Z_2	0.983
1.0	JRC = 32.29 + 33.84 log Z_2	0.995
1.3	JRC = 32.73 + 32.95 log Z_2	0.998
1.5	JRC = 33.13 + 32.54 log Z_2	0.992
2.0	JRC = 33.58 + 31.69 log Z_2	0.968

CHAPTER SIX

ANALYSIS AND INTERPRETATION

CHAPTER 6: ANALYSIS AND INTERPRETATION

6.1 Comparison of Methods

In all, 67 joints, from six Antarctic lithologies, were subjected to profile comparison, tilt testing, pull testing, and numerical characterisation, in order to estimate their roughness coefficients (JRC). The distribution of testing is shown in Table 6.1 .

TABLE 6.1 Distribution of testing

ROCK		COMP(1)	TILT(2)	PULL(3)	NUMC(4)
Quartz arenite	(OQ)	18	7	-	18
Dolerite	(AD)	9	-	9	9
Granite	(BG)	10	-	3	10
Gneissic granite	(SG)	10	-	4	10
Schist	(SS)	10	10	10	10
Marble	(SM)	10	9	10	10
TOTAL		67	26	36	67

(1) profile comparison
(2) tilt testing
(3) pull testing
(4) numerical characterisation

6.1.1 Summary of experimental results

Tilt tests are limited to joints smooth enough for the test to be possible without the tilt angle becoming so large that overturning failure dominates sliding failure. Rougher joints can be tested using pull tests. For joints that are too rough even for pull tests to be performed, the only field orientated method of predicting JRC is to compare their surface roughness with standard joint surfaces of known JRC. Barton and Choubey (1977) present tables depicting the range of

application of tilt and pull tests for determining JRC values of joints. According to Barton and Choubey (1977), for an average residual friction angle of between 25° and 30°, joints in this study with a maximum JRC value of around 8 could be tested satisfactorily by tilt tests. Similarly, joints with JRC values up to around 12 could be tested using pull tests.

Surface roughness profiles of 67 joints, obtained in the field, were compared to the ten standard profiles of Barton and Choubey (1977) (Figure 3.1), and a visual estimation of JRC was made. The results of this profile comparison are shown in Section A2.1 . JRC was estimated to the nearest whole number.

Tilt tests on 26 joints were carried out in the field as described in Section 3.3 . The computer program TILT (A1.1.1) was used to calculate JRC from the parameters obtained in these tests. The results are tabulated in Section A2.2 .

Field pull tests were conducted on 36 joints, as described in Section 3.3 . JRC values were calculated from the parameters obtained, using the computer program PULL (A1.1.2). The results are shown in Section A2.3 . All tilt and pull tests were carried out on dry rock.

Three roughness profiles from each of 67 joints were digitised, and numerically characterised by computer program INTER (A1.1.5) to calculate the Z_2 surface roughness parameter. JRC was calculated from the Z_2 values by a logarithmic relationship of the same form as that presented by Tse and Cruden (1979), but for a sampling interval of 1.0 mm (equation 3.10). The JRC values for the three profiles from each joint were averaged to obtain a JRC estimate for each joint. The results are tabulated in Section A2.4 .

Estimates of JRC resulting from the four different methods used are shown in Table 6.2 .

TABLE 6.2 JRC estimates from profile comparison, tilt testing, pull testing, and numerical calculation.

JOINT	COMP	TILT	PULL	NUMC
OQ1	9	-	-	10.4
OQ2	10	-	-	11.0
OQ3	10	-	-	9.9
OQ4	14	-	-	13.1
OQ5	14	-	-	9.4
OQ6	10	-	-	7.3
OQ7	8	-	-	5.4
OQ8	10	-	-	8.5
OQ9	8	-	-	6.4
OQ10	9	-	-	5.1
OQ11	12	5.9	-	7.1
OQ12	13	4.4	-	7.9
OQ13	10	8.0	-	8.2
OQ14	10	-	-	9.1
OQ15	8	6.4	-	6.9
OQ16	10	7.1	-	7.2
OQ17	8	6.6	-	7.4
OQ18	6	4.4	-	5.4
AD1	8	-	9.2	9.0
AD2	6	-	7.4	4.6
AD3	10	-	6.5	10.0
AD4	12	-	6.3	7.8
AD5	8	-	4.8	5.9
AD6	9	-	8.5	8.4
AD7	10	-	3.7	7.8
AD8	6	-	5.6	5.7
AD9	8	-	3.8	8.3
BG1	14	-	-	14.0
BG2	16	-	-	14.4
BG3	14	-	12.7	13.4
BG4	16	-	-	15.2
BG5	15	-	-	15.2
BG6	14	-	-	14.1
BG7	14	-	-	12.8
BG8	15	-	-	13.4
BG9	13	-	10.7	12.4
BG10	12	-	9.3	10.8

TABLE 6.2 continued

JOINT	COMP	TILT	PULL	NUMC
SG1	14	-	10.5	10.7
SG2	11	-	-	10.4
SG3	10	-	5.6	9.3
SG4	14	-	8.5	11.0
SG5	14	-	-	13.3
SG6	13	-	-	11.8
SG7	14	-	-	14.3
SG8	15	-	-	12.3
SG9	9	-	9.2	11.0
SG10	14	-	-	13.8
SS1	8	4.8	6.0	7.0
SS2	7	6.0	7.9	5.1
SS3	9	7.5	8.0	8.9
SS4	6	9.3	10.0	6.8
SS5	8	8.1	9.8	6.6
SS6	6	7.5	7.1	5.7
SS7	9	8.4	10.5	7.4
SS8	5	9.3	8.9	4.3
SS9	10	8.4	11.1	8.6
SS10	6	6.8	9.4	7.5
SM1	8	4.9	7.6	5.4
SM2	6	4.1	5.7	4.3
SM3	8	-	9.4	9.8
SM4	10	7.8	8.8	7.4
SM5	7	6.5	7.6	3.3
SM6	8	7.2	7.1	7.3
SM7	10	7.8	9.6	6.2
SM8	10	7.5	8.7	7.3
SM9	10	8.2	8.2	6.9
SM10	8	7.1	6.4	3.3

6.1.2 Statistical summary

Estimation of JRC by numerical calculation (NUMC) is based on a mathematical characterisation of the surface geometry. As a technique, this is a more precise computerised approach to what the eye approximates using the profile comparison method (COMP) recommended by Barton and Choubey (1977). As such it is a useful laboratory standard, with which the field orientated tilt (TILT) and pull (PULL) tests can be compared. Statistical comparison of the

reliability of each method was achieved by linearly regressing each method against the numerical calculation technique. If the two methods considered are measuring the same property, the resulting regression line should be close to y = x (a gradient equal to 1). Ideally, the degree of scatter about the line should be minimised (the larger the coefficient of determination, r^2, the better the linearity of the data considered). The results of the regression analysis are shown in Table 6.3, and Figures 6.1 and 6.2 . In the regressions conducted, when observations with a large standardised residual (the residual, the difference between observed and predicted y-values, divided by the estimated standard deviation of that residual) were removed, the correlation improved dramatically. Removal of these few observations was considered necessary in revealing the underlying relationships involved.

TABLE 6.3 Results of the regression analysis of four methods of estimating JRC, for six Antarctic lithologies.

Relationship	a	r^2	t	s	df
All lithologies					
NUMC vs COMP	0.981	0.884	20.12	1.090	54
NUMC vs TILT	0.474	0.355	3.52	0.927	21
NUMC vs PULL	0.515	0.188	2.76	2.279	34
PULL vs TILT	0.771	0.537	4.44	1.060	18
Salmon Marble					
NUMC vs TILT	0.784	0.649	4.26	0.599	6
NUMC vs PULL	1.120	0.478	2.70	1.582	9

a = gradient;
r^2 = coefficient of determination;
t = obtained t-ratio;
s = estimated standard deviation around the regression line;
df = total degrees of freedom;

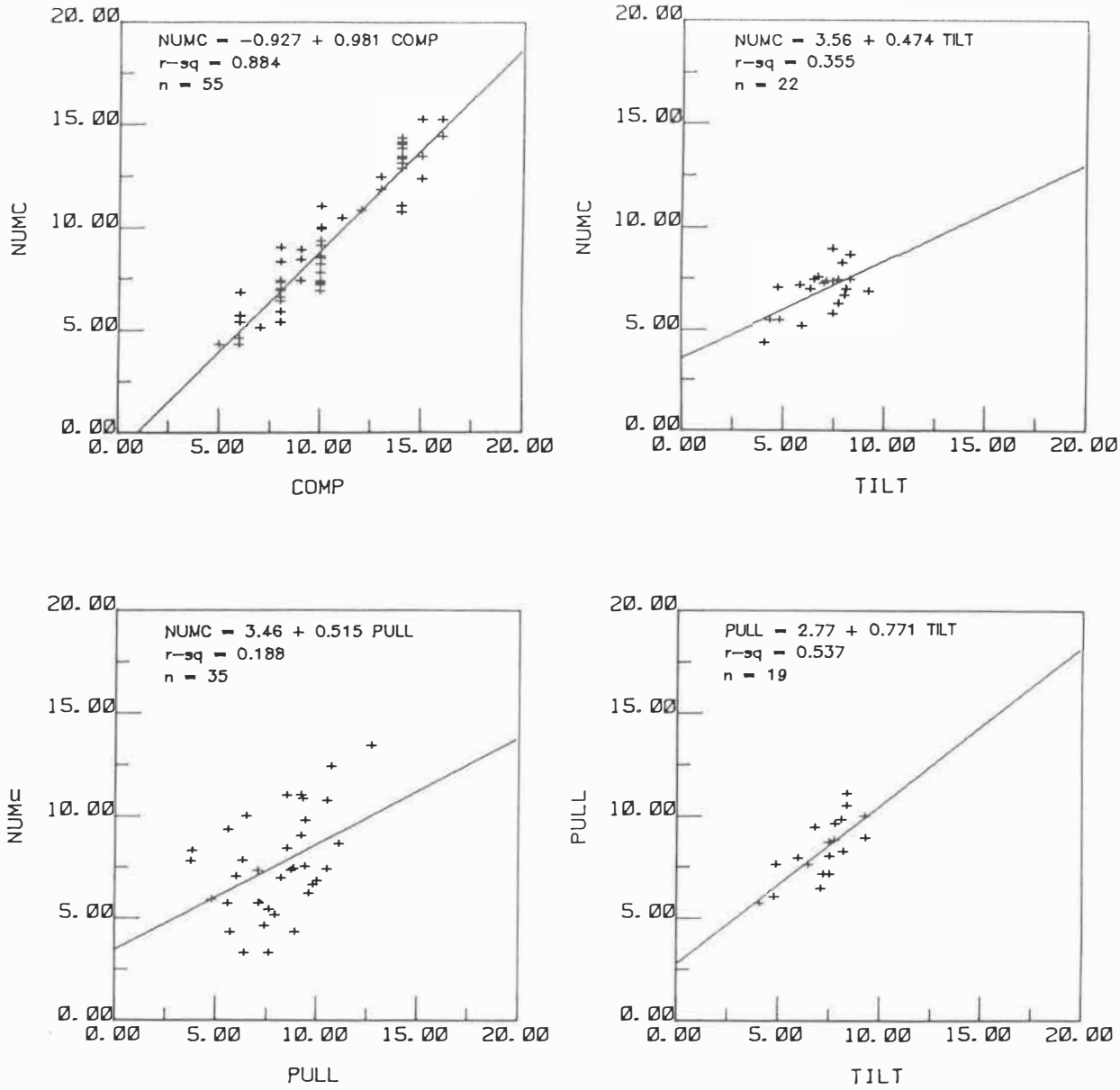

FIGURE 6.1 Relationships between the four methods of estimating JRC for six Antarctic lithologies.

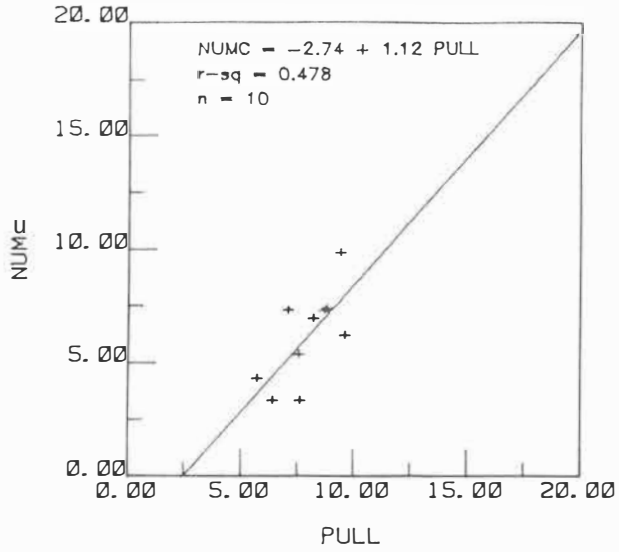

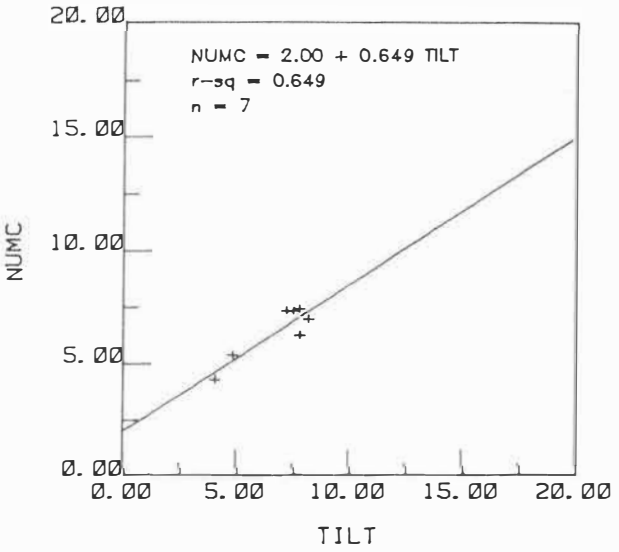

FIGURE 6.2 Relationships between methods of estimating JRC for Salmon Marble, Koettlitz Group, Antarctica.

If the obtained t-ratio for the regression is greater than the tabulated t value, for the appropriate degrees of freedom, at $\alpha = 0.05$, then the gradient of the regression line is significantly different from zero at that alpha level. As would be expected all the regression lines have a gradient significantly different from zero. Also, by comparing the absolute difference between the obtained gradient and 1, against the standard deviation around the regression line (s), it can be determined that none of the regression lines have gradients significantly different from 1 (at $\alpha = 0.05$). However, consideration of r^2 is less satisfactory. The obtained results suggest that:

(1) An excellent relationship exists between the profile comparison method (COMP) and the standard numerical calculation technique (NUMC). This is not unexpected since both methods assume a JRC dominated by surface geometry.

(2) While individual joint types (e.g. Salmon Marble, Figure 6.2) can produce adequate relationships between the field tilt and pull tests (TILT, PULL) and numerical calculation (NUMC), overall the degree of linearity is nowhere near as good as the relationship between profile comparison and numerical calculation.

(3) A definite relationship exists between the field conducted tilt (TILT) and pull tests (PULL). Again, this is not unexpected since both tests involve the sliding of one joint block against another.

All this suggests that the tilt and pull tests, while both measuring the same property, measure something that is slightly different from that measured by numerical calculation or profile comparison methods. It is tempting to postulate that the tilt and pull tests measure a JRC composed of some material property of the rock (such as the shear strength of asperities), in addition to the geometric roughness measured by profile comparison and numerical calculation. This

questions the validity of using tilt and pull tests to measure JRC.

Barton and Choubey (1977) describe an experimental study involving these simple index tests for the estimation of JRC. They admit that tilt and push/pull tests sound rather crude, but reassure the reader of their applicability by reporting from their experimental study that "despite the inevitable scatter of data" the mean predicted and measured JRC values for 57 (tilt tested) and 45 (push tested) joint specimens were "remarkably close". It is this author's opinion that any attempt to average the results of 8 different rock types and some 15 different joint types can only result in a false and misleading sense of confidence. To further compound the error Barton and Choubey (1977) then combine the tilt test and push test results and report the mean predicted and measured JRC values for 102 joint specimens.

If an attempt is made to isolate individual results from the mean values reported the story becomes less convincing. Barton and Choubey (1977) report a range of errors in the mean predicted JRC for combined tilt and pull tests of greater than ±1. The range of errors within each test type is even larger, (a function of decreasing sample size), and even these are the means of a number of joint specimens for each joint type. The range of errors in the predicted JRC for individual joint specimens is not given.

A similar exercise was conducted on the data reported in this study (Table 6.4). The range of errors in the mean predicted JRC for the tilt test was approximately ±1, while that of the pull tests was ±2. The mean value of JRC predicted from the tilt tests on 26 joints was 6.9, while the measured mean obtained from numerical calculation was 6.5 The mean value of JRC predicted from pull tests on 36

joints was 8.1, while the measured was 7.6 . These results are comparable with those reported by Barton and Choubey (1977). However, the degree of scatter shown in Figure 6.1 dispels the misleading degree of accuracy that such calculations generate. These calculations merely reflect that the index tilt and pull tests show a bias in overestimating JRC for some joint types and underestimating JRC for others. When all the joint types studied are considered the errors happen to cancel out each other. Interest is invariably centred on one particular joint type, and the range of errors that can be expected in the predicted JRC from this type of study is large enough to be of significance. Errors in individual predicted JRC values for both the tilt tests and pull tests in this study generally lie between ±3.5 .

TABLE 6.4 JRC prediction based on tilt and pull tests.

	TILT TESTS (JRC ≤ 8.0)				PULL TESTS (JRC ≤ 12.0)			
Joint type	No.[1]	JRC[2] (meas.)	JRC[3] (pred.)	ERROR[4]	No.[1]	JRC[2] (meas.)	JRC[3] (pred.)	ERROR[4]
OQ	7	7.2	6.1	-0.9	-	-	-	-
AD	-	-	-	-	9	7.5	6.2	-1.3
BG	-	-	-	-	3	12.2	10.9	-1.3
SG	-	-	-	-	4	10.5	8.5	-2.0
SS	10	6.8	7.6	+0.8	10	6.8	8.9	+2.1
SM	9	5.7	6.8	+1.1	10	6.1	7.9	+1.8
ALL	26	6.5	6.9	+0.4	36	7.6	8.1	+0.5

(1) number of samples of suitable roughness for tilt/pull testing
(2) mean measured JRC from numerical calculation;
(3) mean predicted JRC from tilt/pull tests on same specimens as (1);
(4) prediction error: (+) over-estimate, (-) under-estimate;

Furthermore, Barton and Choubey (1977) carried out their tests using a direct shear box to conduct push tests and a laboratory tilting frame with a mounted scale for conducting tilt tests. In the field, the use of a stress gauge and tape loop for pull tests, and hand tilting and a structural compass for tilt tests, introduces a decrease in general accuracy.

6.2 Rock Characterisation

Analysis of variance (ANOVA) procedures are techniques for comparing the means of several populations. Such procedures construct ANOVA F tests by comparing mean squares relative to their expected values under a null hypothesis of equal means, (assuming equal variances). The ratio of the two mean squares is an F statistic. Large F values lead to rejection of the null hypothesis. It is important to note that failure to reject the null hypothesis does not necessarily imply that the population means are equal but rather implies that the difference between population means, if any, is not large enough to be detected with the given sample size. A one-way ANOVA test was conducted on the JRC results from the numerical characterisation technique (Table 6.5), using a MINITAB computer procedure (AOVONEWAY; Ryan *et al.*, 1982) which accepts unequal sample sizes. The resultant ANOVA table is reproduced in Table 6.6 . Since the obtained F ratio (28.05) exceeds the tabulated F value (2.37; Quinn, 1974) for the appropriate degrees of freedom (5,61) at $\alpha = 0.05$, the null hypothesis of no differences is rejected, concluding that significant evidence exists that there is some difference between the six means.

TABLE 6.5 JRC estimates by lithology.

JOINT	BG	SG	OQ	AD	SS	SM
1	14.0	10.7	10.4	9.0	7.0	5.4
2	14.4	10.4	11.0	4.6	5.1	4.3
3	13.4	9.3	9.9	10.0	8.9	9.8
4	15.2	11.0	13.1	7.8	6.8	7.4
5	15.2	13.3	9.4	5.9	6.6	3.3
6	14.1	11.8	7.3	8.4	5.7	7.3
7	12.8	14.3	5.4	7.8	7.4	6.2
8	13.4	12.3	8.5	5.7	4.3	7.3
9	12.4	11.0	6.4	8.3	8.6	6.9
10	10.8	13.8	5.1		7.5	3.3
11			7.1			
12			7.9			
13			8.2			
14			9.1			
15			6.9			
16			7.2			
17			7.4			
18			5.4			

TABLE 6.6 ANOVA table for JRC by lithology.

ANALYSIS OF VARIANCE

SOURCE	DF	SS	MS	F
FACTOR	5	452.73	90.55	28.05
ERROR	61	196.88	3.23	
TOTAL	66	649.62		

LEVEL	N	MEAN	STDEV
BG	10	13.57	1.34
SG	10	11.79	1.61
OQ	18	8.09	2.11
AD	9	7.50	1.74
SS	10	6.79	1.45
SM	10	6.12	2.06

POOLED STDEV = 1.80

INDIVIDUAL 95 PCT CI'S FOR MEAN
BASED ON POOLED STDEV

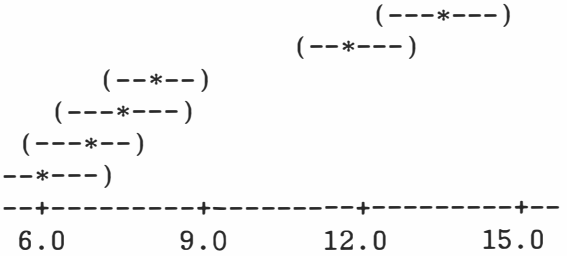

When two or more means are compared an ANOVA F test concludes whether the means are significantly different from each other, but it does not decide which means differ from other means. Multiple comparison methods produce more detailed information about differences among means. However, if many comparisons are made using the same alpha level to judge significance, the probability of making a Type 1 error (incorrectly rejecting an equal means hypothesis) is much higher than the alpha level, simply because there are more chances to make the error. As the number of means compared increases, the chances of making at least one Type 1 error approaches 1. Statistical methods for making multiple inferences while controlling the probability of making at least one Type 1 error are called simultaneous inference methods. The Tukey method is a moderately powerful test designed for pairwise comparisons based on a studentised range, that controls the Type 1 error rate when the sample sizes are equal. The Tukey-Kramer method is a modification for unequal sample sizes. A Tukey-Kramer test was carried out on the data in Table 6.5 using a SAS computer procedure (GLM, TUKEY; SAS Institute Inc., 1982). The results are shown in Table 6.7

Interpretation of the Tukey-Kramer test is straightforward. At the $\alpha = 0.05$ level the two granites (BG,SG) have JRC means which are significantly different from those of the other lithologies (OQ,AD,SS,SM). However, the mean JRC values of the two granites are not significantly different from each other, and neither are the mean JRC values of the other lithologies different from each other. This is not to say that the mean JRC values of the granite and the gneissic granite are the same, or that the quartz arenite, dolerite, schist, and marble have equal JRC means. Rather, characteristic JRC values for the individual granites or for the remaining lithologies can not

be isolated using the relatively small sample sizes involved.

TABLE 6.7 Tukey-Kramer test for JRC by lithology.

GENERAL LINEAR MODELS PROCEDURE

CLASS LEVEL INFORMATION

CLASS	LEVELS	VALUES
ROCK	6	AD BG OQ SG SM SS

NUMBER OF OBSERVATIONS IN DATA SET = 67

TUKEY'S STUDENTIZED RANGE (HSD) TEST FOR VARIABLE: JRC
NOTE: THIS TEST CONTROLS THE TYPE I ERROR RATE

ALPHA=.05 CONFIDENCE=0.95 DF=61 MSE=3.23
CRITICAL VALUE OF STUDENTIZED RANGE=4.16

COMPARISONS SIGNIFICANT AT THE .05 LEVEL ARE INDICATED BY '***'

ROCK COMPARISON	SIMULTANEOUS LOWER CONFIDENCE LIMIT	DIFFERENCE BETWEEN MEANS	SIMULTANEOUS UPPER CONFIDENCE LIMIT	
BG - SG	-0.58	1.78	4.14	
BG - OQ	3.39	5.48	7.56	***
BG - AD	3.64	6.07	8.50	***
BG - SS	4.41	6.78	9.14	***
BG - SM	5.09	7.45	9.81	***
SG - OQ	1.61	3.70	5.78	***
SG - AD	1.86	4.29	6.72	***
SG - SS	2.64	5.00	7.36	***
SG - SM	3.31	5.67	8.03	***
OQ - AD	-1.56	0.59	2.75	
OQ - SS	-0.78	1.30	3.39	
OQ - SM	-0.11	1.97	4.06	
AD - SS	-1.72	0.71	3.14	
AD - SM	-1.05	1.38	3.81	
SS - SM	-1.69	0.67	3.03	

One point which could be made is that the increase in mean JRC value between the dolerite and the granites is paralleled by an increase in overall grain size from the fine grained dolerite to the

coarser grained granites. It would be interesting to determine mean JRC values for a group of rocks forming a plutonic and hyperbyssal intrusive sequence, resulting in a progressive decrease in grain size. With larger sample sizes, perhaps significantly characteristic JRC values could be isolated from each rock type, and the contribution of grain size to joint roughness be estimated.

CHAPTER SEVEN

TIME SERIES ANALYSIS OF JOINT PROFILES

CHAPTER 7: TIME SERIES ANALYSIS OF JOINT PROFILES

7.1 Introduction

Data arranged along a continuum of time or space are referred to as a series or sequence. A time series is a function of time (or space) which exhibits random properties - a stochastic process. Time series analysis, therefore, involves techniques for the examination of data exhibiting a single positional characteristic. One possible approach to characterising the surface roughness of joint profiles is to consider the profile as a result of a stochastic process, that is, a time series, and to analyse it statistically (Wu and Ali, 1978; Krahn and Morgenstern, 1979; Dight and Chiu, 1981). Two statistical functions used to describe the properties of random data are the autocorrelation function and the spectral density function.

7.2 Autocorrelation Function

We could observe if a series of observations was cyclic or periodic if we could compare the series with itself at successive positions, locating the maximum correspondence, and measuring the degree of similarity or dissimilarity, between corresponding segments. This is achieved using the autocorrelation function (ACF), essentially the linear correlation between a time series and the same series at a later interval of time or space. The amount of offset between the two series being compared is known as the lag. A series of data may consist of three parts - a linear trend or drift in the mean value of the data; various periodic or cyclic components (signals); and superimposed random components (noise). The main use of the ACF is to detect an underlying periodic signal which may be masked in a seemingly random profile (Davis, 1973).

The ACF (Bendat and Piersol, 1971) describes the general dependence of data values at one position on the values at another position. For the profile function h(x) (Figure 7.1), an estimate of the autocorrelation between the values of h(x) at distances x and x+R can be obtained by taking the product of the two variables and averaging over the profile length, N. The resulting average product will produce an exact autocorrelation function as N tends to infinity. In equation form the ACF is defined as,

$$ACF(R) = \frac{1}{N} \int_0^N h(x)\, h(x+R)\, dx \qquad (7.1)$$

where h(x) is the amplitude of the asperity height at the distance, x, along the length, N, and R is a constant distance lag.

For discrete data, the autocorrelation function is calculated (Dight and Chiu , 1981) as the autocovariance at lag R divided by the autocovariance at lag zero. Autocovariance is computed by,

$$A_R = \frac{\sum_{i=1}^{N-R} Y_i\, Y_{i+R}}{N - R} \qquad (7.2)$$

for R = 0,1,2,...,L where L is the maximum lag number.

That is,

$$ACF(R) = \frac{A_R}{A_0}$$

$$= \frac{\sum_{i=1}^{N-R} Y_i\, Y_{i+R}}{\sum_{i=1}^{N-R} Y_i^{\,2}} \qquad (7.3)$$

for R = 0,1,2,...,L

This computation places certain requirements on the data used,

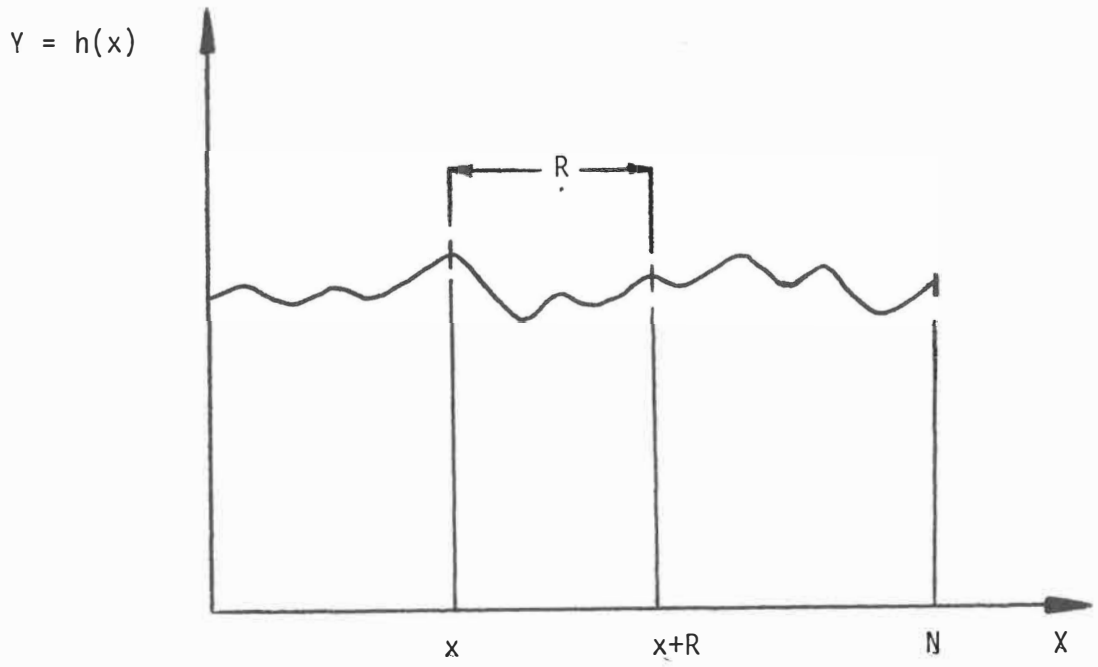

FIGURE 7.1 Idealised joint profile.

(1) the data must be equally spaced;

(2) the data must fluctuate about a constant mean;

and (3) any trend present in the original data must have been removed.

By plotting the autocorrelation function versus the lag we obtain a diagram known as an autocorrelogram. A typical autocorrelogram will fall from a maximum correlation of +1.0 at zero lag, to possibly negative values. At lags corresponding to positions of near coincidence of profile elements, the autocorrelogram will show peaks of high autocorrelation. Thus, examination of the autocorrelogram will reveal lags, or intervals of distance, at which the profile has a repetitive nature. An autocorrelogram which diminishes to zero autocorrelation with increasing lag reflects a lack of regular wave or signal within random background (Davis, 1973; Krahn and Morgenstern, 1979).

With regard to the parameters used, N should exceed 50, while L, the maximum lag, should intuitively, not exceed N/2. Some authors suggest more conservative limits on L, such as N/4 or even N/10 (Bendat and Piersol, 1971; Davis, 1973). These restrictions reflect the fact that as the lag increases, the autocorrelation is based on progressively fewer data points, thereby increasing the variance of the autocorrelation function. Also, as the lag becomes larger, the underlying assumption that the autocorrelation is a sample from an infinitely long time series becomes invalid. Therefore little confidence can be placed in high autocorrelations at large lag intervals, unless the profile is itself many times larger. Difficulties can arise, then, in analysing short roughness profiles if long wavelength periodic components occur in the joint (Davis, 1973; Dight and Chiu, 1981).

7.3 Spectral Density Function

The spectral density function (SDF) is the Fourier transform of the autocorrelation function. It yields information similar to the autocorrelation function, but with respect to frequency rather than distance. The spectral density function is used to determine the frequency of any periodic components that may exist in the roughness profile. This will occur if the spectral density is a maximum for a given frequency.

The spectral density function (Bendat and Piersol, 1971) is defined as,

$$SDF(f) = 2 \int_{-\infty}^{\infty} ACF(R) \exp[-j2\pi fR] \, dR \qquad (7.4)$$

This equation can be approximated by the determination of raw spectral estimates, T_R,

$$T_R = 2d \left(A_0 + 2 \sum_{r=1}^{L-1} A_r \cos\frac{rR\pi}{L} + A_L \cos R\pi \right) \qquad (7.5)$$

for R = 0,1,2,...,L

where A_r is the estimate of the autocorrelation at lag r, L is the maximum lag number, and d is the distance interval between sample points.

Because the variability of the raw spectral estimates does not improve with increased sample size, the raw estimates must be "smoothed" to obtain a better approximation of the true spectral density (Dight and Chiu, 1981). This is achieved by applying a Hanning filter (Bendat and Piersol, 1971). The refined spectral estimates are calculated as,

$$G_0 = 0.5T_0 + 0.5T_1 \tag{7.6}$$

$$G_R = 0.25T_{R-1} + 0.5T_R + 0.25T_{R+1} \tag{7.7}$$

$$G_L = 0.5T_{L-1} + 0.5T_L \tag{7.8}$$

for R = 1,2,3,...,L-1

The frequency is computed by,

$$f = \frac{R\ f_c}{L} \tag{7.9}$$

for R = 0,1,2,...,L

where f_c is the cutoff frequency or Nyquist frequency, and is equal to 1/2d, d being the sampling interval. Definition of the frequency of a periodic component in the data requires a minimum of two samples points per cycle. Therefore, the highest frequency which can be defined by sampling at a rate of one sample per distance d, is 1/2d cycles per distance units (Bendat and Piersol, 1971). The spectral density function is computed over the frequency range,

$$0 \leqslant f \leqslant f_c$$

A plot of spectral density versus frequency is termed a power spectrum. A peak in spectral density at a specific frequency reflects periodic undulations, which have a predominant wavelength equal to the reciprocal of the frequency.

7.4 Analysis and Interpretation

7.4.1 Summary of experimental results

125 joint surface profiles from 6 Antarctic lithologies (Section A2.4) were digitised on a Summagraphics digitising table (Model ID2-CTR-3648) at 0.1 mm spacings. Each profile was then interpolated to a linear spacing of 0.5 mm. The length of the profiles was 300 mm, producing a sample size, N, of 600. Autocorrelations and spectral densities were determined for each profile using the computer program STAT (A1.1.6), which is based on the theory discussed in the previous sections. The resultant autocorrelograms and power spectra are presented in Section A3.1 . The distribution of profiles used, with respect to rock type and JRC range, is shown in Table 7.1 . Note that spectral densities were normalised as a percentage of the total energy of the spectra (which was recorded), and plotted on a logarithmic scale. Dominant lags and frequencies were isolated from the autocorrelograms and power spectra in order to determine the presence of regular wavelengths greater than 10 mm. The results of the analysis are tabulated in Table 7.2 .

The frequency interval used by program STAT, for the profiles analysed, was 0.033 cm^{-1}. At the low end of the frequency range the difference between adjacent frequency intervals produces a large difference in corresponding wavelength. That is, the resolution of wavelengths is less at low frequencies. The relevant autocorrelograms are used to determine the larger wavelengths (although they do not easily reflect the smaller wavelengths). For instance, the 0.067 cm^{-1} frequency corresponds to a wavelength of 150 mm. The frequency intervals on either side, 0.033 cm^{-1} and 0.100 cm^{-1}, reflect wavelengths of 300 mm (the length of the profile) and 100 mm,

respectively. Thus, the 0.067 cm^{-1} frequency actually reflects a range of wavelengths between 100-150 mm. The autocorrelograms demonstrate this variation, which is tabulated in Table 7.3 .

TABLE 7.1 Distribution of profiles analysed.

JRC	Quartz arenite OQ	Dolerite AD	Granite BG	Gneissic granite SG	Schist SS	Marble SM	ALL
2-4	9a	2a,2b,8a	-	-	-	2b,2c,5a 5b,5c,10b	10
4-6	7a,7b,10a 10b,10c 11b,16a	1c,9b	-	-	2a,2b,2c 4a,4b,5b 6b,10c	7a,9b	19
6-8	1a,7c,8b 9b,11c 12b,13a 14a,15a 15b,15c 16b	6a,7a,7b 8b,8c	-	-	3b,5c,6a 7b,7c,9c 10b	2a,4c,7b 7c,8b,8c 9a,9c	32
8-10	2b,3a,3b 5c,6a,8a 8c,12a 13b,13c 14c	2c,6b,7c	-	1b,3b,3c	1b,1c,3a 3c,4c,7a 9b,10a	4b,8a	27
10-12	1b,2a,2c 3c,4b,14b	-	6a,8a,9c	1a,4b,4c 6b,9a,9b	9a	-	16
12-14	1c,4c	-	7a,7b,8c 9b	1c,5b,5c 6a,7b,8c 10b	-	-	13
14-16	4a	-	2a,2b,2c 6b	5a,7c,10c	-	-	8
ALL	40	13	11	19	24	18	125

TABLE 7.2 Dominant wavelengths representing periodic undulations.

Wavelength (mm)	Profiles displaying the wavelength
150	$OQ^{1a,1c,2a,2b,3b,3c,4b,4c,5c,6a,7b,9a,10a,10c,11b,11c,12a}$ $OQ^{13a,13b,13c,14a,14b,14c,15b,15c,16a,16b}$ $AD^{2a,2c,6a,6b,7c,8b,8c,9b}$ $BG^{2a,2b,2c,6b,8a,9b}$ $SG^{1a,1c,3b,3c,4b,4c,5a,6a,7c,8c,9a,9b}$ $SS^{1b,1c,2a,2b,2c,5b,5c,7a,7b,10a}$ $SM^{2b,4b,5a,7a,7b,7c,8c}$
100	OQ^{12b} SG^{6b} SS^{3b}
75	$OQ^{9b,10b}$ $SS^{6a,10c}$ $SM^{7a,9b}$
60	OQ^{13a} SS^{7a}
50	OQ^{9a} BG^{8c} SG^{3b} $SS^{3a,5c,6b}$
43	$OQ^{11c,14a,15c}$ $AD^{2b,8b}$ $SS^{1b,2a,9a}$
37	$OQ^{5c,7a,8c,10b,15b}$ $AD^{2c,7b}$ SG^{6b} SS^{4a} $SM^{2c,9a}$
33	$OQ^{7b,8b}$ AD^{7c} $SS^{3b,6a,7c}$
30	$OQ^{1c,3b,7c,10c}$ $AD^{1c,2a}$ BG^{9b} SG^{8c} $SM^{2b,5b}$
27	$OQ^{8c,9b,10a,11b}$ $AD^{7b,8a}$ $SG^{3b,3c,4b,7b,10b}$ $SS^{2a,2c,5b,9b,10c}$
25	$OQ^{10b,13b,13c,14a,15a,15b,16b}$ $AD^{2c,7a,8b}$ $BG^{6b,8c}$ SM^{5a}
23	$OQ^{7a,12a,14b}$ $SS^{3c,4c}$ SM^{7a}
21	$OQ^{1a,1c,6a}$ $AD^{2b,9b}$ $BG^{2c,7b,8a}$ $SG^{5a,7c,8c,9b}$ $SS^{2b,10a}$ $SM^{8a,9c}$
20	$OQ^{4a,4b,13a,15c}$ AD^{6a} $SG^{4c,9a,10c}$ $SS^{6a,7a}$ $SM^{2a,2b,5c,10b}$
19	$OQ^{2a,4c,11c}$ BG^{9b} $SS^{2c,3a}$ SM^{7b}
18	$OQ^{3b,3c,5c,12b,13b}$ $AD^{1c,7a,7c,8c}$ SG^{1a} $SS^{1b,2a,4a,7c,10b}$ $SM^{4b,7c,9b}$
17	$OQ^{3a,9a,11b,13c,14b,14c}$ $AD^{2a,8a}$ $SG^{5c,6a}$ $SS^{7b,9c}$
16	$OQ^{6a,13a}$ $AD^{7b,9b}$ BG^{8a} SG^{7c} $SS^{4b,10c}$ $SM^{2b,5a}$
15	$OQ^{1c,2c,7c,8a,11c,16a}$ AD^{6b} BG^{9b} $SG^{3c,9b,10c}$ $SM^{8c,10b}$
14	$OQ^{4a,8b,9b,12a}$ AD2c,8b,8c $BG^{2b,6b}$ $SG^{1c,3b}$ $SS^{1c,4c,5c,9b}$ $SM^{2c,4c,7b,9c}$
13	$OQ^{1b,2b,6a,8c,9a,10a,14a,15b,16b}$ $AD^{2b,6a}$ $BG^{2c,8a,8c,9c}$ $SG^{1b,4c,5a,5b,6a,7c,8c}$ $SS^{2b,5b,7b,7c,10b,10c}$ $SM^{4b,7c}$
12	$OQ^{1a,3a,4c,5c,7a,7b,9b,11b,13a,15a,15c}$ $AD^{1c,2a,6b,9b}$ $BG^{2a,6a,7a}$ $SG^{3c,4b,6b}$ $SS^{2a,3a,3b,3c,4b,6a,7a,7b,9a,10a}$ $SM^{2b,5a,5b,7a,8b,10b}$
11	$OQ^{1b,2a,7c,8b,10a,12b,16a}$ $SG^{1a,1b,1c,3b,8c,9b}$ $SS^{2b,4a,9b,9c}$ $SM^{4b,8a,9b}$

Representative autocorrelograms, power spectra, and their associated joint profiles, are shown in Figures 7.2 and 7.3 . Figure 7.2(a) demonstrates a typical autocorrelogram for a profile lacking large wavelength components. In contrast, Figure 7.2(b) shows the power spectrum of a profile displaying a dominant frequency at 0.067 cm^{-1}, which corresponds to a wavelength of 150 mm. Note how the autocorrelogram reflects a more precise estimate at 130 mm. Figure 7.2(c) shows the behaviour of a profile with a wavelength of 50 mm.

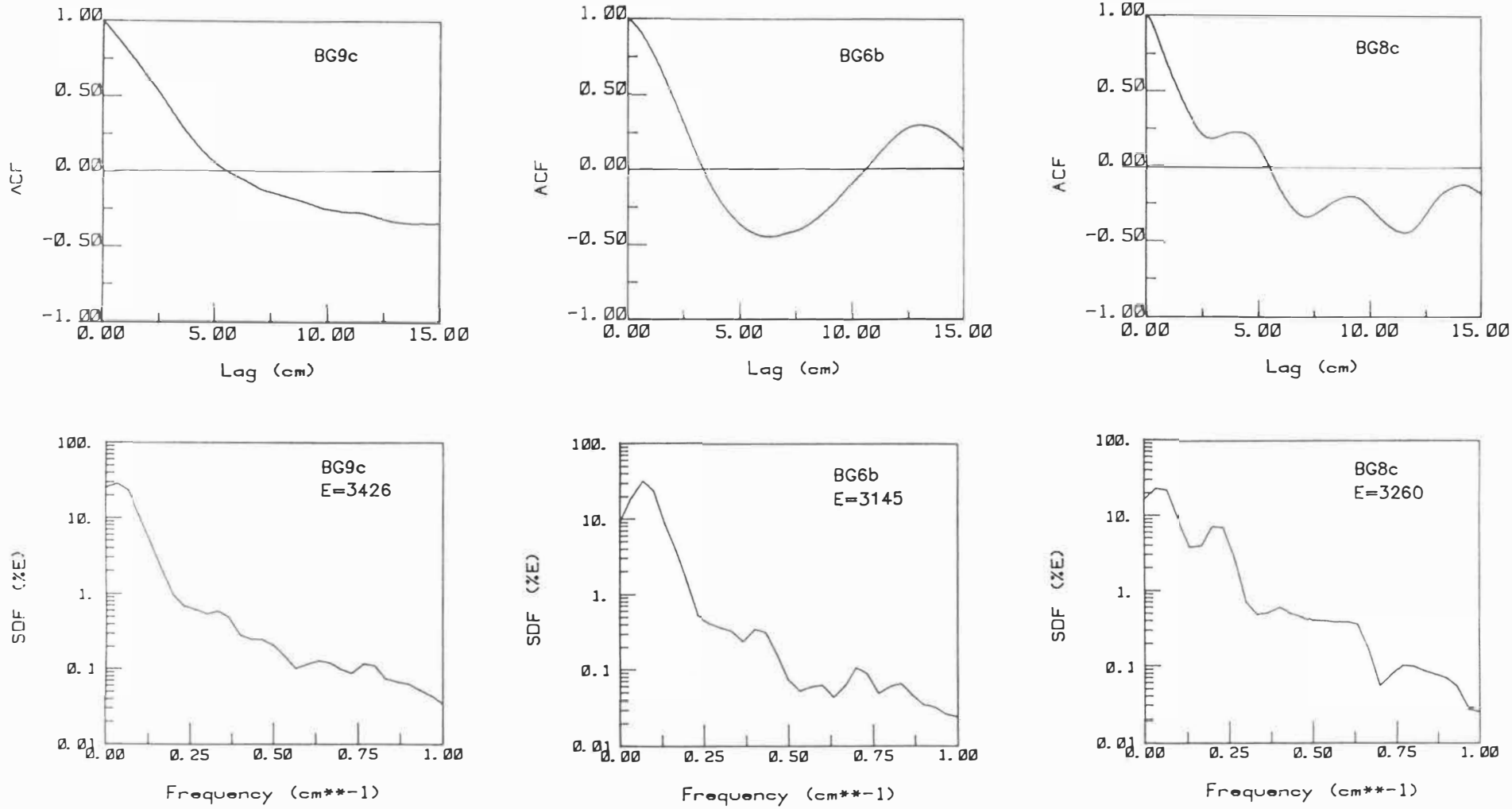

FIGURE 7.2 Typical autocorrelograms and associated power spectra

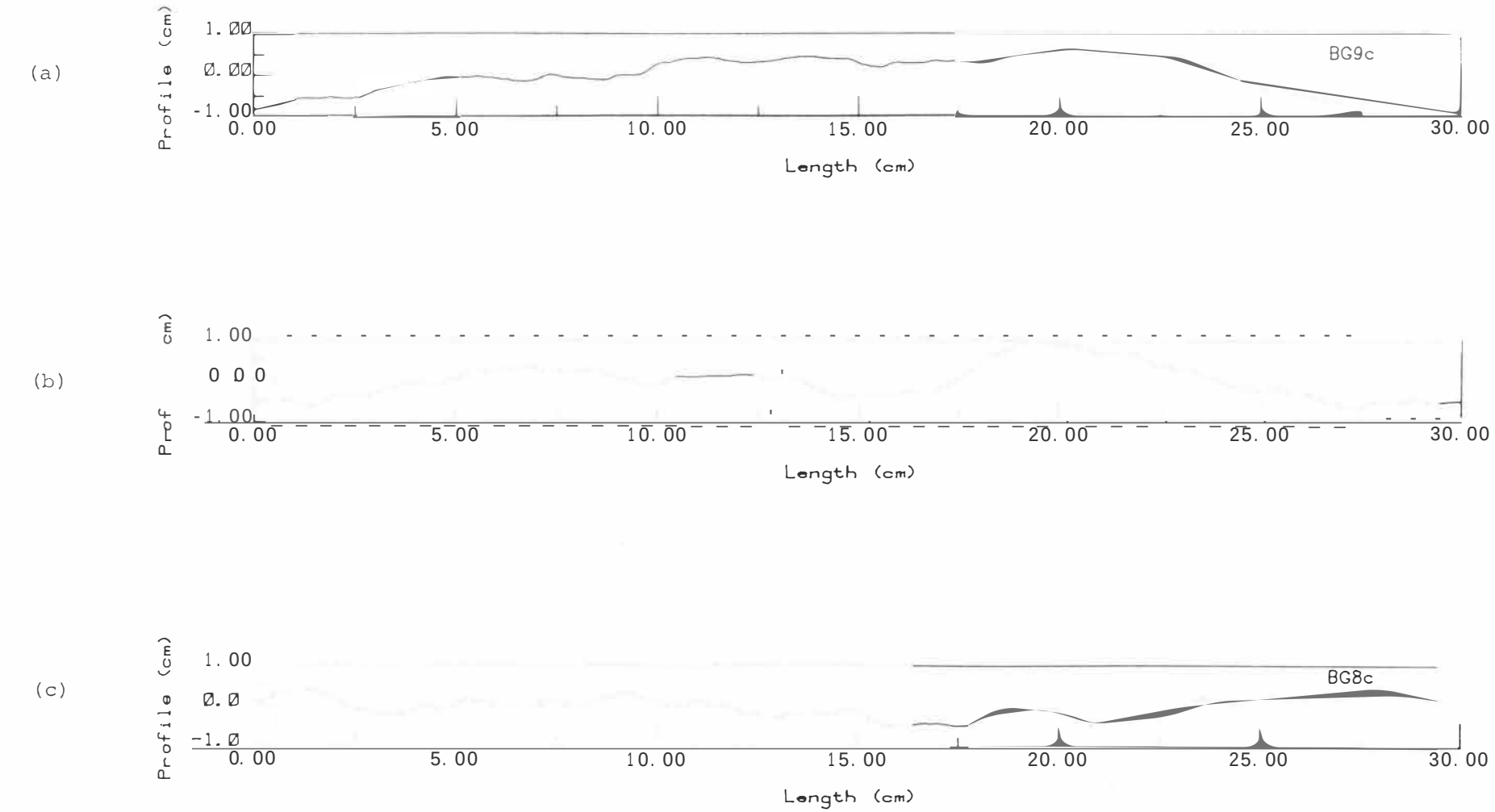

FIGURE 7.3 Representative joint surface profiles.

TABLE 7.3 Distribution of wavelengths interpreted for the 150 mm peak.

Wavelength (mm)	Profiles displaying the wavelength
150	$OQ^{1c,2a,3c,7b,9a,13a,13b,13c,14a,14b,15b,15c,16a}$ $AD^{2a,7c,8b,9b}$ BG^{2a} $SG^{1a,1c,3b,3c,8c}$ $SS^{1c,2c,10a}$ $SM^{4b,7b,7c,8c}$
140	$OQ^{2b,3b,11b,11c,16b}$ AD^{6b} BG^{8a} SS^{2b} SM^{7a}
130	$OQ^{4b,6a,10c,14c}$ $AD^{2c,6a}$ $BG^{2b,6b}$ $SG^{4b,4c,6a}$ $SS^{1b,5b,5c,7a,7b}$ SM^{5a}
120	$OQ^{4c,10a,12a}$ AD^{8c} $BG^{2c.9b}$ SG^{7c} SM^{2b}
110	$OQ^{1a,5c}$ $SG^{5a,9a,9b}$ SS^{2a}

The maximum lag, L, used in program STAT was N/2, which for the 125 profiles studied equals 300 (150 mm). The number of degrees of freedom, N/L, was therefore 2. However, it is generally recognised (e.g. Dight and Chiu, 1981) that the number of degrees of freedom should be at least 20 for statistical independence. This implies that while analysis of the profiles shows the existence of a periodic roughness in some cases, the statistical inferences can not necessarily be relied on, because of the reduced number of degrees of freedom. To overcome this problem, individual spectra from the same rock type and JRC range were combined and normalised to form a cumulative spectrum, with an increased number of degrees of freedom. Since all the profiles analysed were 300 mm in length, the frequency interval generated by computer program STAT for production of the power spectra was a constant 0.033 cm^{-1}. As a result, energies for each individual frequency (spaced 0.033 cm^{-1} apart) from a number of spectra, could be added together and renormalised using computer program NORM (A1.1.8) to produce a cumulative spectrum. Any peaks observed in such a spectrum have a much higher degree of statistical

significance. The corresponding wavelengths of the frequencies determined from these cumulative spectra (Section A3.2) are shown in Table 7.4 . In analysing power spectra with less than 10 degrees of freedom only major peaks were considered, but for spectra with more than 10 degrees of freedom all peaks were used, due to the "smoothing" effect of combining many individual spectra.

TABLE 7.4 Wavelengths obtained from analysis of cumulative spectra.

	Wavelengths (mm)	Degrees of freedom
Quartz arenite (OQ)		
JRC = 2-4	150, 50, 17, 13, 11	2
JRC = 4-6	150, 12	14
JRC = 6-8	150, 15, 11	24
JRC = 8-10	150	22
JRC = 10-12	150, 19, 12	12
JRC = 12-14	150, 21, 12	4
JRC = 14-16	20,14	2
Dolerite (AD)		
JRC = 2-4	150, 27, 17, 12	6
JRC = 4-6	17, 12	4
JRC = 6-8	150, 14	10
JRC = 8-10	150, 25, 15	6
Granite (BG)		
JRC = 10-12	21, 13	6
JRC = 12-14	20, 12	8
JRC = 14-16	150, 14	8
Gneissic granite (SG)		
JRC = 8-10	150, 27, 15, 13	6
JRC = 10-12	150, 12	12
JRC = 12-14	150, 23, 11	14
JRC = 14-16	150, 21, 16, 13	6
Schist (SS)		
JRC = 4-6	150, 27, 13	16
JRC = 6-8	150, 20, 14, 12	14
JRC = 8-10	21, 12	16
JRC = 10-12	43, 19, 12	2
Marble (SM)		
JRC = 2-4	27, 21, 16, 12	12
JRC = 4-6	150, 23, 18, 12	4
JRC = 6-8	14	16
JRC = 8-10	150, 23, 11	4

7.4.2 Modal analysis

By plotting the data contained in Table 7.2 as a histogram, the modal, most commonly occurring, wavelengths can be isolated. Figure 7.4 shows such an exercise where a differentiation on the basis of lithology is attempted. What becomes evident on examination of Figure 7.4 is that there are two major wavelength modes at opposite ends of the wavelength scale, 150 mm and 12 mm. In addition to these, there are a number of common frequencies (e.g. 25-27 mm, 20-21 mm, 17-18 mm, 14-15 mm) distributed amongst all the lithologies.

When the data are plotted so as to differentiate JRC ranges the picture becomes clearer. Figure 7.5 incorporates three roughness divisions:

(1) low roughness (JRC 2-6);

(2) moderate roughness (JRC 6-10);

(3) high roughness (JRC 10-16).

While all three roughness divisions show definite modes at 150 mm and around 12 mm, the subordinate modal frequencies begin to group separately. High roughness shows a mode at 21 mm, moderate roughness at 14, 18, and 25 mm, and low roughness at 27 and 16 mm.

Figure 7.6 shows a histogram approach to the wavelengths obtained from the cumulative power spectra which were grouped according to lithology and JRC range (Table 7.4). These results have a much higher degree of confidence associated with them, and consequently any modal wavelengths inferred from them can be relied on to a greater extent. Once again, the dominant modes occur at 150 and 12 mm. However, the subordinate modes both confirm the previous results and enhance the separation. The high roughness division shows a mode at 21 mm, the moderate roughness division at 14-15 mm, and the low roughness

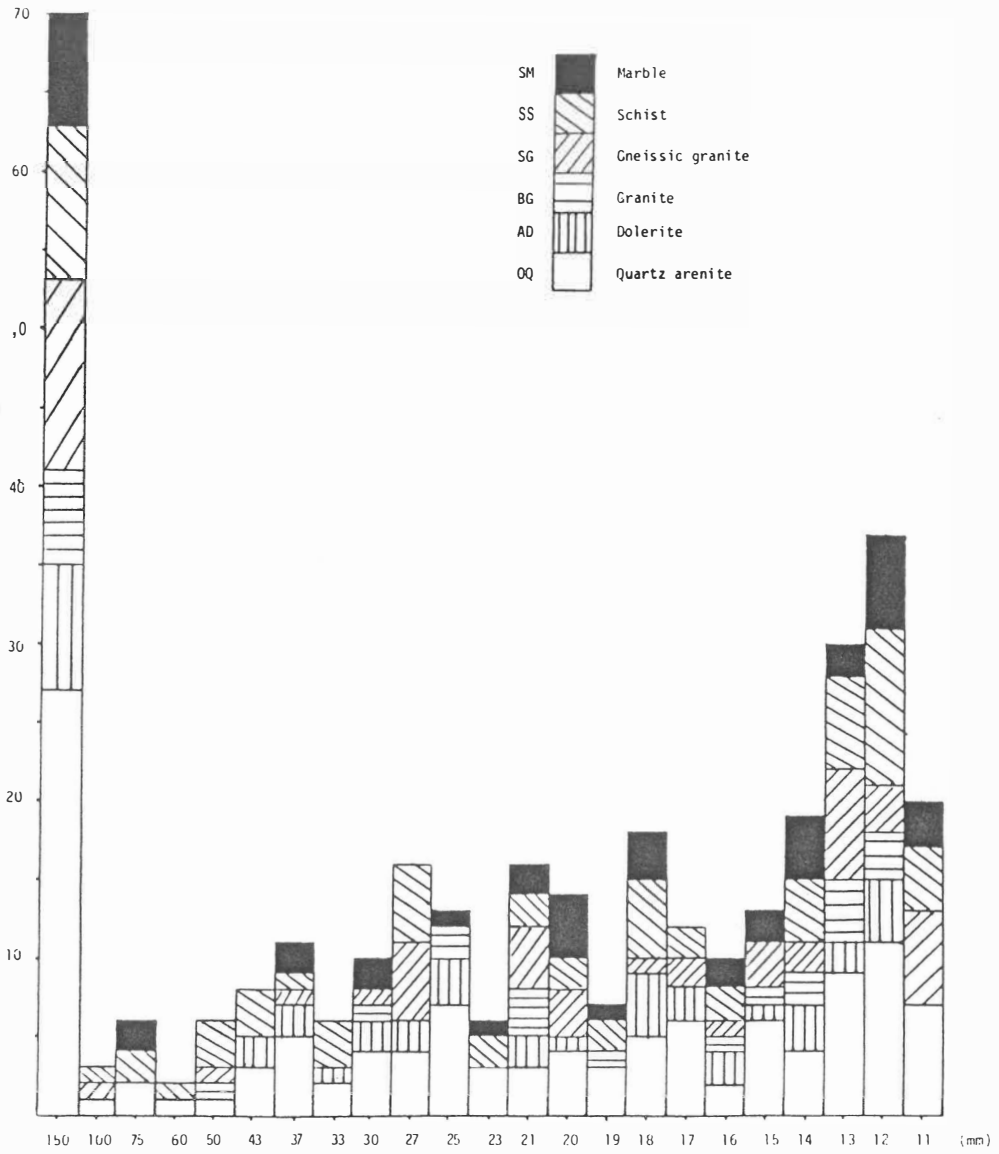

FIGURE 7.4 Wavelengths isolated from individual spectra; differentiated by lithology.

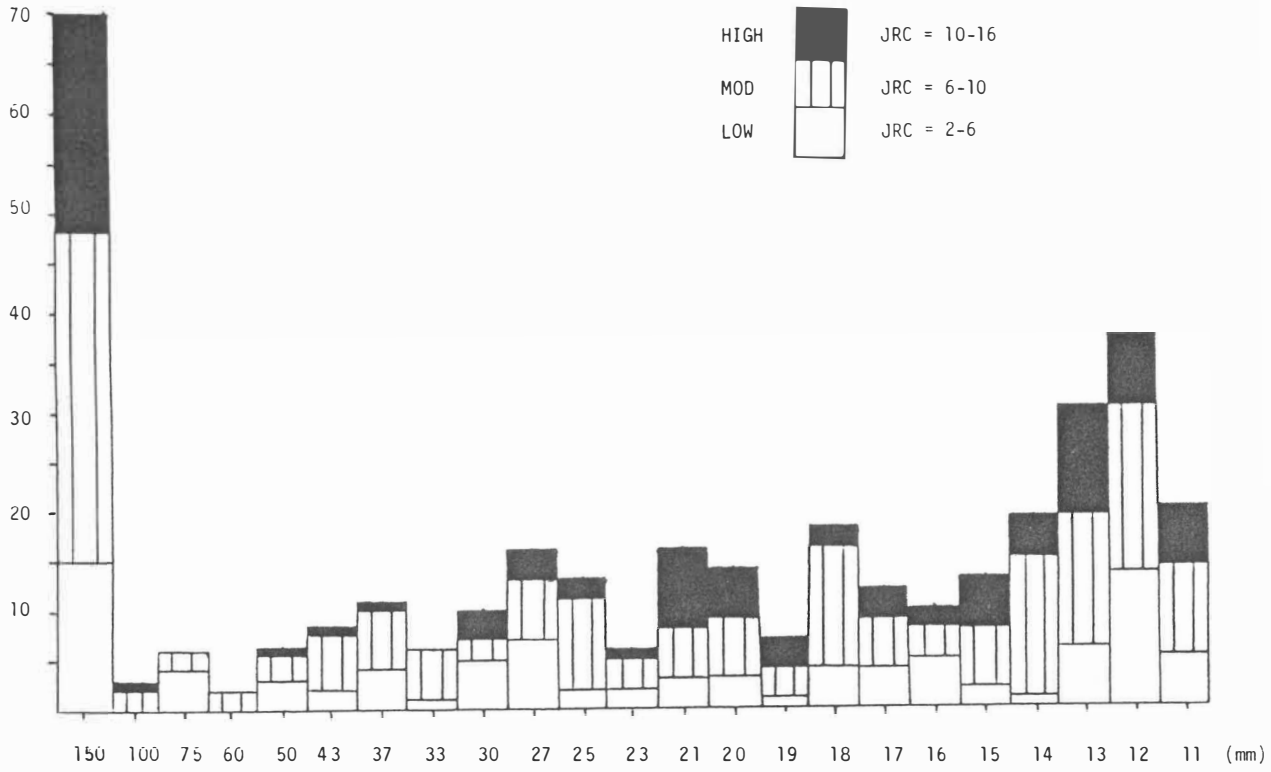

FIGURE 7.5 Wavelengths isolated from individual spectra; differentiation by JRC range.

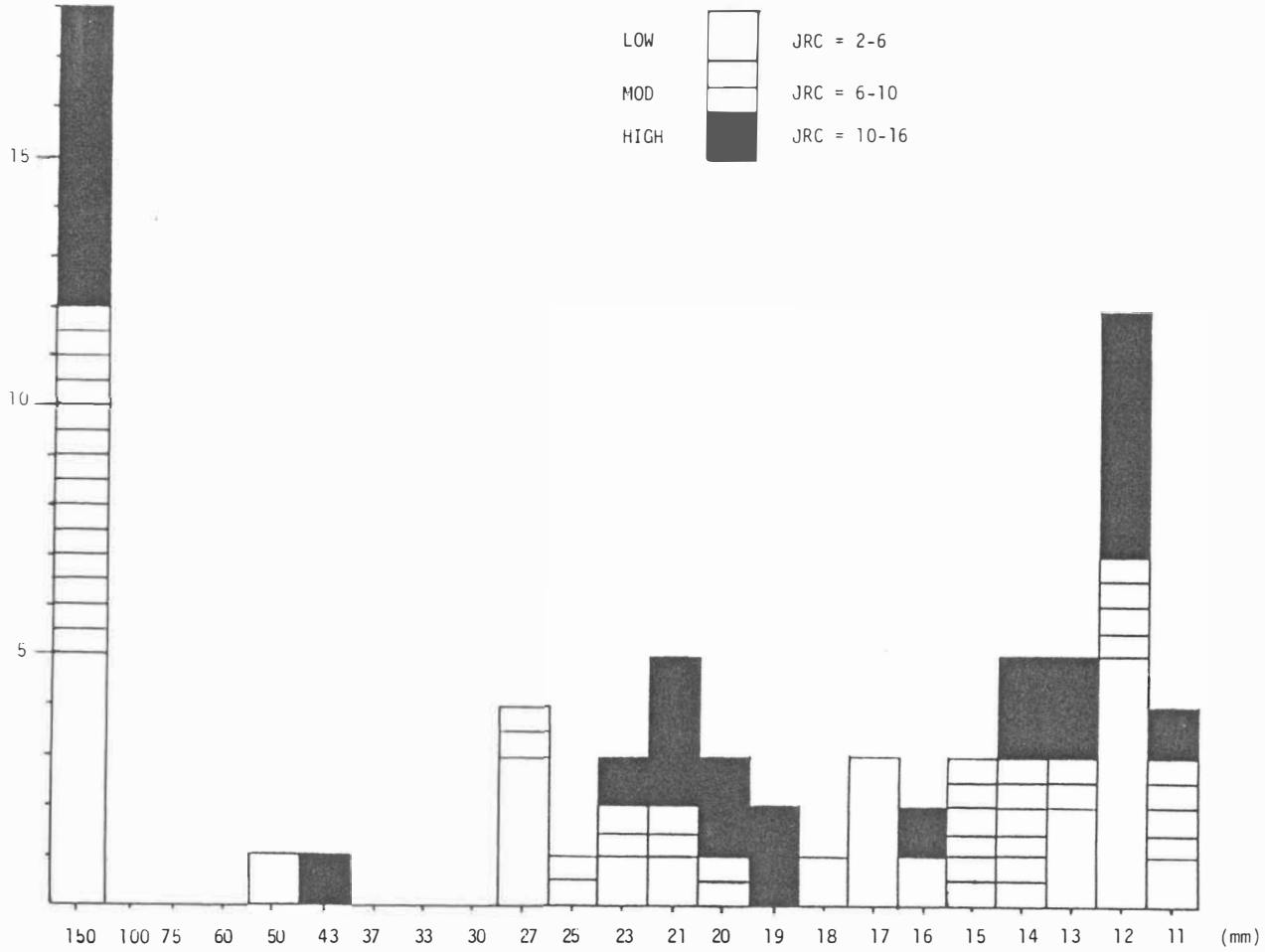

FIGURE 7.6 Wavelengths isolated from cumulative spectra; differentiation by JRC range.

division shows modes at 27 and 17 mm. Consideration of Table 7.3 suggests that the 150 mm mode represents a range of wavelengths from 110 to 150 mm, but most commonly 150 mm and 130 mm.

The amplitude of a particular waveform whose wavelength is represented as a peak on a power spectrum is proportional to the square root of the energy contained in the peak. For the power spectra produced in this study the low frequency, high wavelength, end of the spectrum was also the high energy end, so that the large wavelengths tend to be accompanied by larger amplitudes. In other words, joint surfaces from all six lithologies studied tend to show a dominant, high amplitude, periodic roughness with a wavelength of around 130 mm or 150 mm, upon which is superimposed a secondary, lower amplitude, roughness with a wavelength of around 12 mm. Joints of low surface roughness often contain an additional subordinate roughness of around 27 or 17 mm, while moderately rough joints tend to display roughnesses of 14-15 mm wavelengths, and joints of high roughness commonly display periodic roughness with a wavelength of 21 mm.

Obviously, further work is required to determine quantitatively the shape and amplitudes of the regular roughness waveforms. Unfortunately, such a study is beyond the scope of this thesis. Generally however, the results presented here optimistically lend support to the idea of replacing a joint surface profile with a regular geometric profile for use in the modelling of joint behaviour (Dight and Chiu, 1981).

CHAPTER EIGHT

CONCLUSIONS

CHAPTER 8: CONCLUSIONS

8.1 Characterisation of Six Rock Types From the McMurdo Sound Area

Six lithologies of an intrusive, metamorphic, and sedimentary nature, from the Taylor Valley, and the Asgard and Olympus Ranges, were used in this study:

(a) Beacon Heights Orthoquartzite, a quartz-sericite cemented quartz arenite of the Taylor Group;

(b) Ferrar Dolerite, a labradorite-augite-pigeonite dolerite of the Ferrar Group;

(c) Larsen Granodiorite, a hornblende-biotite granite of the Granite Harbour Intrusives;

(d) Olympus Granite-gneiss, another hornblende-biotite granite, with crude gneissic foliations and plagioclase augens, belonging to the Granite Harbour Intrusives;

(e) Schist, an unnamed biotite schist of the Koettlitz Group of metasediments;

(f) Salmon Marble, a crystalline forsterite-antigorite-phlogopite marble of the Koettlitz Group.

A summary of their geotechnical properties, determined in this study, is presented in Table 8.1 . Statistical tests suggest that characteristic mean JRC values for each individual rock type cannot be determined given the present low number of joints sampled. However, the coarser grained granites have mean JRC values which are significantly different from those of the other lithologies.

TABLE 8.1 Selected geotechnical properties of six Antarctic lithologies.

Lithology	γ (kN/m^3)	ϕ_b °	R	$I_{s(50)}$ (MPa)	σ_c (MPa)	JRC
Quartz arenite (Beacon Heights Orthoquartzite)	24.1	32.2	49	-	-	8.1
Dolerite (Ferrar Dolerite)	28.1	30.9	62	9.8	216	7.5
Granite (Larsen Granodiorite)	26.9	32.7	50	3.6	79	13.6
Gneissic granite (Olympus Granite-gneiss)	26.7	30.8	54	3.4	75	11.8
Schist (Koettlitz Group)	26.4	28.4	59	7.0	154	6.8
Marble (Salmon Marble)	28.0	30.6	58	5.3	117	6.1

γ = unit weight;
ϕ_b = basic friction angle;
R = Schmidt rebound hardness (Type N hammer);
$I_{s(50)}$ = point load strength index;
σ_c = compressive strength;
JRC = joint roughness coefficient;

8.2 Applicability of Field Tests Used to Determine the Roughness Coefficient of Natural Joints

Barton and Choubey (1977) recommend, in addition to comparison of joint profiles with standard profiles, the use of tilt and push/pull tests for the determination of JRC in the field. Applicability of these tests is limited. Generally tilt tests are effective for joints measuring JRC$\leq$8, while push or pull tests extend the range to JRC$\leq$12 . Statistical comparison and the subsequent analysis of the above three field orientated methods with numerically calculated JRC values yielded interesting results:

(a) The close agreement between mean measured JRC and mean predicted JRC from tilt and push/pull tests reported by Barton and Choubey (1977) is misleading. Differences between predicted and measured JRC for individual joint specimens are significantly larger than they suggest. Results from this study which produce comparable differences in mean and measured JRC values, exhibit error ranges of up to ±3.5 on an individual basis.

(b) Although results from this study confirm that the general relationships proposed by Barton and Choubey (1977) for tilt and pull tests do exist, the degree of correlation between predicted JRC values from tilt and pull tests and numerically measured JRC values is not always good. These index tests can not as accurately estimate JRC for a particular joint specimen as previously thought. Indeed, even their validity to do so is suspect.

(c) If the mean behaviour of joint types is of interest then tilt and push/pull tests might be used to estimate JRC provided that the number of joint specimens tested is large (a minimum of 10 specimens is suggested by Barton and Choubey, (1977)). If, however, individual joints are of interest, then visual profile comparison will be probably just as, if not more, accurate than tilt or push/pull tests. At least three profiles spaced across a joint surface are required to obtain a representative JRC estimate. If facilities, budget, and time allow it, the use of a shear box to back-calculate JRC, or a digitiser to numerically estimate JRC, is recommended for precise determination.

During the testing of the field methods of Barton and Choubey (1977) certain techniques for the estimation of component parameters were examined. In particular, the use of the Schmidt test hammer was

confirmed as a useful tool to estimate *in situ* the degree of weathering, and the joint compressive strength of a joint wall. A simple relationship was developed with the point load strength index for lithologies used in this study, allowing the quantitative estimation of compressive strength from Schmidt hammer rebound hardness for a Type N hammer.

In addition, the tilting of three rock cores, arranged as an elongated pyramid, provided a useful technique for estimating basic friction angle. The relatively simple equipment required, plus the general availability of cores in investigative projects, often makes it an attractive alternative to shear box determinations. The method recommended by Stimpson (1981) is modified in this study to correct inherent mathematical uncertainities present in the original proposal.

It was possible to expand the technique of numerically characterising surface profiles by digitisation, (and thereby numerically estimating JRC), developed by Tse and Cruden (1979), so as to encompass a wider range of data sampling intervals, thereby increasing its general applicability. Numerical characterisation provides a more accurate determination of JRC than the visual profile comparison method suggested by Barton and Choubey (1977), since the computer measures quantitatively what the eye estimates relatively. Numerical characterisation was used in this study as a laboratory standard against which to compare other techniques of JRC estimation.

8.3 Regularity in the Surface Roughness Profiles of Natural Joints

The autocorrelation function, and its Fourier transform, the spectral density function, are two powerful statistical tools in the analysis of joint profiles. They may be used to determine the frequency or wavelength of such periodic components that may exist in the roughness profile. Both functions are incorporated into the computer program STAT and were used in the analysis of 125 joint surface profiles collected from the six lithologies studied.

On the basis of the analysis conducted, the following generalisations can be made:

(a) A primary, high amplitude, regular wavelength can be isolated from the majority of joints analysed. This occurs somewhere between 100 and 150 mm. Although the size of this wavelength compared to the size of the profile sampled is large, both the regularity of its occurrence, and the variation in its actual value between individual profiles, suggest it exists in reality.

(b) Secondary, lower amplitude, wavelengths fall into five groupings, 25-27 mm, 20-21 mm, 16-18 mm, 14-15 mm, and 11-13 mm. By far the most commonly appearing secondary wavelength is that centred around 12 mm. Its occurrence is recorded in a majority of joint profiles from all of the six lithologies.

(c) The other, subordinate, secondary wavelengths are less evenly distributed amongst the six lithologies. Their occurrence appears to be dependent on the degree of roughness displayed by the joint. If the joint profiles are divided into low (JRC = 2-6), moderate (JRC = 6-10), and high (JRC = 10-16) roughness categories, the subordinate wavelengths separate out relatively clearly. Low roughness joints show a preference for

the 27 and 17 mm wavelengths, while high roughness joints most often show a 21 mm wavelength. Joints of moderate roughness tend to display subordinate secondary wavelengths of 14-15 mm.

While more information is required on the amplitudes and shapes of the periodic roughness undulations detected, these preliminary results suggest that it may indeed be possible to model joint surfaces with a regular geometric equivalent. It is convenient to suggest that the 150 mm wavelength observed corresponds to the 1st order roughness described by Patton (1966), the subordinate wavelengths reflecting 2nd or even 3rd order roughness. If this is so, joints of at least 300 mm length should be used to estimate JRC. More accurate definition of high amplitude wavelengths requires even longer joint profiles. This also implies that shear box testing using small joint samples could provide misleading data.

APPENDIX ONE

PROGRAMMING

APPENDIX 1: PROGRAMMING

A1.1 Computer Programs

Inevitably, when dealing with groups of numbers or the large quantity of points associated with a line or profile, the use of a computer's memory and calculating ability facilitates rapid and accurate manipulation. In this study a number of computer programs and routines were written by the author or borrowed. Almost all were written in FORTRAN computer language, (program DIGIT was written in PASCAL language), and all were used on the University of Waikato's VAX computer system. The programs used are listed in this appendix. Their application is discussed elsewhere.

Programs TILT, PULL, FILTER, and NORM were written solely by the author. Programs INTER, and STAT were written by the author with assistance (P.G. Scadden, pers. comm., 1984). Subroutine LEASTS was written by K.P. Black. Program TEST was written by the author with assistance (K.P. Black, pers. comm., 1985). Program DIGIT was written by Yeo Chun Cheng.

A1.1.1 TILT

```
      PROGRAM TILT
C     CALCULATES JRC FROM RESULTS OF FIELD TILT TESTS
C
      CHARACTER FNAME*10
      CHARACTER TNAME*8
      INTEGER CS, RJ
C
C     ************************************************************
C             VARIABLES USED
C     A     : TILT ANGLE (degrees)
C     BF    : BASIC FRICTION ANGLE (degrees)
C     CS    : JOINT WALL COMPRESSIVE STRENGTH (MPa)
C     FNAME : FILENAMES
C     H     : THICKNESS OF UPPER BLOCK (cm)
C     RC    : JOINT ROUGHNESS COEFFICIENT
C     RF    : RESIDUAL FRICTION ANGLE (degrees)
C     RJ    : SCHMIDT HARDNESS FOR JOINT SURFACE
C     RU    : SCHMIDT HARDNESS FOR UNWEATHERED ROCK
C     TNAME : INDIVIDUAL TEST NAMES
C     UW    : UNIT WEIGHT OF ROCK TYPE (kN/cubic m)
C     X     : TEMPORARY HOLDING VARIABLE
C     XS    : NORMAL STRESS INDUCED BY SELF WEIGHT OF UPPER BLOCK
C     ************************************************************
C
C     GET THE FILENAMES FOR THE INPUT AND OUTPUT DATA
C     THEN OPEN THOSE FILES
C
100   TYPE*,' ENTER OUTPUT FILENAME'
      ACCEPT 120, FNAME
      OPEN(UNIT=2, NAME=FNAME, TYPE='NEW', ERR=100)
110   TYPE*,' ENTER INPUT FILENAME'
      ACCEPT 120, FNAME
      OPEN(UNIT=1, NAME=FNAME, TYPE='OLD', ERR=110, READONLY)
120   FORMAT(A)
      TYPE*,' ENTER UNWEATHERED ROCK SCHMIDT HARDNESS (use decimal point)'
      ACCEPT*, RU
      TYPE*,' ENTER BASIC FRICTION ANGLE'
      ACCEPT*, BF
      TYPE*,' ENTER UNIT WEIGHT (kN/cubic m)'
      ACCEPT*, UW
C
C     CALCULATE JOINT ROUGHNESS COEFFICIENT
C
      WRITE(2,130)
130   FORMAT('  RESIDUAL FRICTION ANGLE (deg), JCS (MPa), JRC')
150   READ(1,155,END=200) TNAME, H, A, RJ
155   FORMAT(A8,2F8.1,I8)
      RF=(BF-20)+20*(RJ/RU)
      X=0.0271*RJ+0.548
      CS=(1.0*10**X)
      XS=UW*(H/100)*COSD(A)*COSD(A)/1000
      RC=(A-RF)/ALOG10(CS/XS)
      WRITE(2,180) TNAME, RF, CS, RC
180   FORMAT(A8,F8.1,I8,F8.1)
      GOTO 150
C
```

```
C       CLOSE OFF FILES
C
200     CLOSE(UNIT=2)
        CLOSE(UNIT=1)
        END
```

A1.1.2 PULL

```
      PROGRAM PULL
C     CALCULATES JRC FROM RESULTS OF FIELD PULL TESTS
C
      CHARACTER FNAME*10
      CHARACTER TNAME*8
      INTEGER A, CS, RJ
C
C     ************************************************************
C               VARIABLES USED
C     A     : AREA OF JOINT SURFACE (entered in sq cm)
C     BF    : BASIC FRICTION ANGLE (degrees)
C     CS    : JOINT WALL COMPRESSIVE STRENGTH (MPa)
C     FNAME : FILENAMES
C     N     : NORMAL COMPONENT OF THE UPPER BLOCK WEIGHT
C     RC    : JOINT ROUGHNESS COEFFICIENT
C     RF    : RESIDUAL FRICTION ANGLE (degrees)
C     RJ    : SCHMIDT HARDNESS FOR JOINT SURFACE
C     RU    : SCHMIDT HARDNESS FOR UNWEATHERED ROCK
C     S     : SLOPE ANGLE RELATIVE TO THE HORIZONTAL (degrees)
C     T1    : TANGENTIAL COMPONENT OF THE UPPER BLOCK WEIGHT
C     T2    : APPLIED PULLING FORCE (entered in kg)
C               (A NEGATIVE SIGN INDICATES T2 WAS APPLIED UPWARDS)
C     TNAME : INDIVIDUAL TEST NAMES
C     W     : WEIGHT OF THE UPPER BLOCK (kg)
C     X1-X5 : TEMPORARY HOLDING VARIABLES
C     ************************************************************
C
C     GET THE FILENAMES FOR THE INPUT AND OUTPUT DATA
C     THEN OPEN THOSE FILES
C
100   TYPE*,' ENTER OUTPUT FILENAME'
      ACCEPT 120, FNAME
      OPEN(UNIT=2, NAME=FNAME, TYPE='NEW', ERR=100)
110   TYPE*,' ENTER INPUT FILENAME'
      ACCEPT 120, FNAME
      OPEN(UNIT=1, NAME=FNAME, TYPE='OLD', ERR=110, READONLY)
120   FORMAT(A)
      TYPE*,' ENTER UNWEATHERED ROCK SCHMIDT HARDNESS (use decimal point)'
      ACCEPT*, RU
      TYPE*,' ENTER BASIC FRICTION ANGLE'
      ACCEPT*, BF
C
C     CALCULATE JOINT ROUGHNESS COEFFICIENT
C
      WRITE(2,130)
130   FORMAT('  RESIDUAL FRICTION ANGLE (deg), JCS (MPa), JRC')
150   READ(1,155,END=200) TNAME, A, S, W, T2, RJ
155   FORMAT(A8,I8,3F8.1,I8)
      RF=(BF-20)+20*(RJ/RU)
      T1=W*SIND(S)
      N=W*COSD(S)
      IF (T2.GE.0) THEN
         GOTO 160
      ELSE
         T1=-T1
         T2=-T2
```

```
        ENDIF
160     X1=(T1+T2)/N
        X2=0.0271*RJ+0.548
        CS=(1.0*10**X2)
        X3=A/10000.
        X4=N*9.81/1000000
        X5=CS*X3/X4
        RC=(ATAND(X1)-RF)/ALOG10(X5)
        WRITE(2,180) TNAME, RF, CS, RC
180     FORMAT(A8,F8.1,I8,F8.1)
        GOTO 150
C
C       CLOSE OFF FILES
C
200     CLOSE(UNIT=2)
        CLOSE(UNIT=1)
        END
```

A1.1.3 DIGIT

```
Program test_digitizer(input, output, outfile);

        {*** a test program for the digitiser ***}

    var
        outfile         : text;
        success,
        finished        : boolean;
        x, y            : integer;
        ch              : char;

{************************************************************************}
{***            Digitiser          functions                          ***}
{************************************************************************}

        [external] procedure digit_init;extern;

        [external] function digit_read(var x, y : integer;
                                       var ch : char):boolean;extern;


{************************************************************************}
{***                    Application Program                           ***}
{************************************************************************}

        procedure read_digitiser;

                {*** read coords from the digitiser ***}

        begin {read_digitiser}
            finished := false;
                {*** read coordinates from the digitiser ***}
            while not finished  do begin
                success := digit_read(x, y, ch);
                if success and (ord(ch) = 255) then begin
                    writeln(outfile, x, y);
                    writeln(output, x, y);
                end
                else if success and (ord(ch) <> -1) then begin
                    writeln(output, 'Specifying new set of data');
                    writeln(output, chr(7));
                end
                else if not success then begin
                    if ord(ch) = 13 then begin          {CR is hit}
                        finished := true;
                    end;
                end;
            end {while};
        end {read_digitiser};


        procedure information;
             {*** info on how to run the program ***}
        begin
            writeln(output);        writeln(output);
            writeln(output, 'To input data hit the GREY key on the digitiser ');
```

```
            writeln(output, 'pad.');
            writeln(output);
            writeln(output, 'Only data input with the GREY key is accepted  ');
            writeln(output, 'and written  ');
            writeln(output, 'to the file OUT.DAT.');
            writeln(output);
            writeln(output, 'To Specify a new set of data, hit any other ');
            writeln(output, 'keys on the');
            writeln(output, 'Digitiser keypad.');
            writeln(output);
            writeln(output, 'To terminate session, hit the <RETURN> key ');
            writeln(output, 'on the V500 keypad.');
            writeln(output);
            writeln(output);
            writeln(output, 'The data [x and y coordinates] are displayed ');
            writeln(output, 'on the screen as well.');
            writeln(output);
            writeln(output);
            writeln(output, 'Please hit <RETURN> to start session');
            readln(input);
        end {information};


begin {test}

        {***  initialise ***}

    open(outfile, 'out.dat', history := new);
    rewrite(outfile);

    digit_init;
    information;
    read_digitiser;             {*** read coords from the digitiser ***}

    writeln(output, 'Bye......');
end {test}.
```

A1.1.4 FILTER

```
      PROGRAM FILTER
C
C     REMOVES ERRORS IN DIGITISING WHICH RESULT IN
C     X VALUES LESS THAN OR EQUAL TO PREVIOUS X VALUE
C
      CHARACTER*10 FNAME
      INTEGER X, Y, XLAST, YLAST
C
C     GET THE FILENAME FOR THE DIGITISED DATA
C     THEN OPEN THAT FILE FOR INPUT
C     OPEN OUTPUT FILE OF SAME NAME
C
100   TYPE*,'ENTER INPUT FILENAME'
      ACCEPT 110, FNAME
      OPEN(UNIT=1, NAME=FNAME, TYPE='OLD', ERR=100, READONLY)
      OPEN(UNIT=2, NAME=FNAME, TYPE='NEW')
110   FORMAT(A)
C
C     FILTER THE DIGITISED VALUES
C     OUTPUT PROBLEM VALUES TO THE SCREEN
C
      READ(1,* ,ERR=150) X, Y
120   WRITE(2,140) X, Y
      XLAST=X
      YLAST=Y
130   READ(1,* ,END=150) X, Y
      IF(X.LE.XLAST) THEN
        TYPE 140, XLAST, YLAST
        TYPE 140, X, Y
        TYPE 140
        GOTO 130
      ENDIF
      GOTO 120
140   FORMAT(2I8)
C
C     CLOSE OFF THE FILES
C
150   CLOSE(UNIT=1)
      CLOSE(UNIT=2)
      END
```

A1.1.5 INTER

```
      PROGRAM INTER
C     INTERPOLATES A DIGITISED DATA TO A REGULAR SAMPLING INTERVAL
C     AND CALCULATES Z2 AND JRC
C
C     DECLARE THE VARIABLES
C
      CHARACTER*10 FNAME
      INTEGER DX
      REAL XN(2000), YN(2000), Y, JRC
C
C     ************************************************************
C             VARIABLES USED
C     DX    : INTERPOLATION INTERVAL (= * 0.1 mm)
C     FNAME : FILENAMES
C     I     : GENERAL PURPOSE COUNTER
C     J     : GENERAL PURPOSE COUNTER
C     JRC   : JOINT ROUGHNESS COEFFICIENT
C     M     : NUMBER OF INTERVALS
C     N     : NUMBER OF INTERPOLATED POINTS
C     RMS   : ROOT MEAN SQUARE
C     X     : DIGITISED X VALUE
C     XLAST : PREVIOUS DIGITISED X COORDINATE
C     XN    : ARRAY OF X COORDINATES ON WHICH YN ARE INTERPOLATED
C     XX    : X VALUE CONVERTED TO CENTIMETRES
C     Y     : DIGITISED Y VALUE
C     YLAST : PREVIOUS DIGITISED VALUE
C     YN    : INTERPOLATED Y VALUES AT POINTS IN XN
C     YY    : Y VALUE CONVERTED TO CENTIMETRES
C     Z2    : RMS OF THE 1ST DERIVATIVE OF THE PROFILE
C     ************************************************************
C
C     GET THE FILENAMES FOR THE DIGITISED DATA
C     AND INTERPOLATED DATA
C     THEN OPEN THOSE FILES
C
100   TYPE*,' ENTER OUTPUT FILENAME'
      ACCEPT 120, FNAME
      OPEN(UNIT=2, NAME=FNAME, TYPE='NEW', ERR=100)
110   TYPE*,' ENTER INPUT FILENAME'
      ACCEPT 120, FNAME
      OPEN(UNIT=1, NAME=FNAME, TYPE='OLD', ERR=110, READONLY)
120   FORMAT(A)
C
C     SET INTERPOLATION INTERVAL TO 1.0 MM
C
      DX=10
C
C     INTERPOLATE THE DIGITISED PROFILE ONTO A REGULAR INTERVAL
C
      J=1
      READ(1,* ,ERR=140) X, Y
      XN(J)=X
      YN(J)=Y
      XLAST=X
      YLAST=Y
      XN(J+1)=XN(1)+J*DX
```

```
        J=J+1
130     IF (XN(J).GE.X) READ(1,* ,END=140) X, Y
        IF (X.GE.XN(J)) THEN
          YN(J)=YLAST+(Y-YLAST)*(XN(J)-XLAST)/(X-XLAST)
          XN(J+1)=XN(1)+J*DX
          J=J+1
          IF (X.LE.XN(J)) THEN
            XLAST=X
            YLAST=Y
          ENDIF
        ELSE
          XLAST=X
          YLAST=Y
        ENDIF
        GOTO 130
C
C       CALCULATE N AND M
C
140     N=J-1
        M=N-1
C
C       DETREND THE PROFILE AND NORMALISE THE INTERPOLATED Y VALUES
C       SO THEY HAVE A MEAN OF ZERO
C
        CALL LEASTS(YN,N)
C
C       CALCULATE Z2 AND JRC
C
        RMS=0.0
        DO I=1,M
          RMS=RMS+(YN(I+1)-YN(I))**2
        ENDDO
        Z2=SQRT(RMS/(M*DX**2))
C
C       THE COEFFICIENTS BELOW ONLY APPLY WHEN DX=10
C
        JRC=32.29+33.84*ALOG10(Z2)
        TYPE 150, Z2,JRC,DX
        WRITE(2,150) Z2, JRC, DX
150     FORMAT(' FOR THIS PROFILE Z2=',F6.3,' AND THE JRC=',F7.2,' WITH
        1 A DX OF ',I4)
C
C       OUTPUT THE INTERPOLATED NORMALISED PROFILE IN CM
C
        DO I=1,N
          XX=(XN(I)-XN(1))*0.01
          YY=YN(I)*0.01
          WRITE(2,160) XX, YY
160     FORMAT(3F8.3,1P5E11.4)
        ENDDO
C
C       CLOSE OFF THE FILES
C
        CLOSE(UNIT=1)
        CLOSE(UNIT=2)
        END
C
      SUBROUTINE LEASTS(Y,N)
C
```

```
C     LINEAR LEAST SQUARES FIT TO DETREND DATA
C
      DIMENSION Y(N)
      DATA IDSH/'-'/
      SUM1=0.
      SUM2=0.
      SUM3=0.
      SUM4=0.
      DO 1 I=1,N
      X=I
      SUM1=SUM1+X*Y(I)
      SUM2=SUM2+X
      SUM3=SUM3+Y(I)
      SUM4=SUM4+X*X
    1 CONTINUE
      Z=N
      A=(SUM1-SUM2*SUM3/Z)/(SUM4-SUM2*SUM2/Z)
      B=(SUM3-A*SUM2)/Z
        TYPE 110
  110 FORMAT('0DATA DETREND')
        TYPE 120, (IDSH,I=1,12)
  120 FORMAT(1X,120A1)
        TYPE 100, A,B
  100 FORMAT('0LINEAR LEAST SQUARES FIT TO Y=AX+B AND A =',1PE12.4,
     *' AND B =',1PE12.4,/)
      DO 2 I=1,N
      X=I
      Y(I)=Y(I)-(A*X+B)
    2 CONTINUE
      RETURN
      END
```

A1.1.6 STAT

```
      PROGRAM STAT
C     INTERPOLATES DIGITISED DATA TO A REGULAR SAMPLING INTERVAL
C     OF 0.5 MM
C     THEN CALCULATES ACF AND SDF
C
C     DECLARE THE VARIABLES
C
      CHARACTER*10 FNAME, ANS
      INTEGER DX, R
      REAL XN(2000), YN(2000), Y, T(2000), AC(2000)
      REAL FF(2000), G(2000)
      DATA PI /3.1415927/
C
C     ************************************************************
C             VARIABLES USED
C     AC    : ARRAY STORING ACF(R)
C     AC0   : NORMALISED SUM OF SQUARES = ACF(0)
C     ANS   : DUMMY VARIABLE STORING SCREEN INTERROGATION ANSWERS
C     DUM   : DUMMY VARIABLE WHERE A SUM IS ACCUMULATED
C             FOR THE 2ND COEFFICIENT IN SDF
C     DX    : INTERPOLATION INTERVAL (= * 0.1 mm)
C     F     : FREQUENCY IN SDF(F)
C     FC    : CUTOFF FREQUENCY
C     FF    : FREQUENCY (cm**-1)
C     FNAME : FILENAMES
C     G     : REFINED SPECTRAL ESTIMATES
C     GTOT  : TOTAL SPECTRAL ENERGY
C     I     : GENERAL PURPOSE COUNTER
C     J     : GENERAL PURPOSE COUNTER
C     M     : NUMBER OF INTERVALS
C     N     : NUMBER OF INTERPOLATED POINTS
C     PI    : VALUE OF PI
C     R     : LAG NUMBER
C     RMAX  : MAXIMUM LAG NUMBER
C     RR    : LAG NUMBER (cm)
C     T     : RAW SPECTRAL ESTIMATES
C     X     : DIGITISED X VALUE
C     XLAST : PREVIOUS DIGITISED X COORDINATE
C     XN    : ARRAY OF X COORDINATES ON WHICH YN ARE INTERPOLATED
C     Y     : DIGITISED Y VALUE
C     YLAST : PREVIOUS DIGITISED VALUE
C     YN    : INTERPOLATED Y VALUES AT POINTS IN XN
C     ************************************************************
C
C     GET THE FILENAMES FOR THE DIGITISED DATA
C     AND THE ACF AND SDF DATA
C     THEN OPEN THOSE FILES
C
100   TYPE*,' ENTER ACF OUTPUT FILENAME'
      ACCEPT 130, FNAME
      OPEN(UNIT=3, NAME=FNAME, TYPE='NEW', ERR=100)
110   TYPE*,' ENTER SDF OUTPUT FILENAME'
      ACCEPT 130, FNAME
      OPEN(UNIT=4, NAME=FNAME, TYPE='NEW', ERR=110)
120   TYPE*,' ENTER INPUT FILENAME'
      ACCEPT 130, FNAME
```

```
      OPEN(UNIT=1, NAME=FNAME, TYPE='OLD', ERR=120, READONLY)
130   FORMAT(A)
C
C     SET INTERPOLATION INTERVAL TO 0.5 MM
C
      DX=5
C
C     INTERPOLATE THE DIGITISED PROFILE ONTO A REGULAR INTERVAL
C
      J=1
      READ(1,* ,ERR=150) X, Y
      XN(J)=X
      YN(J)=Y
      XLAST=X
      YLAST=Y
      XN(J+1)=XN(1)+J*DX
      J=J+1
140   IF (XN(J).GE.X) READ(1,* ,END=150) X, Y
      IF (X.GE.XN(J)) THEN
        YN(J)=YLAST+(Y-YLAST)*(XN(J)-XLAST)/(X-XLAST)
        XN(J+1)=XN(1)+J*DX
        J=J+1
        IF (X.LE.XN(J)) THEN
          XLAST=X
          YLAST=Y
        ENDIF
      ELSE
        XLAST=X
        YLAST=Y
      ENDIF
      GOTO 140
C
C     CALCULATE N AND  M
C
150   N=J-1
      M=N-1
C
C     DETREND THE INTERPOLATED PROFILE AND NORMALISE THE
C     INTERPOLATED Y VALUES SO THEY HAVE A MEAN OF ZERO
C
      CALL LEASTS(YN,N)
C
C     CALCULATE THE NORMALISED SUM OF SQUARES (AC0) FOR LATER USE
C
      AC0=0
      DO I=1,N
        AC0=AC0+YN(I)*YN(I)
      ENDDO
C
C     CALCULATE AUTOCORRELATION FUNCTION (ACF)
C
      WRITE(3,160)
160   FORMAT('  LAG (cm) AND ACF')
      RMAX=N/2
      DO R=0,RMAX
        AC(R)=0.0
        DO I=1,(N-R)
          AC(R)=AC(R)+(YN(I)*YN(I+R))
        ENDDO
```

```
          AC(R)=AC(R)/AC0
          RR=R*DX*0.01
          WRITE(3,170) RR,AC(R)
170       FORMAT(F8.2,F8.4)
        ENDDO
C
C       CALCULATE SPECTRAL DENSITY FUNCTION (SDF)
C       BEGIN BY CALCULATING RAW ESTIMATES T(R)
C
        DO R=0,RMAX
          DUM=0.0
          DO I=1,RMAX-1
            DUM=DUM+AC(I)*COS(I*R*PI/RMAX)
          ENDDO
          T(R)=2*DX*(AC(0)+2*DUM+AC(RMAX)*COS(R*PI))
        ENDDO
C
C       REFINE BY HANNING
C
        R=0
        G(R)=0.5*T(R)+0.5*T(R+1)
        FC=1.0/(2.0*DX)
        F=(R*FC)/RMAX
        FF(R)=F/0.01
        DO R=1,RMAX-1
          G(R)=0.5*T(R)+0.25*T(R-1)+0.25*T(R+1)
        FC=1.0/(2.0*DX)
        F=(R*FC)/RMAX
        FF(R)=F/0.01
        ENDDO
        R=R+1
        G(R)=0.5*T(R)+0.5*T(R-1)
        FC=1.0/(2.0*DX)
        F=(R*FC)/RMAX
        FF(R)=F/0.01
C
C       CALCULATE TOTAL SPECTRAL ENERGY
C
180     GTOT=G(0)
        DO R=1,RMAX
          GTOT=GTOT+G(R)
        ENDDO
        TYPE 190, GTOT
190     FORMAT(' TOTAL SPECTRAL ENERGY =',F8.2)
C
C       INTERROGATE TO DETERMINE IF NORMALISATION
C       IS REQUIRED
C
200     TYPE*,' DO YOU WANT TO NORMALISE THE SDF? (Y/N)'
        ACCEPT 210, ANS
210     FORMAT(A)
        IF(ANS.EQ.'N') GOTO 220
        IF(ANS.EQ.'Y') GOTO 250
        GOTO 200
C
C       OUTPUT UNNORMALISED SDF
C
220     WRITE(4,230)
230     FORMAT('  FREQUENCY (cm**-1) AND SDF')
```

```
        DO R=0,RMAX
           WRITE(4,240) FF(R),G(R)
240     FORMAT(F8.3,F8.2)
        ENDDO
        GOTO 280
C
C       NORMALISE SDF
C       OUTPUT AS PERCENTAGE OF TOTAL ENERGY
C
250     WRITE(4,260)
260     FORMAT('  FREQUENCY (cm**-1) AND PERCENTAGE SDF')
        DO R=0,RMAX
           G(R)=(G(R)/GTOT)*100
           WRITE(4,270) FF(R),G(R)
270     FORMAT(2F8.3)
        ENDDO
C
C       CLOSE OFF THE FILES
C
280     CLOSE(UNIT=4)
        CLOSE(UNIT=3)
        CLOSE(UNIT=1)
        END
C
      SUBROUTINE LEASTS(Y,N)
C
C     LINEAR LEAST SQUARES FIT TO DETREND DATA
C
      DIMENSION Y(N)
      DATA IDSH/'-'/
      SUM1=0.
      SUM2=0.
      SUM3=0.
      SUM4=0.
      DO 1 I=1,N
      X=I
      SUM1=SUM1+X*Y(I)
      SUM2=SUM2+X
      SUM3=SUM3+Y(I)
      SUM4=SUM4+X*X
    1 CONTINUE
      Z=N
      A=(SUM1-SUM2*SUM3/Z)/(SUM4-SUM2*SUM2/Z)
      B=(SUM3-A*SUM2)/Z
        TYPE 110
  110 FORMAT('0DATA DETREND')
        TYPE 120, (IDSH,I=1,12)
  120 FORMAT(1X,120A1)
        TYPE 100, A,B
  100 FORMAT('0LINEAR LEAST SQUARES FIT TO Y=AX+B AND A =',1PE12.4,
     *' AND B =',1PE12.4,/)
      DO 2 I=1,N
      X=I
      Y(I)=Y(I)-(A*X+B)
    2 CONTINUE
      RETURN
      END
```

A1.1.7 TEST

```
        PROGRAM TEST
C
C       GENERATE A TEST CURVE BY SUPERIMPOSING TWO SINE WAVES
C       (THE FIRST WITH AN AMPLITUDE OF 2 AND A WAVELENGTH OF 10
C       THE SECOND WITH AN AMPLITUDE OF 3 AND A WAVELENGTH OF 3)
C       AND A LINEAR TREND OF Y=2X+5; DETREND AND NORMALISE THE
C       CURVE USING THE SUBROUTINE LEASTS
C
        DIMENSION YY(128),XX(128)
        DATA PI2 /6.2831854/
        OPEN(UNIT=2, NAME='TEST.DAT', TYPE='NEW')
        N=128
        DO I=1,N
         Y=2.*COS(PI2*I/10.)+3.*COS(PI2*I/3.)+2.*I+5.
         XX(I)=I
         YY(I)=Y
        ENDDO
        CALL LEASTS(YY,N)
        WRITE(2,100)
100     FORMAT(' TEST.DAT')
        WRITE(2,120) ((XX(I),YY(I)),I=1,N)
120     FORMAT(F8.2,F8.4)
        CLOSE(UNIT=2)
        END
C
      SUBROUTINE LEASTS(Y,N)
C
C     LINEAR LEAST SQUARES FIT TO DETREND DATA
C
      DIMENSION Y(N)
      DATA IDSH/'-'/
      SUM1=0.
      SUM2=0.
      SUM3=0.
      SUM4=0.
      DO 1 I=1,N
      X=I
      SUM1=SUM1+X*Y(I)
      SUM2=SUM2+X
      SUM3=SUM3+Y(I)
      SUM4=SUM4+X*X
    1 CONTINUE
      Z=N
      A=(SUM1-SUM2*SUM3/Z)/(SUM4-SUM2*SUM2/Z)
      B=(SUM3-A*SUM2)/Z
        TYPE 110
  110 FORMAT('0DATA DETREND')
        TYPE 120, (IDSH,I=1,12)
  120 FORMAT(1X,120A1)
        TYPE 100, A,B
  100 FORMAT('0LINEAR LEAST SQUARES FIT TO Y=AX+B AND A =',1PE12.4,
     *' AND B =',1PE12.4,/)
      DO 2 I=1,N
      X=I
      Y(I)=Y(I)-(A*X+B)
    2 CONTINUE
```

```
RETURN
END
```

A1.1.8 NORM

```
      PROGRAM NORM
C     COMBINES NORMALISED POWER SPECTRA
C     WITH THE SAME FREQUENCY INTERVAL
C     AND OUTPUTS THE RESULTANT SPECTRUM
C
      CHARACTER FNAME*10
      REAL XN(2000), YN(2000), XT(2000), YT(2000)
      REAL FF(2000), EN(2000)
C
C     ***************************************************
C             VARIABLES USED
C     ANS   : DUMMY VARIABLE STORING INTERROGATION ANSWERS
C     EN    : NORMALISED CUMULATIVE SPECTRAL DENSITY
C     ETOT  : TOTAL SPECTRAL ENERGY
C     FF    : FREQUENCY (cm**-1)
C     FNAME : FILENAMES
C     I     : GENERAL PURPOSE COUNTER
C     N     : NUMBER OF OBSERVATIONS
C     X     : INPUTTED FREQUENCY
C     XN    : ARRAY STORING INPUTTED FREQUENCY
C     XT    : ARRAY STORING CUMULATIVE FREQUENCY
C     Y     : INPUTTED ENERGY
C     YN    : ARRAY STORING INPUTTED ENERGY
C     YT    : ARRAY STORING CUMULATIVE ENERGY
C     ***************************************************
C
C     OPEN OUTPUT FILE
C
100   TYPE*,'ENTER OUTPUT FILENAME'
      ACCEPT 105, FNAME
      OPEN(UNIT=2, NAME=FNAME, TYPE='NEW', ERR=100)
105   FORMAT (A)
C
C     OPEN INITIAL INPUT FILE AND READ INTO ARRAY
C     THEN CLOSE INITIAL INPUT FILE
C
110   TYPE*,'ENTER INITIAL INPUT FILENAME'
      ACCEPT 115, FNAME
      OPEN(UNIT=1, NAME=FNAME, TYPE='OLD', ERR=110, READONLY)
115   FORMAT (A)
C
      I=1
120   READ(1,*,END=125) X, Y
      XT(I)=X
      YT(I)=Y
      I=I+1
      GOTO 120
125   N=I-1
C
      CLOSE(UNIT=1)
C
C     OPEN NEXT INPUT FILE AND READ INTO ARRAY
C     THEN COMBINE WITH PREVIOUS DATA AND CLOSE INPUT FILE
C
130   TYPE*,'ANOTHER INPUT FILE ? (Y/N)'
      ACCEPT 135, ANS
```

```
135     FORMAT (A)
        IF(ANS.EQ.'N') GOTO 155
        IF(ANS.EQ.'Y') GOTO 140
        GOTO 130
140     TYPE*,'ENTER NEXT INPUT FILENAME'
        ACCEPT 145, FNAME
        OPEN(UNIT=1, NAME=FNAME, TYPE='OLD', ERR=140, READONLY)
145     FORMAT (A)
C
        DO I=1,N
           READ(1,*,ERR=150) X, Y
           XN(I)=X
           YN(I)=Y
           XT(I)=XN(I)
           YT(I)=YT(I)+YN(I)
        ENDDO
        CLOSE(UNIT=1)
        GOTO 130
150     TYPE*,'ERROR IN DATA INPUT'
C
C       CALCULATE TOTAL SPECTRAL ENERGY
C
155     ETOT=0.0
        DO I=1,N
           ETOT=ETOT+YT(I)
        ENDDO
C
C       OUTPUT NORMALISED CUMULATIVE SDF
C       AS PERCENTAGE OF TOTAL ENERGY
C
        WRITE(2,160)
160     FORMAT(' FREQUENCY (cm**-1) AND SDF (%E)')
        DO I=1,N
           FF(I)=XT(I)
           EN(I)=(YT(I)/ETOT)*100
           WRITE(2,165) FF(I), EN(I)
165     FORMAT(2F8.3)
        ENDDO
C
        CLOSE(UNIT=2)
        END
```

A1.2 Program Testing

Testing of calculative routines was accomplished by working through by hand specific examples. Testing of interpolative routines was achieved by matching digitised profiles before and after interpolation, and checking the degree of correspondence. By far the most important test was whether the program STAT with its routines for calculating ACF and SDF, could detrend a digitised profile and isolate regular frequencies or wavelengths. Program TEST generates a test consisting of two superimposed sine waves (one with a wavelength of 10, the other with a wavelength of 3) and a linear trend of $y=2x+5$. Program TEST attempts to detrend this curve using the subroutine LEASTS, which produces a linear leasts squares fit of $Y=1.9994X+4.9873$, obviously a good correction. The detrended test curve (Figure A1.1) was run through a version of STAT. The resulting autocorrelation (Figure A1.2) shows two predominant lags with peaks every 3 and 10 units. The power spectrum generated (Figure A1.3) clearly shows two peaks at frequencies of 0.10 and 0.33, corresponding to wavelengths of 10 and 3, respectively. Hence, some confidence must be placed in the ability of program STAT to predict regular wavelengths.

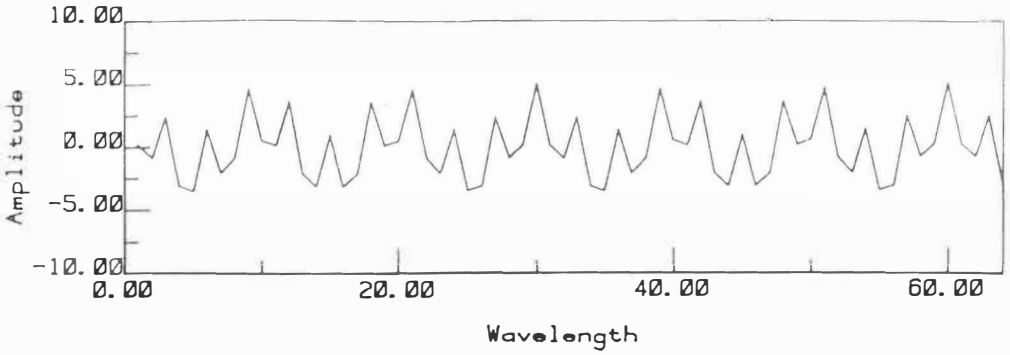

FIGURE A1.1 Detrended test curve generated by program TEST.

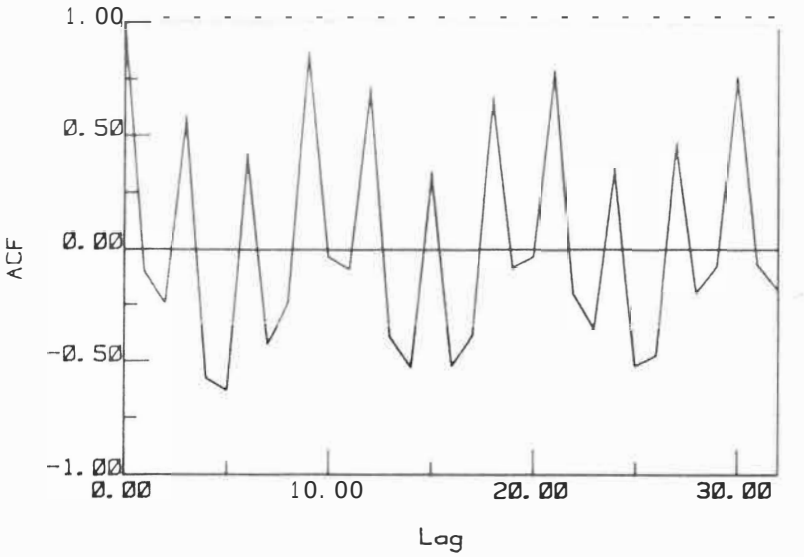

FIGURE A1.2 Autocorrelogram of test curve; produced by program STAT.

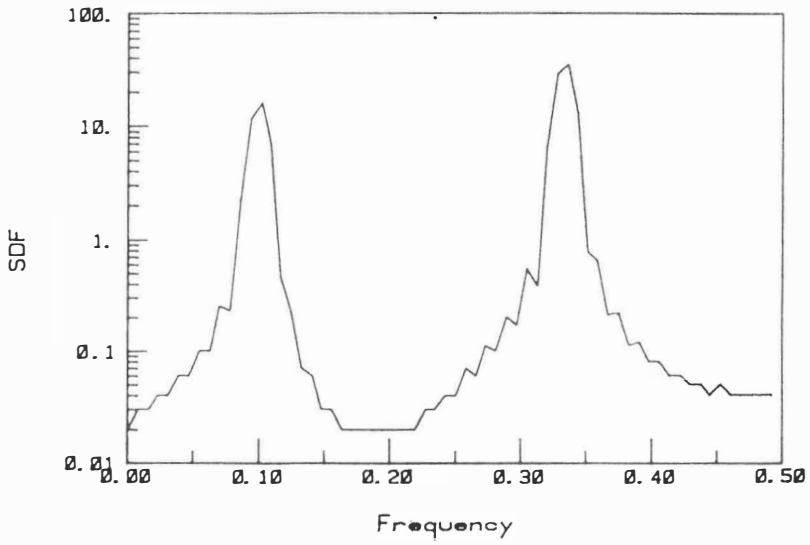

FIGURE A1.3 Power spectrum of test curve; produced by program STAT.

APPENDIX TWO

RESULTS OF JRC ESTIMATION

APPENDIX 2: RESULTS OF JRC ESTIMATION

A2.1 Profile Comparison

JOINT	JRC	JOINT	JRC	JOINT	JRC	JOINT	JRC	JOINT	JRC	JOINT	JRC
OQ1	9	AD1	8	BG1	14	SG1	14	SS1	8	SM1	8
OQ2	10	AD2	6	BG2	16	SG2	11	SS2	7	SM2	6
OQ3	10	AD3	10	BG3	14	SG3	10	SS3	9	SM3	8
OQ4	14	AD4	12	BG4	16	SG4	14	SS4	6	SM4	10
OQ5	14	AD5	8	BG5	15	SG5	14	SS5	8	SM5	7
OQ6	10	AD6	9	BG6	14	SG6	13	SS6	6	SM6	8
OQ7	8	AD7	10	BG7	14	SG7	14	SS7	9	SM7	10
OQ8	10	AD8	6	BG8	15	SG8	15	SS8	5	SM8	10
OQ9	8	AD9	8	BG9	13	SG9	9	SS9	10	SM9	10
OQ10	9			BG10	12	SG10	14	SS10	6	SM10	8
OQ11	12										
OQ12	13										
OQ13	10										
OQ14	10										
OQ15	8										
OQ16	10										
OQ17	8										
OQ18	6										

A2.2 Tilt Testing

JOINT	h (cm)	$\alpha°$	r	$\phi_r°$	JCS (MPa)	JRC
OQ11	10.5	50.0	30	24.4	22	5.9
OQ12	7.0	48.2	38	27.7	37	4.4
OQ13	6.0	65.8	33	25.7	27	8.0
OQ15	6.5	57.3	35	26.5	31	6.4
OQ16	6.5	54.0	25	22.4	16	7.1
OQ17	6.5	50.1	23	21.6	14	6.6
OQ18	6.5	46.5	34	26.1	29	4.4
SS1	7.0	46.3	44	23.3	55	4.8
SS2	6.0	52.9	43	23.0	51	6.0
SS3	4.0	60.1	38	21.3	37	7.5
SS4	3.5	70.9	34	19.9	29	9.3
SS5	3.5	65.1	39	21.6	40	8.1
SS6	2.0	59.8	34	19.9	29	7.5
SS7	3.0	61.8	31	18.9	24	8.4
SS8	2.5	68.2	29	18.2	21	9.3
SS9	4.5	63.6	36	20.6	33	8.4
SS10	2.5	54.9	34	19.9	29	6.8
SM1	11.0	46.4	40	24.4	42	4.9
SM2	11.0	43.3	42	25.1	48	4.1
SM4	5.5	58.9	32	21.6	26	7.8
SM5	6.5	55.4	39	24.0	40	6.5
SM6	7.0	60.8	41	24.7	45	7.2
SM7	4.5	66.9	42	25.1	48	7.8
SM8	4.5	61.3	37	23.4	35	7.5
SM9	7.5	64.2	38	23.7	37	8.2
SM10	8.0	56.0	36	23.0	33	7.1

h = thickness of upper joint block;
α = average tilt angle;
r = joint wall Schmidt rebound number;
ϕ_r = residual friction angle;
JCS = joint wall compressive strength;

A2.3 Pull Testing

JOINT	A (cm^2)	β°	W (kg)	T_2 (kg)	r	ϕ_r°	JCS (MPa)	JRC
AD1	644	3.0	10.0	-24.0	47	26.1	66	9.2
AD2	912	4.0	14.0	20.0	42	24.4	48	7.4
AD3	525	10.0	29.0	-46.6	54	28.3	102	6.5
AD4	621	3.0	37.0	-49.8	50	27.0	79	6.3
AD5	729	18.0	15.0	-19.6	45	25.4	58	4.8
AD6	1176	32.0	31.0	-73.0	49	26.7	75	8.5
AD7	972	8.0	44.0	-48.3	54	28.3	102	3.7
AD8	1164	29.0	26.5	18.3	51	27.4	85	5.6
AD9	1185	26.0	24.0	-32.7	54	28.3	102	3.8
BG3	297	21.0	3.5	9.6	23	21.9	14	12.7
BG9	533	19.0	11.0	16.5	23	21.9	14	10.7
BG10	460	20.0	9.0	9.5	22	21.5	13	9.3
SG1	497	31.0	8.5	10.5	28	21.2	20	10.5
SG3	575	1.0	8.5	-8.8	33	23.0	27	5.6
SG4	667	10.0	12.0	-21.8	36	24.1	33	8.5
SG9	364	3.0	8.0	16.6	43	26.7	51	9.2
SS1	624	1.0	14.0	-15.7	44	23.3	55	6.0
SS2	600	8.0	13.0	-20.9	43	23.0	51	7.9
SS3	1240	0.5	18.0	-26.2	38	21.3	37	8.0
SS4	943	3.0	7.0	13.5	34	19.9	29	10.0
SS5	506	2.0	5.5	-12.0	39	21.6	40	9.8
SS6	675	6.0	4.5	-5.8	34	19.9	29	7.1
SS7	550	4.0	6.0	10.6	31	18.9	24	10.5
SS8	546	4.0	4.0	-5.3	29	18.2	21	8.9
SS9	480	5.0	6.5	15.9	36	20.6	33	11.1
SS10	950	7.0	5.0	-9.3	34	19.9	29	9.4
SM1	368	12.0	5.5	-9.3	40	24.4	42	7.6
SM2	330	3.0	13.0	-14.3	42	25.1	48	5.7
SM3	190	2.0	3.5	5.6	34	22.3	29	9.4
SM4	370	2.0	5.5	-8.6	32	21.6	26	8.8
SM5	950	1.0	15.0	-22.5	39	24.0	40	7.6
SM6	1716	1.0	13.0	19.8	41	24.7	45	7.1
SM7	546	18.0	11.5	20.7	42	25.1	48	9.6
SM8	696	4.0	11.0	-19.1	37	23.4	35	8.7
SM9	624	5.0	14.5	21.6	38	23.7	37	8.2
SM10	442	8.0	8.5	8.4	36	23.0	33	6.4

A = joint area;
β = test inclination;
W = weight of upper joint block;
T_2 = applied pulling force; a negative sign indicates T2 was applied in an upwardly inclined direction;
r = joint wall Schmidt rebound number;
ϕ_r = residual friction angle;
JCS = joint wall compressive strength;

A2.4 Numerical Calculation

JOINT	a	b	c	JRC
OQ1	7.8	10.1	13.3	10.4
OQ2	10.9	10.0	12.0	11.0
OQ3	9.9	8.7	11.1	9.9
OQ4	14.3	12.0	12.9	13.1
OQ5	11.8	6.3	10.0	9.4
OQ6	8.7	5.1	8.0	7.3
OQ7	4.6	5.6	6.1	5.4
OQ8	8.3	7.3	10.0	8.5
OQ9	4.0	6.1	9.1	6.4
OQ10	4.6	5.1	5.7	5.1
OQ11	9.3	5.7	6.2	7.1
OQ12	8.8	7.4	7.5	7.9
OQ13	6.7	8.1	9.8	8.2
OQ14	7.1	11.1	9.0	9.1
OQ15	7.6	6.3	6.8	6.9
OQ16	5.9	7.0	8.6	7.2
OQ17	9.7	4.3	8.1	7.4
OQ18	4.0	4.6	7.5	5.4
AD1	10.8	11.0	5.1	9.0
AD2	2.8	2.9	8.1	4.6
AD3	12.1	8.3	9.7	10.0
AD4	8.3	7.8	7.3	7.8
AD5	8.9	6.7	2.0	5.9
AD6	7.6	8.6	9.0	8.4
AD7	8.0	7.1	8.3	7.8
AD8	3.2	6.3	7.5	5.7
AD9	11.6	4.9	8.4	8.3
BG1	17.7	12.8	11.4	14.0
BG2	14.3	14.7	14.2	14.4
BG3	15.5	12.4	12.3	13.4
BG4	16.4	16.3	12.9	15.2
BG5	13.9	15.0	16.7	15.2
BG6	11.8	14.1	16.4	14.1
BG7	12.7	13.3	12.4	12.8
BG8	12.0	14.7	13.5	13.4
BG9	12.5	13.5	11.4	12.4
BG10	11.7	10.1	10.6	10.8
SG1	11.7	8.2	12.1	10.7
SG2	10.3	8.7	12.2	10.4
SG3	9.7	9.2	8.9	9.3
SG4	11.7	10.5	10.7	11.0
SG5	15.0	12.1	12.7	13.3
SG6	12.1	12.0	11.2	11.8
SG7	12.9	13.9	16.0	14.3
SG8	12.8	11.2	12.8	12.3
SG9	10.2	10.2	12.6	11.0
SG10	14.6	12.1	14.9	13.8

A2.4 Numerical Calculation continued

JOINT	a	b	c	JRC
SS1	3.5	9.0	8.7	7.0
SS2	5.3	5.4	4.7	5.1
SS3	9.8	7.9	9.2	8.9
SS4	5.7	5.6	9.1	6.8
SS5	8.1	4.4	7.3	6.6
SS6	6.1	5.2	5.7	5.7
SS7	8.2	8.0	6.1	7.4
SS8	4.4	5.7	2.9	4.3
SS9	10.1	8.1	7.6	8.6
SS10	8.9	8.0	5.6	7.5
SM1	5.7	4.2	6.3	5.4
SM2	6.4	3.6	2.9	4.3
SM3	8.0	8.4	13.2	9.8
SM4	4.8	9.5	7.9	7.4
SM5	3.6	3.0	3.1	3.3
SM6	6.6	6.1	9.2	7.3
SM7	6.0	6.5	6.1	6.2
SM8	8.7	6.2	7.1	7.3
SM9	7.3	5.8	7.5	6.9
SM10	4.3	3.7	1.9	3.3

APPENDIX THREE

RESULTS OF TIME SERIES ANALYSIS

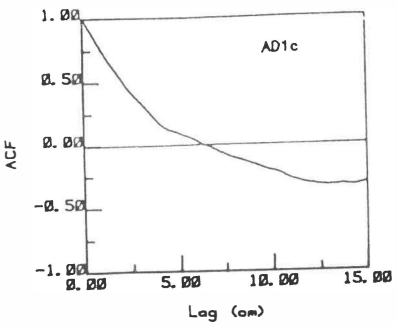
AD1c
ACF
1.00
0.50
0.00
-0.50
-1.00
0.00
5.00
10.00
15.00
Lag (cm)

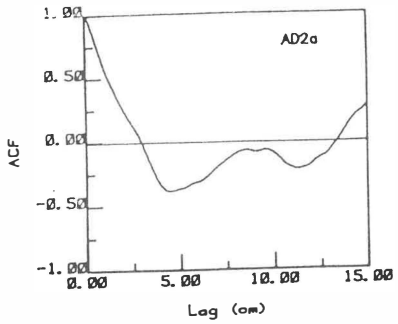
AD2a
ACF
1.00
0.50
0.00
-0.50
-1.00
0.00
5.00
10.00
15.00
Lag (cm)

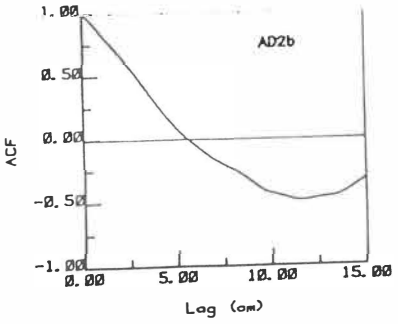
AD2b
ACF
1.00
0.50
0.00
-0.50
-1.00
0.00
5.00
10.00
15.00
Lag (cm)

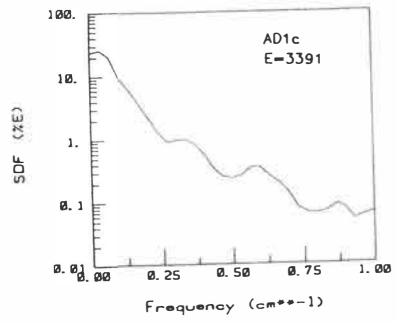
AD1c
E=3391
SDF (%E)
100.
10.
1.
0.1
0.01
0.00
0.25
0.50
0.75
1.00
Frequency (cm**-1)

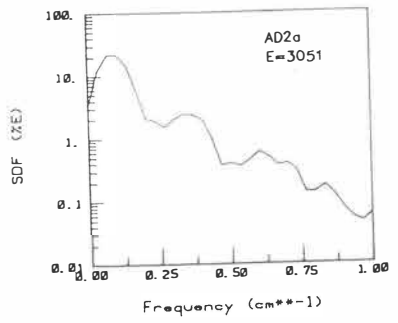
AD2a
E=3051
SDF (%E)
100.
10.
1.
0.1
0.01
0.00
0.25
0.50
0.75
1.00
Frequency (cm**-1)

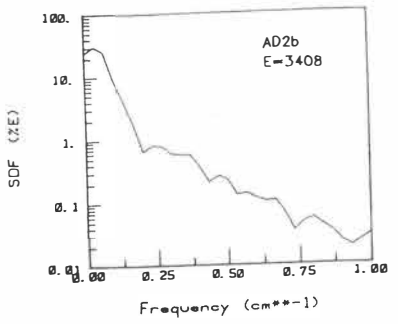
AD2b
E=3408
SDF (%E)
100.
10.
1.
0.1
0.01
0.00
0.25
0.50
0.75
1.00
Frequency (cm**-1)

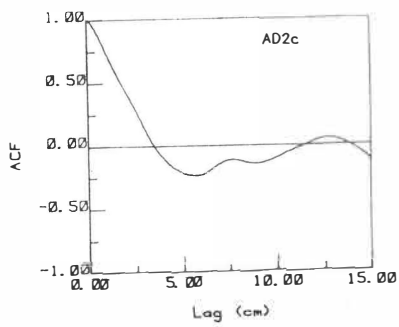
AD2c
ACF
1.00
0.50
0.00
-0.50
-1.00
0.00
5.00
10.00
15.00
Lag (cm)

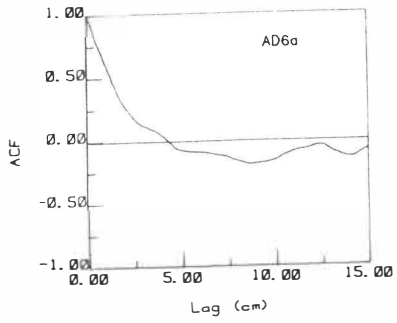
AD6a
ACF
1.00
0.50
0.00
-0.50
-1.00
0.00
5.00
10.00
15.00
Lag (cm)

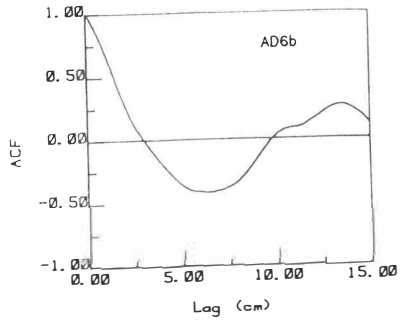
AD6b
ACF
1.00
0.50
0.00
-0.50
-1.00
0.00
5.00
10.00
15.00
Lag (cm)

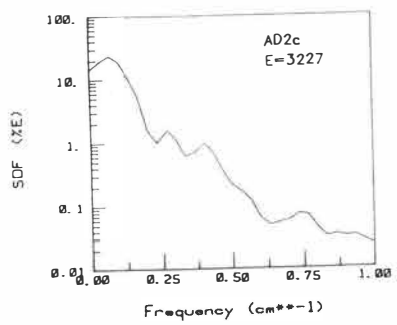
AD2c
E=3227
SDF (%E)
100.
10.
1.
0.1
0.01
0.00
0.25
0.50
0.75
1.00
Frequency (cm**-1)

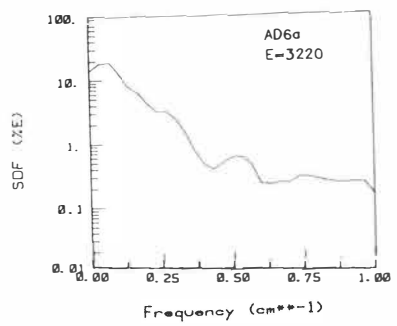
AD6a
E=3220
SDF (%E)
100.
10.
1.
0.1
0.01
0.00
0.25
0.50
0.75
1.00
Frequency (cm**-1)

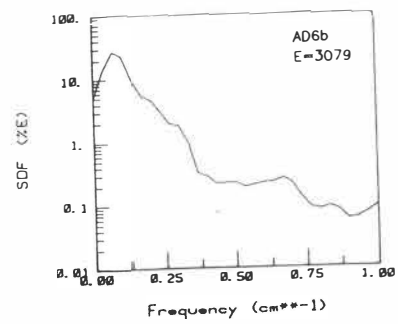
AD6b
E=3079
SDF (%E)
100.
10.
1.
0.1
0.01
0.00
0.25
0.50
0.75
1.00
Frequency (cm**-1)

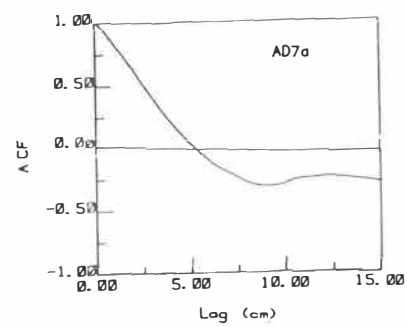
AD7a
ACF
1.00
0.50
0.00
-0.50
-1.00
0.00
5.00
10.00
15.00
Lag (cm)

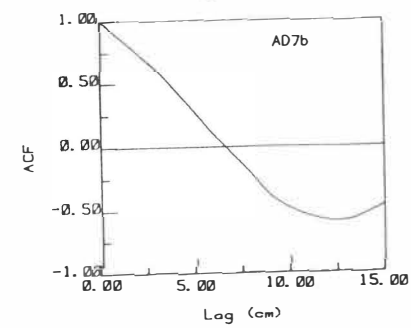
AD7b
ACF
1.00
0.50
0.00
-0.50
-1.00
0.00
5.00
10.00
15.00
Lag (cm)

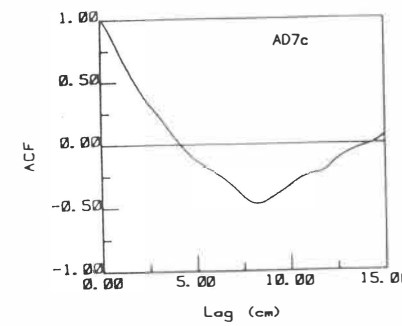
AD7c
ACF
1.00
0.50
0.00
-0.50
-1.00
0.00
5.00
10.00
15.00
Lag (cm)

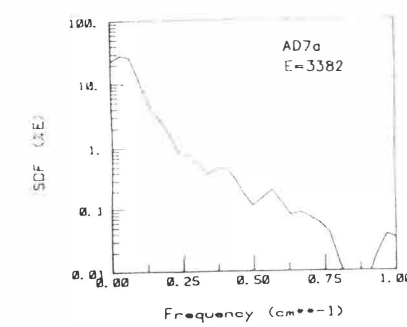
AD7a
E=3382
SDF (%E)
100.
10.
1.
0.1
0.01
0.00
0.25
0.50
0.75
1.00
Frequency (cm**-1)

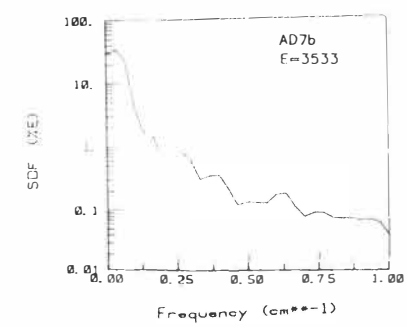
AD7b
E=3533
SDF (%E)
100.
10.
1.
0.1
0.01
0.00
0.25
0.50
0.75
1.00
Frequency (cm**-1)

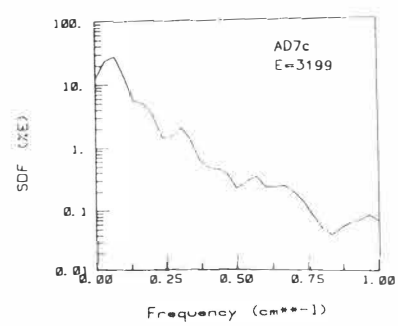
AD7c
E=3199
SDF (%E)
100.
10.
1.
0.1
0.01
0.00
0.25
0.50
0.75
1.00
Frequency (cm**-1)

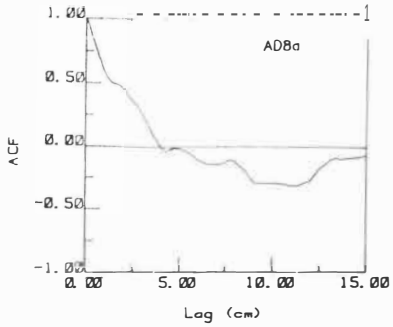
AD8a
ACF
1.00
0.50
0.00
-0.50
-1.00
0.00
5.00
10.00
15.00
Lag (cm)

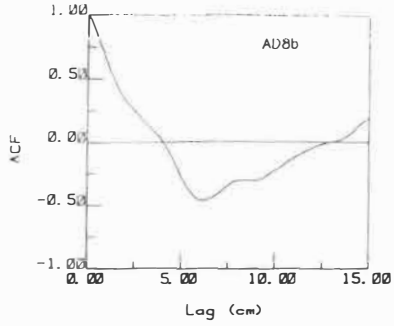
AD8b
ACF
1.00
0.50
0.00
-0.50
-1.00
0.00
5.00
10.00
15.00
Lag (cm)

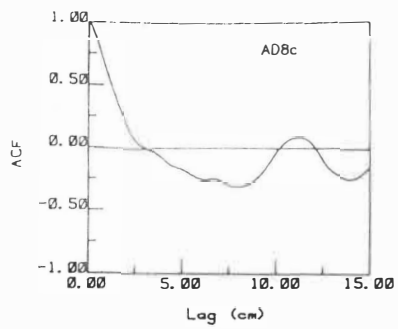
AD8c
ACF
1.00
0.50
0.00
-0.50
-1.00
0.00
5.00
10.00
15.00
Lag (cm)

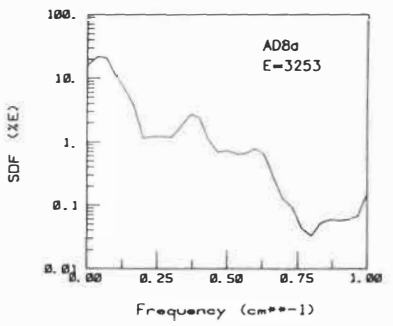
AD8a
E=3253
SDF (%E)
100.
10.
1.
0.1
0.01
0.00
0.25
0.50
0.75
1.00
Frequency (cm**-1)

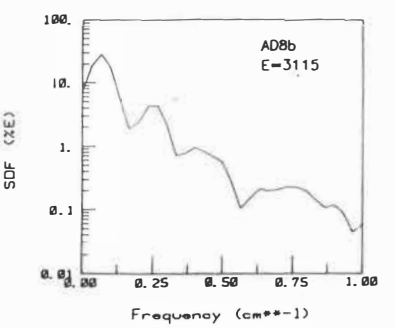
AD8b
E=3115
SDF (%E)
100.
10.
1.
0.1
0.01
0.00
0.25
0.50
0.75
1.00
Frequency (cm**-1)

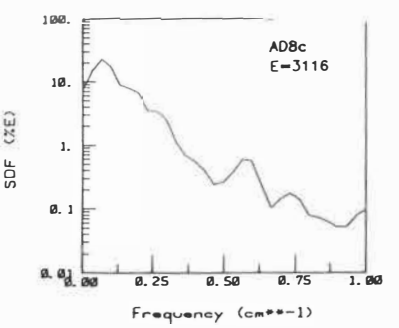
AD8c
E=3116
SDF (%E)
100.
10.
1.
0.1
0.01
0.00
0.25
0.50
0.75
1.00
Frequency (cm**-1)

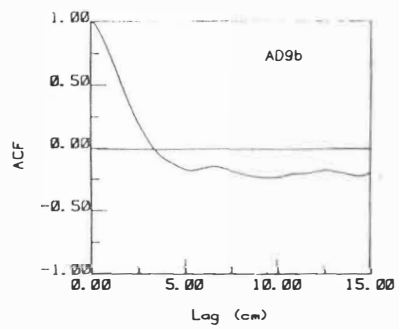
AD9b
ACF
1.00
0.50
0.00
-0.50
-1.00
0.00
5.00
10.00
15.00
Lag (cm)

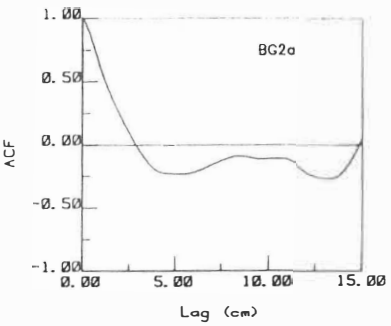
BG2a
ACF
1.00
0.50
0.00
-0.50
-1.00
0.00
5.00
10.00
15.00
Lag (cm)

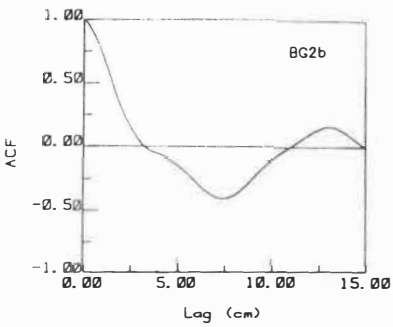
BG2b
ACF
1.00
0.50
0.00
-0.50
-1.00
0.00
5.00
10.00
15.00
Lag (cm)

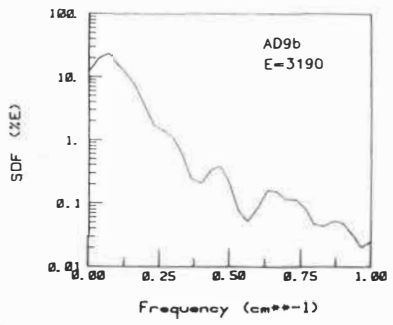
AD9b
E=3190
SDF (%E)
100.
10.
1.
0.1
0.01
0.00
0.25
0.50
0.75
1.00
Frequency (cm**-1)

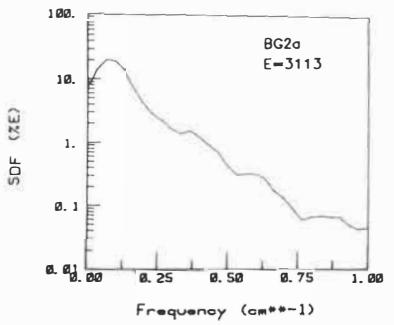
BG2a
E=3113
SDF (%E)
100.
10.
1.
0.1
0.01
0.00
0.25
0.50
0.75
1.00
Frequency (cm**-1)

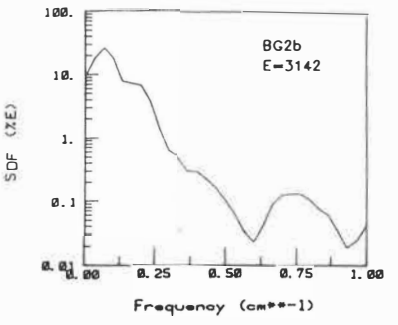
BG2b
E=3142
SDF (%E)
100.
10.
1.
0.1
0.01
0.00
0.25
0.50
0.75
1.00
Frequency (cm**-1)

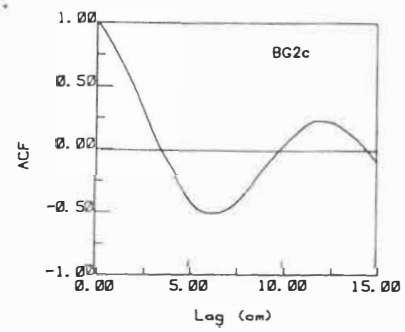
BG2c
ACF
1.00
0.50
0.00
-0.50
-1.00
0.00
5.00
10.00
15.00
Lag (cm)

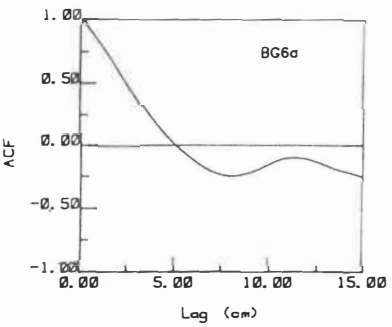
BG6a
ACF
1.00
0.50
0.00
-0.50
-1.00
0.00
5.00
10.00
15.00
Lag (cm)

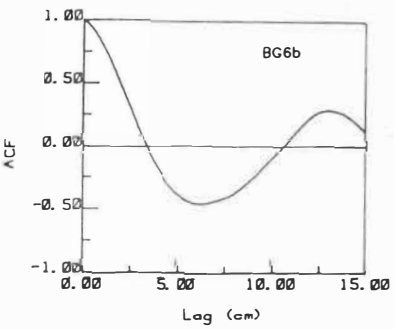
BG6b
ACF
1.00
0.50
0.00
-0.50
-1.00
0.00
5.00
10.00
15.00
Lag (cm)

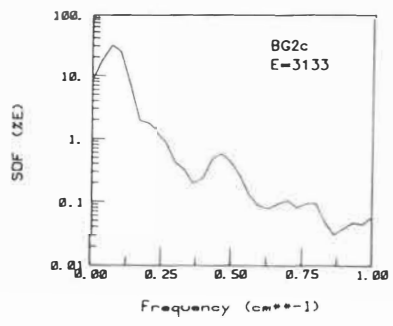
BG2c
E=3133
SDF (%E)
100.
10.
1.
0.1
0.01
0.00
0.25
0.50
0.75
1.00
Frequency (cm**-1)

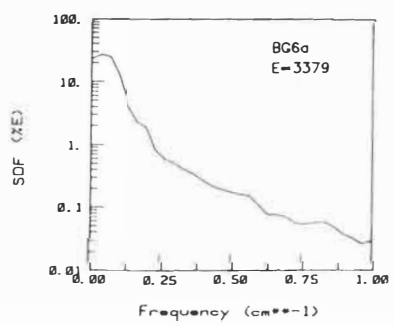
BG6a
E=3379
SDF (%E)
100.
10.
1.
0.1
0.01
0.00
0.25
0.50
0.75
1.00
Frequency (cm**-1)

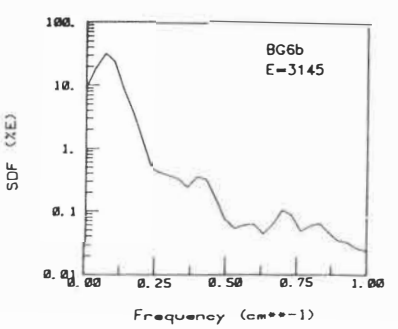
BG6b
E=3145
SDF (%E)
100.
10.
1.
0.1
0.01
0.00
0.25
0.50
0.75
1.00
Frequency (cm**-1)

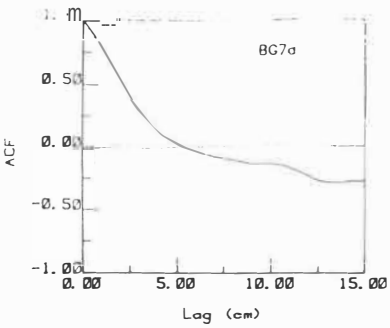
BG7a
ACF
Lag (cm)

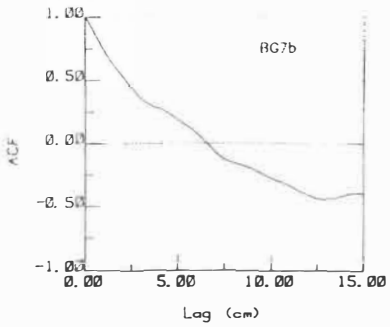
BG7b
ACF
Lag (cm)

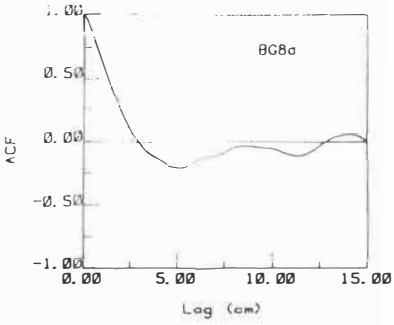
BG8a
ACF
Lag (cm)

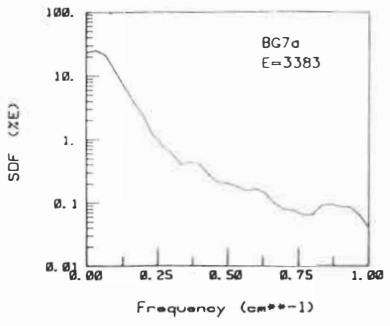
BG7a
E=3383
SDF (%E)
Frequency (cm**-1)

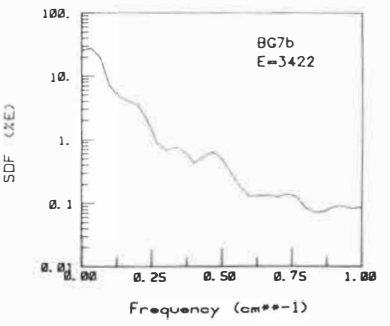
BG7b
E=3422
SDF (%E)
Frequency (cm**-1)

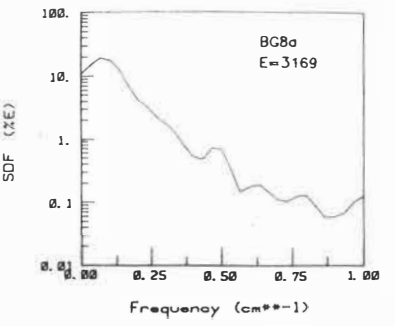
BG8a
E=3169
SDF (%E)
Frequency (cm**-1)

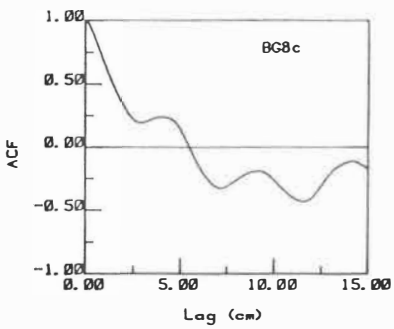
BG8c
ACF
Lag (cm)

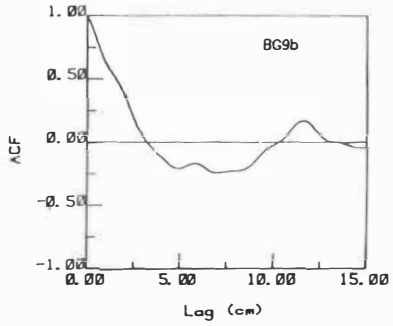
BG9b
ACF
Lag (cm)

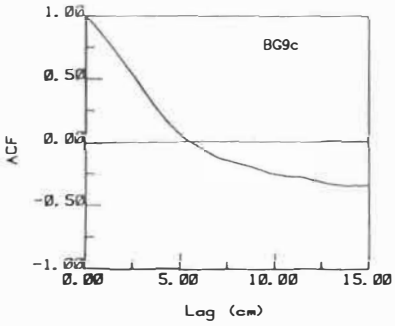
BG9c
ACF
Lag (cm)

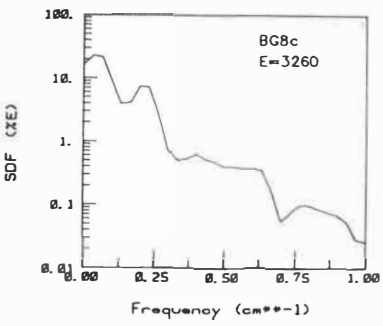
BG8c
E=3260
SDF (%E)
Frequency (cm**-1)

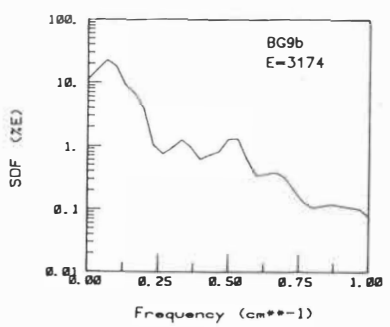
BG9b
E=3174
SDF (%E)
Frequency (cm**-1)

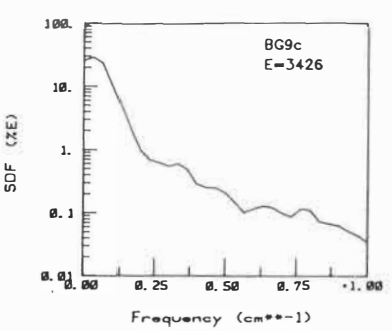
BG9c
E=3426
SDF (%E)
Frequency (cm**-1)

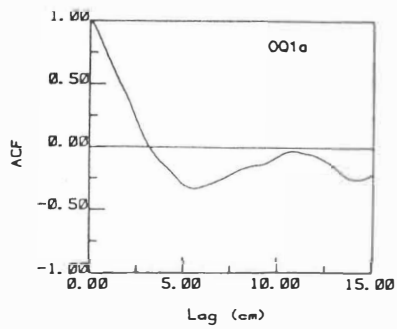
OQ1a
ACF
Lag (cm)

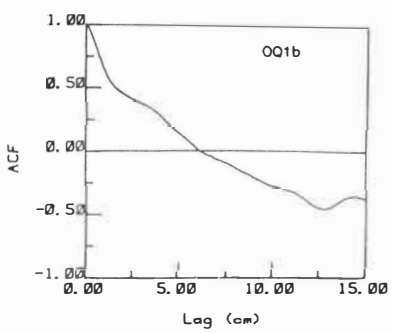
OQ1b
ACF
Lag (cm)

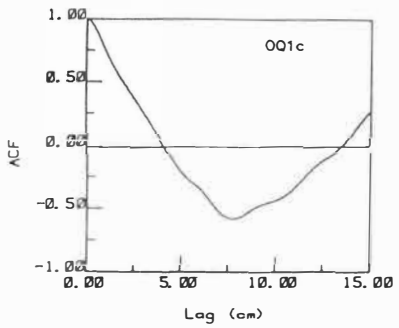
OQ1c
ACF
Lag (cm)

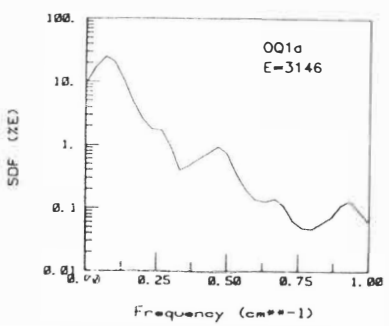
OQ1a
E=3146
SDF (%E)
Frequency (cm**-1)

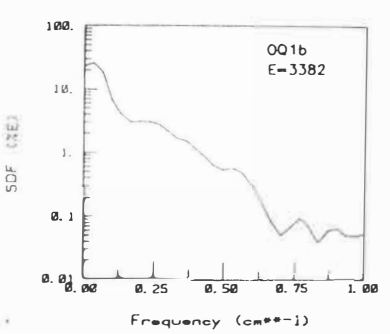
OQ1b
E=3382
SDF (%E)
Frequency (cm**-1)

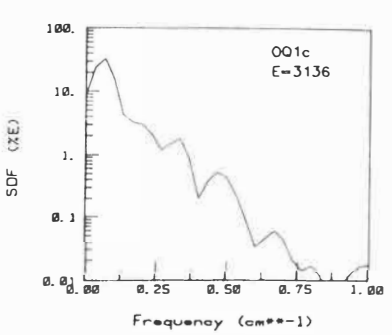
OQ1c
E=3136
SDF (%E)
Frequency (cm**-1)

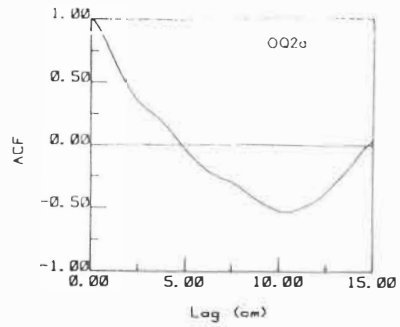
OQ2a
ACF
Lag (cm)

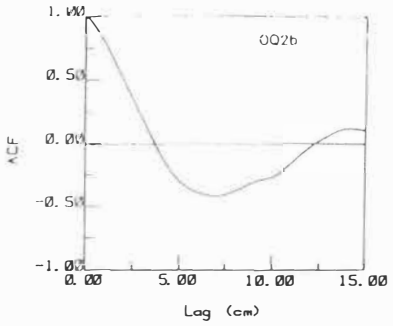
OQ2b
ACF
Lag (cm)

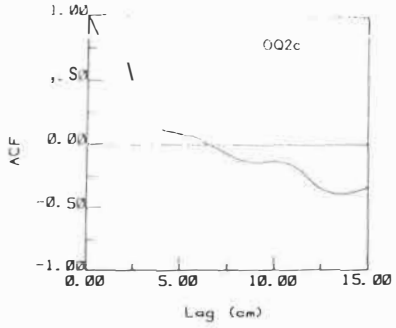
OQ2c
ACF
Lag (cm)

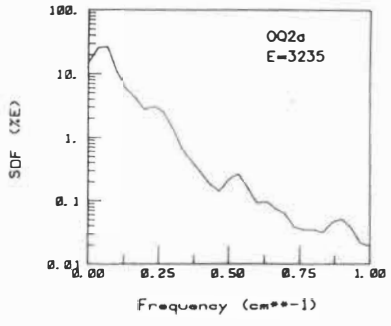
OQ2a
E=3235
SDF (%E)
Frequency (cm**-1)

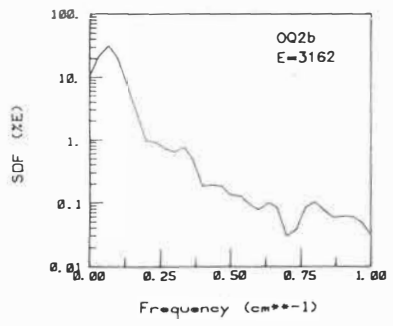
OQ2b
E=3162
SDF (%E)
Frequency (cm**-1)

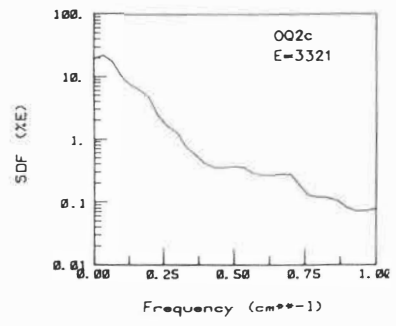
OQ2c
E=3321
SDF (%E)
Frequency (cm**-1)

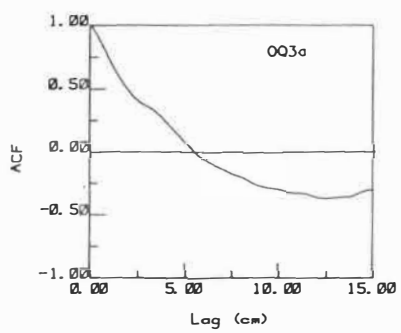
OQ3a
ACF
Lag (cm)

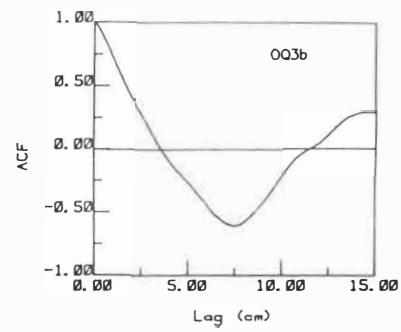
OQ3b
ACF
Lag (cm)

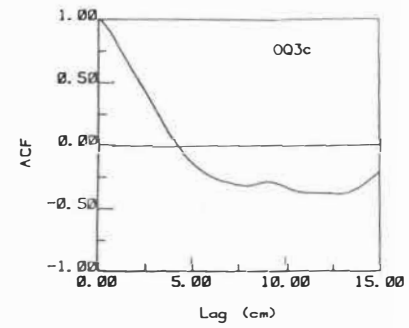
OQ3c
ACF
Lag (cm)

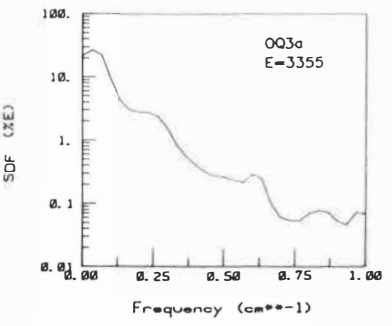
OQ3a
E=3355
SDF (%E)
Frequency (cm**-1)

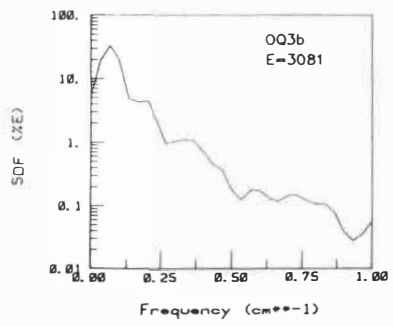
OQ3b
E=3081
SDF (%E)
Frequency (cm**-1)

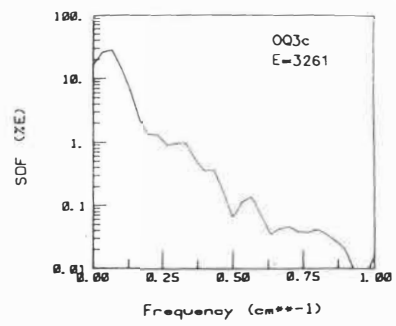
OQ3c
E=3261
SDF (%E)
Frequency (cm**-1)

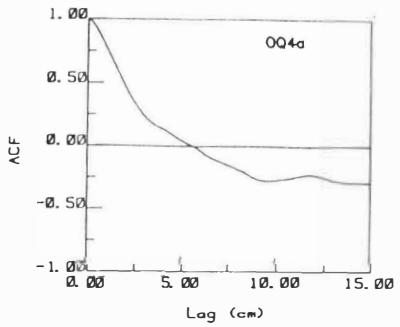
OQ4a
ACF
Lag (cm)

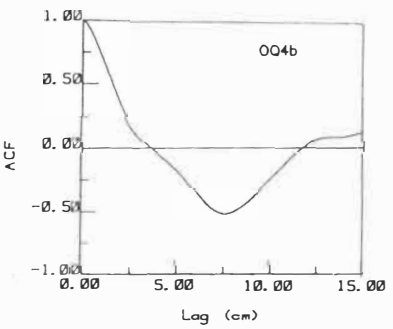
OQ4b
ACF
Lag (cm)

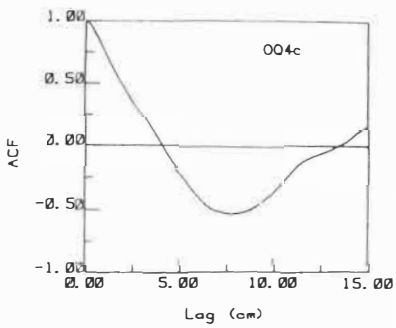
OQ4c
ACF
Lag (cm)

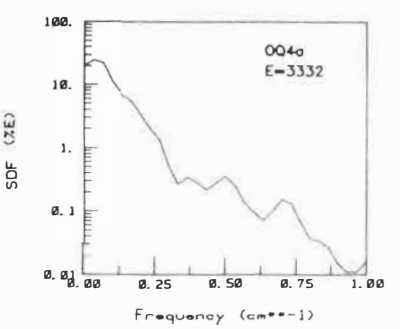
OQ4a
E=3332
SDF (%E)
Frequency (cm**-1)

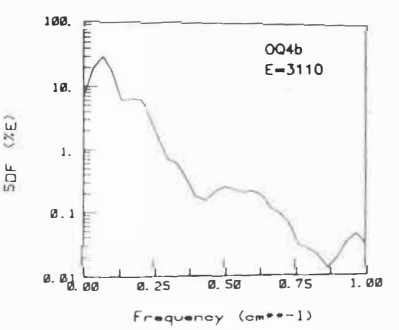
OQ4b
E=3110
SDF (%E)
Frequency (cm**-1)

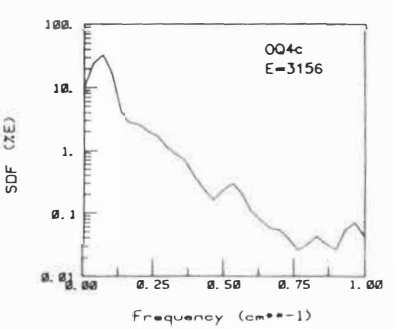
OQ4c
E=3156
SDF (%E)
Frequency (cm**-1)

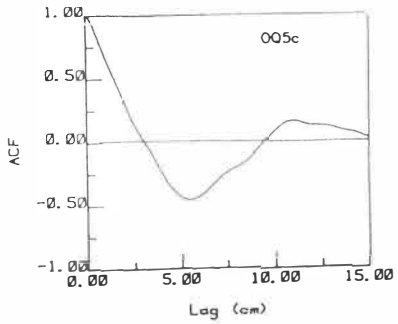
0Q5c
ACF
Lag (cm)

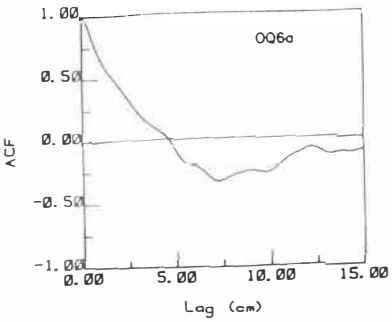
0Q6a
ACF
Lag (cm)

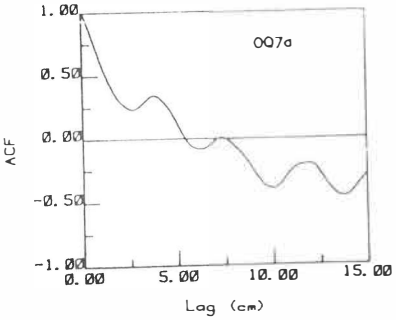
0Q7a
ACF
Lag (cm)

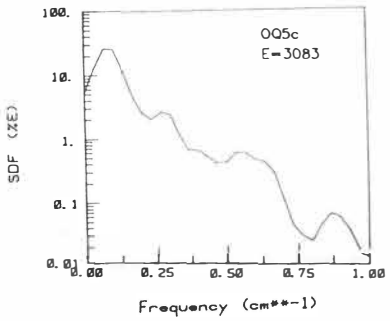
0Q5c
E=3083
SDF (%E)
Frequency (cm**-1)

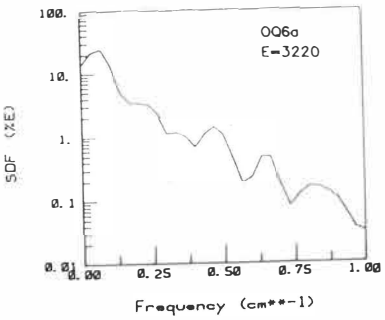
0Q6a
E=3220
SDF (%E)
Frequency (cm**-1)

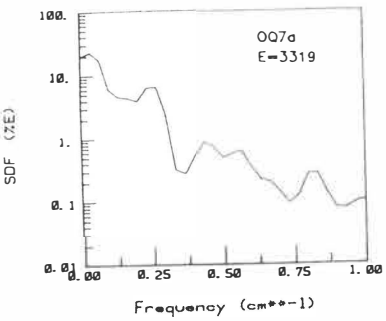
0Q7a
E=3319
SDF (%E)
Frequency (cm**-1)

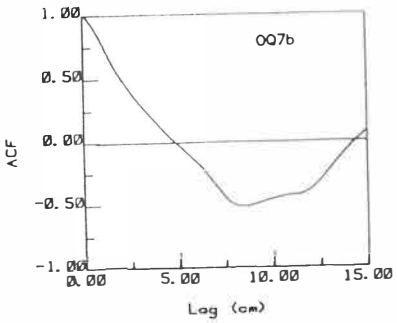
0Q7b
ACF
Lag (cm)

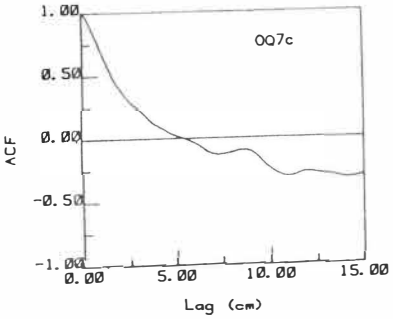
0Q7c
ACF
Lag (cm)

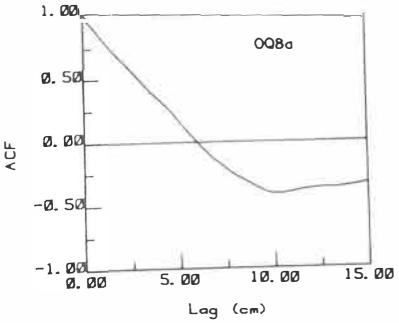
0Q8a
ACF
Lag (cm)

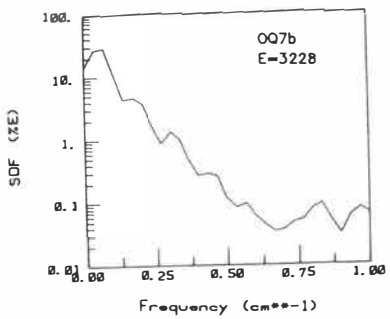
0Q7b
E=3228
SDF (%E)
Frequency (cm**-1)

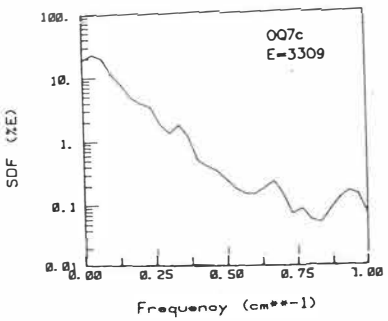
0Q7c
E=3309
SDF (%E)
Frequency (cm**-1)

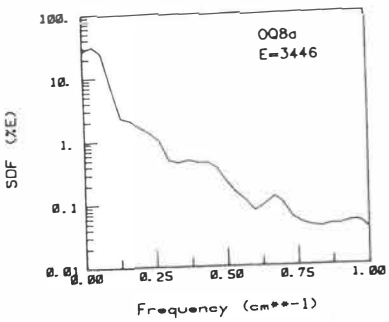
0Q8a
E=3446
SDF (%E)
Frequency (cm**-1)

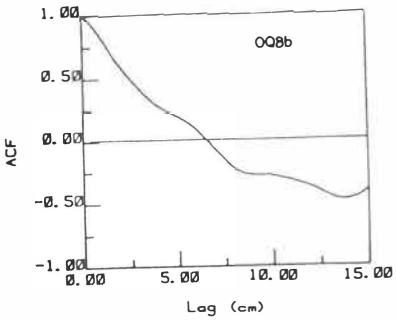
0Q8b
ACF
Lag (cm)

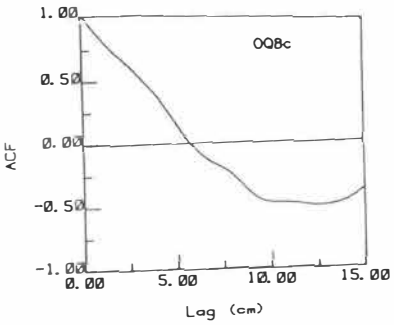
0Q8c
ACF
Lag (cm)

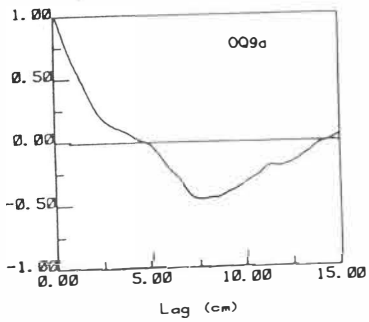
0Q9a
ACF
Lag (cm)

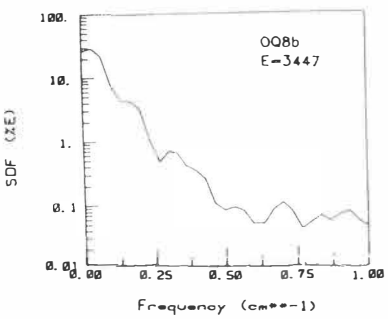
0Q8b
E=3447
SDF (%E)
Frequency (cm**-1)

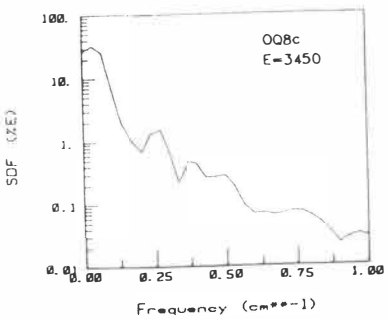
0Q8c
E=3450
SDF (%E)
Frequency (cm**-1)

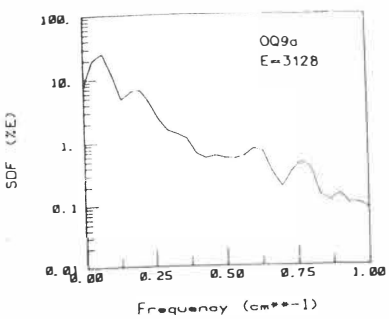
0Q9a
E=3128
SDF (%E)
Frequency (cm**-1)

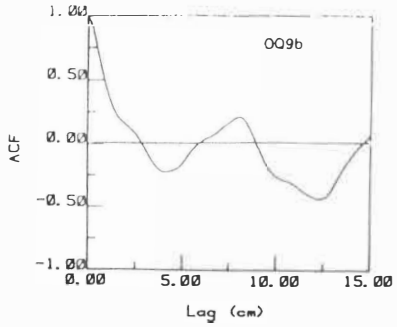
OQ9b
ACF
Lag (cm)

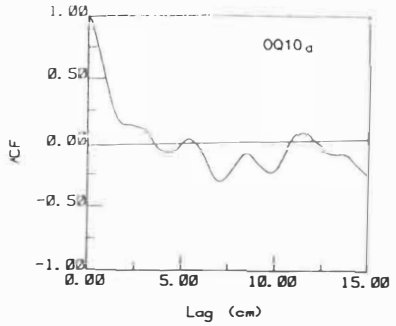
OQ10a
ACF
Lag (cm)

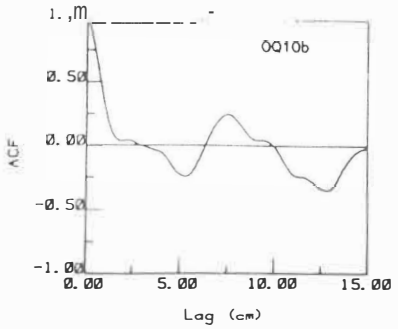
OQ10b
ACF
Lag (cm)

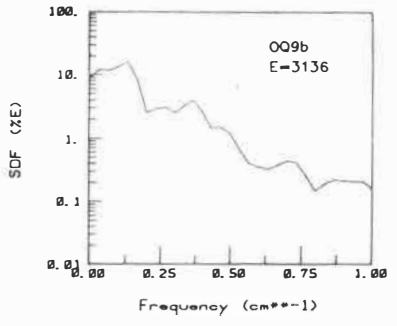
OQ9b
E=3136
SDF (%E)
Frequency (cm**-1)

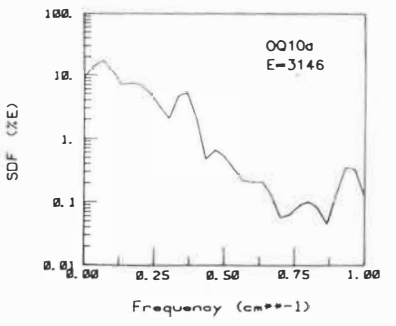
OQ10a
E=3146
SDF (%E)
Frequency (cm**-1)

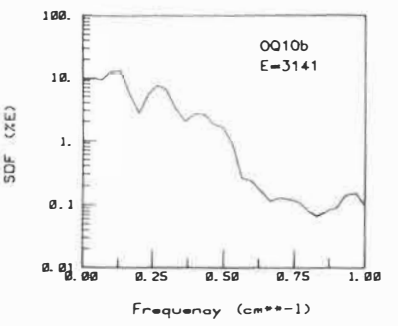
OQ10b
E=3141
SDF (%E)
Frequency (cm**-1)

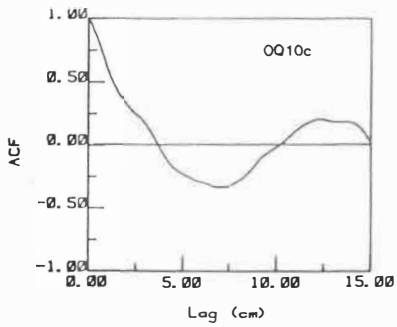
OQ10c
ACF
Lag (cm)

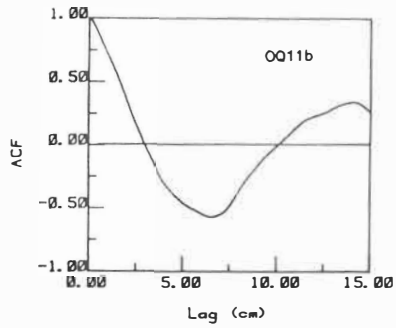
OQ11b
ACF
Lag (cm)

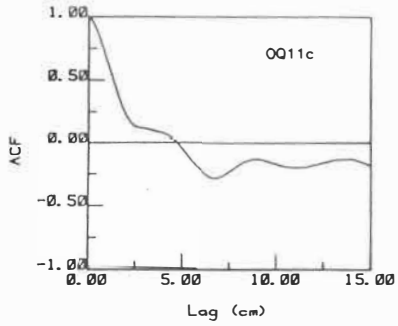
OQ11c
ACF
Lag (cm)

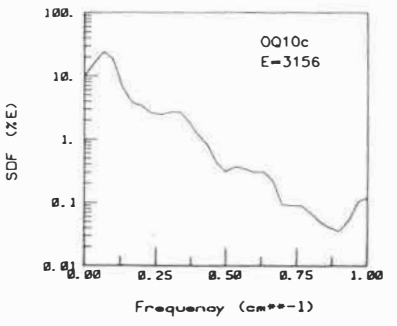
OQ10c
E=3156
SDF (%E)
Frequency (cm**-1)

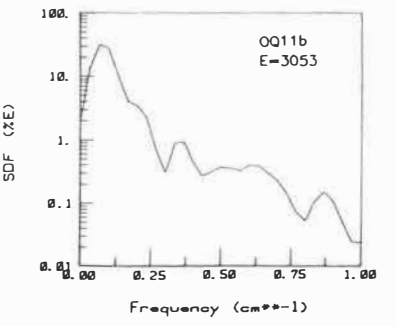
OQ11b
E=3053
SDF (%E)
Frequency (cm**-1)

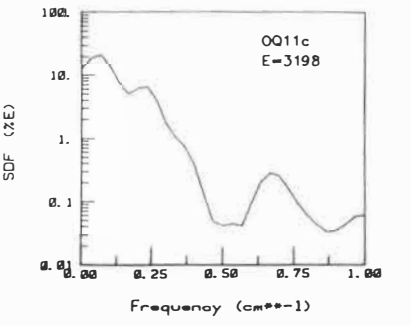
OQ11c
E=3198
SDF (%E)
Frequency (cm**-1)

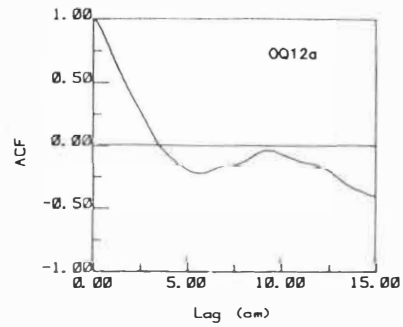
OQ12a
ACF
Lag (cm)

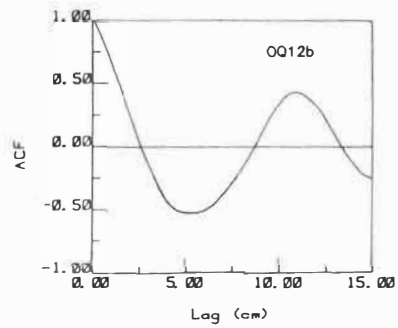
OQ12b
ACF
Lag (cm)

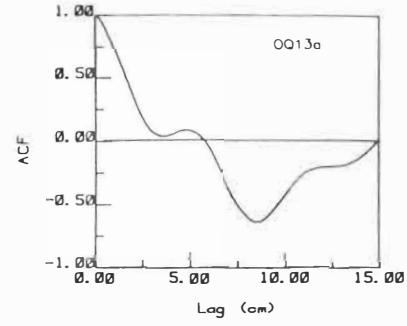
OQ13a
ACF
Lag (cm)

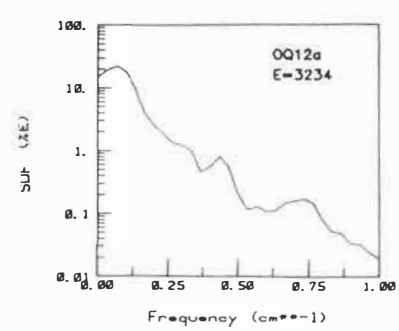
OQ12a
E=3234
Frequency (cm**-1)

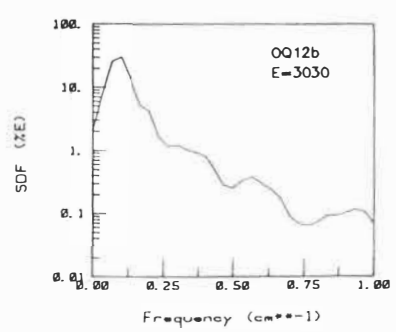
OQ12b
E=3030
SDF (%E)
Frequency (cm**-1)

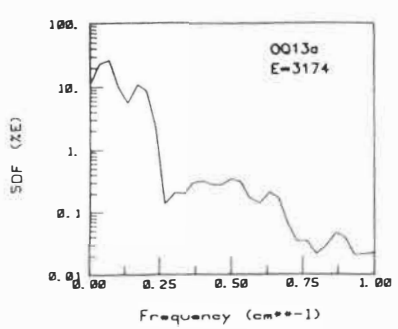
OQ13a
E=3174
SDF (%E)
Frequency (cm**-1)

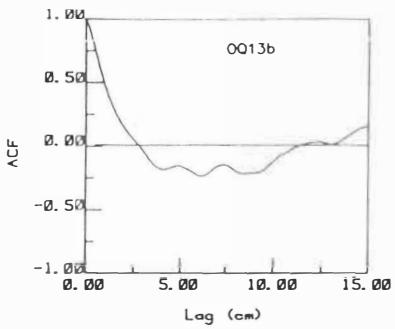
0Q13b
ACF
Lag (cm)

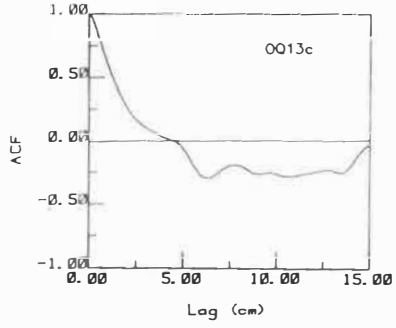
0Q13c
ACF
Lag (cm)

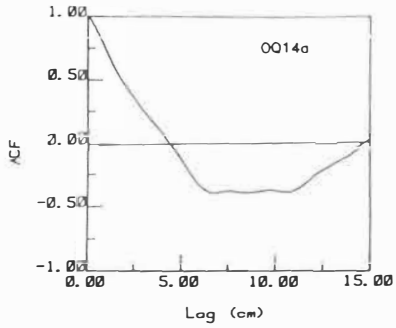
0Q14a
ACF
Lag (cm)

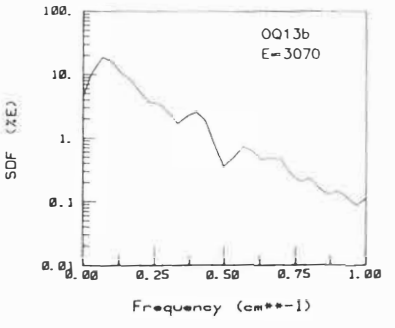
0Q13b
E=3070
SDF (%E)
Frequency (cm**-1)

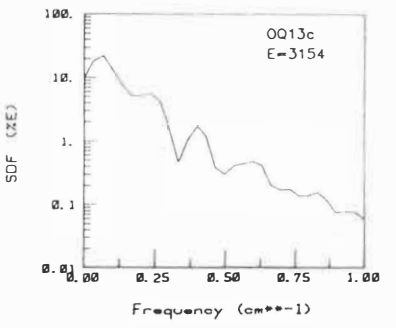
0Q13c
E=3154
SDF (%E)
Frequency (cm**-1)

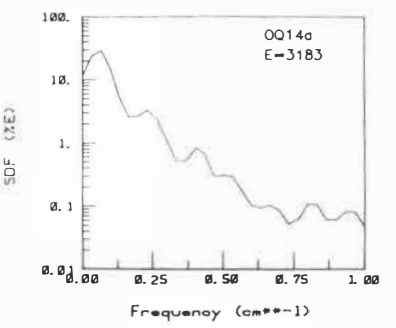
0Q14a
E=3183
SDF (%E)
Frequency (cm**-1)

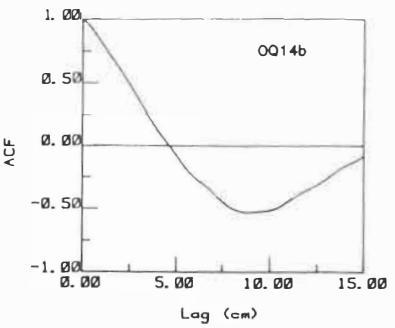
0Q14b
ACF
Lag (cm)

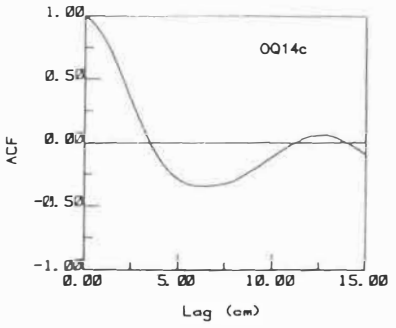
0Q14c
ACF
Lag (cm)

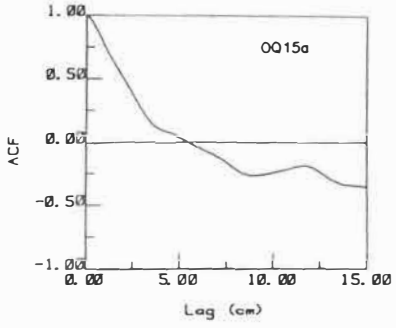
0Q15a
ACF
Lag (cm)

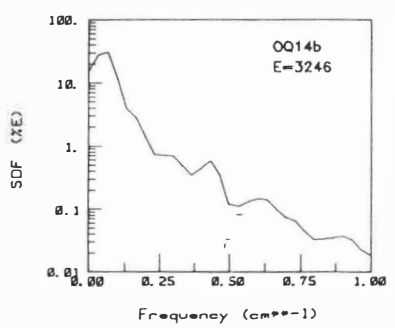
0Q14b
E=3246
SDF (%E)
Frequency (cm**-1)

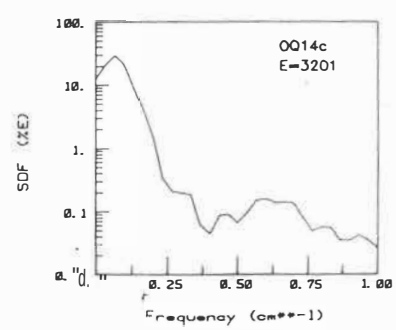
0Q14c
E=3201
SDF (%E)
Frequency (cm**-1)

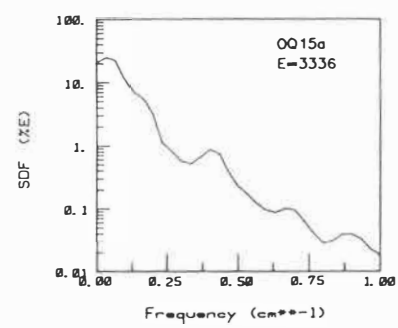
0Q15a
E=3336
SDF (%E)
Frequency (cm**-1)

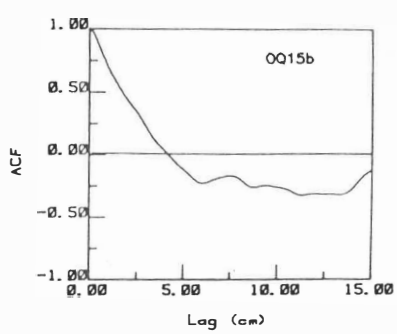
0Q15b
ACF
Lag (cm)

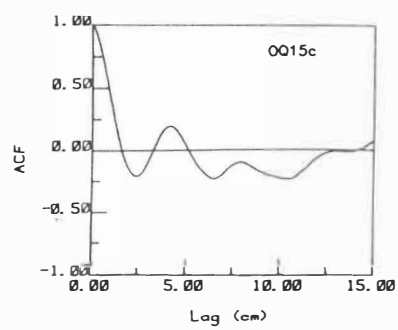
0Q15c
ACF
Lag (cm)

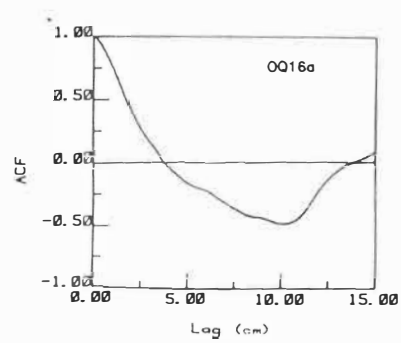
0Q16a
ACF
Lag (cm)

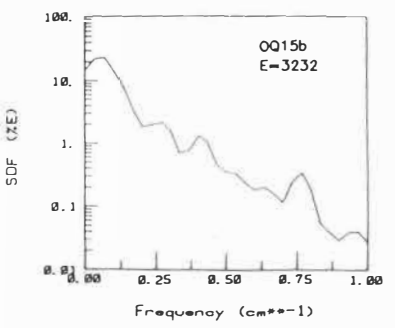
0Q15b
E=3232
SDF (%E)
Frequency (cm**-1)

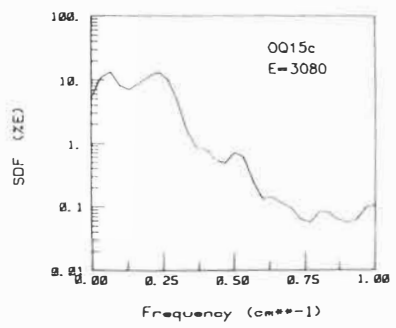
0Q15c
E=3080
SDF (%E)
Frequency (cm**-1)

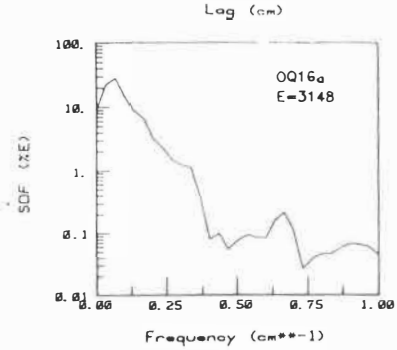
0Q16a
E=3148
SDF (%E)
Frequency (cm**-1)

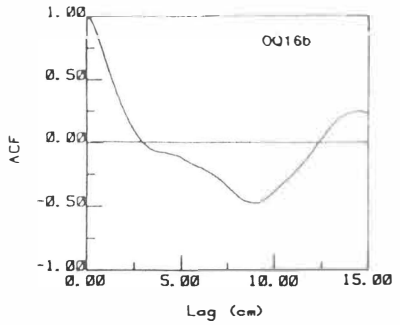
OQ16b
ACF
Lag (cm)

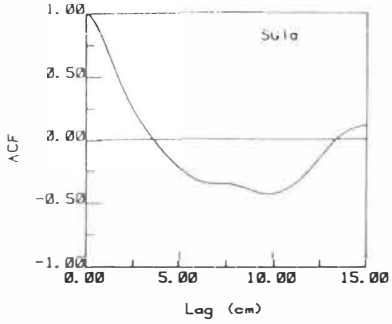
SG1a
ACF
Lag (cm)

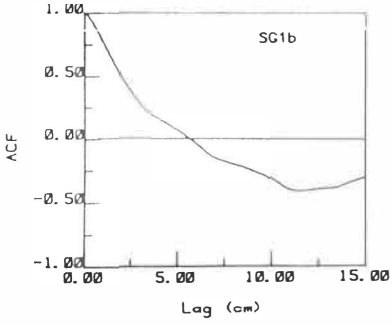
SG1b
ACF
Lag (cm)

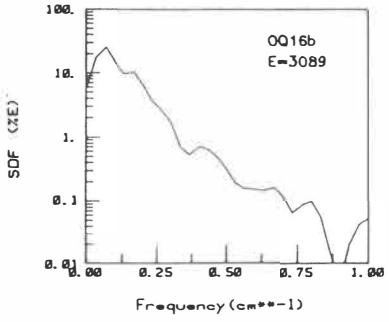
OQ16b
E=3089
SDF (%E)
Frequency (cm**-1)

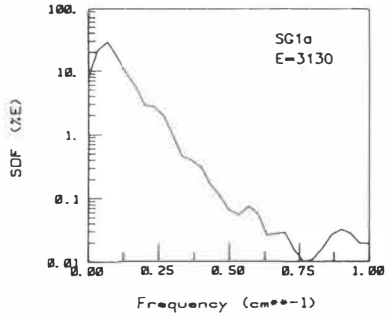
SG1a
E=3130
SDF (%E)
Frequency (cm**-1)

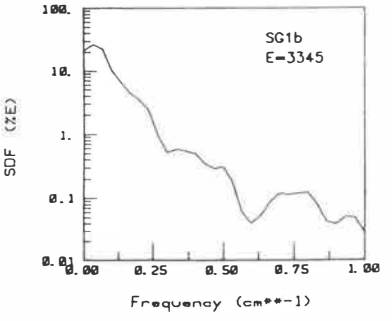
SG1b
E=3345
SDF (%E)
Frequency (cm**-1)

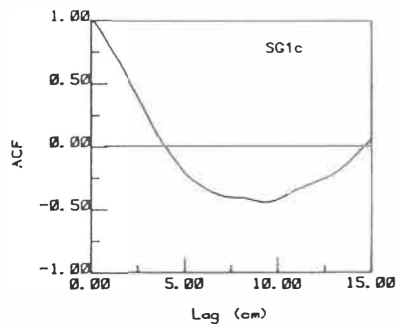
SG1c
ACF
Lag (cm)

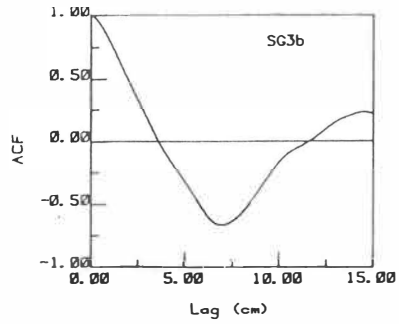
SG3b
ACF
Lag (cm)

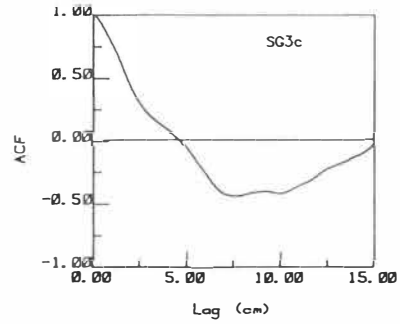
SG3c
ACF
Lag (cm)

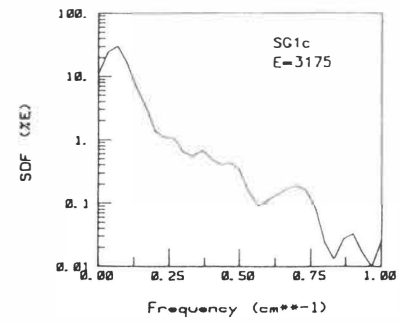
SG1c
E=3175
SDF (%E)
Frequency (cm**-1)

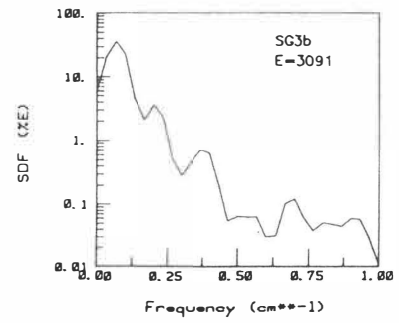
SG3b
E=3091
SDF (%E)
Frequency (cm**-1)

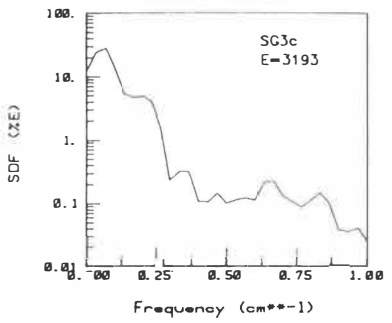
SG3c
E=3193
SDF (%E)
Frequency (cm**-1)

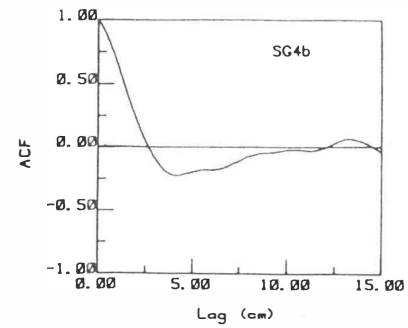
SG4b
ACF
Lag (cm)

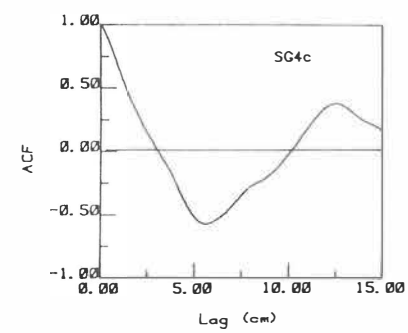
SG4c
ACF
Lag (cm)

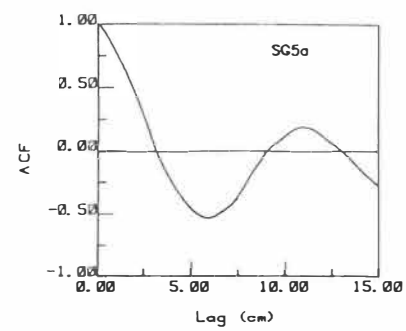
SG5a
ACF
Lag (cm)

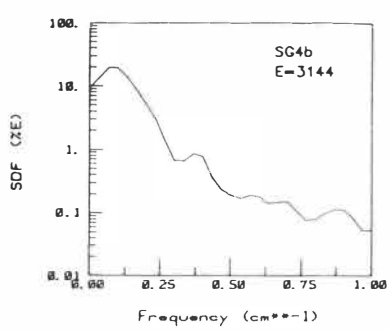
SG4b
E=3144
SDF (%E)
Frequency (cm**-1)

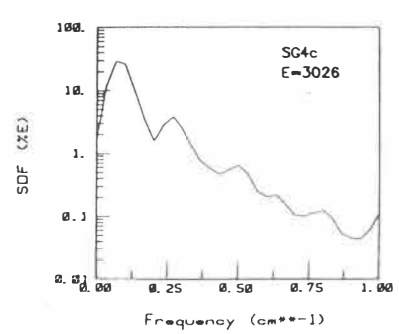
SG4c
E=3026
SDF (%E)
Frequency (cm**-1)

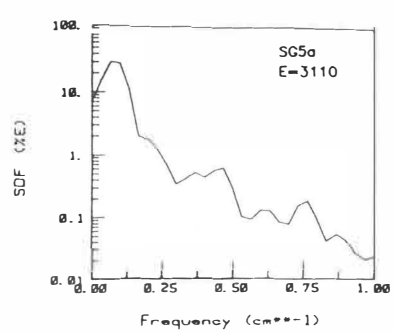
SG5a
E=3110
SDF (%E)
Frequency (cm**-1)

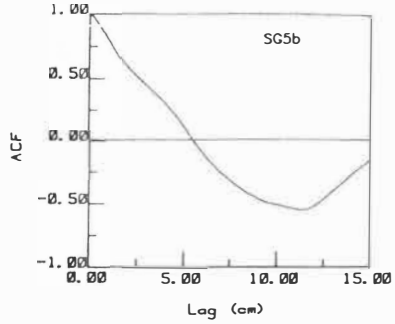
SG5b
ACF
Lag (cm)

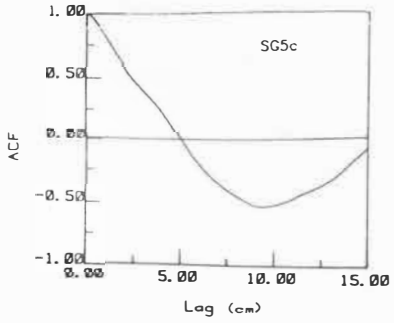
SG5c
ACF
Lag (cm)

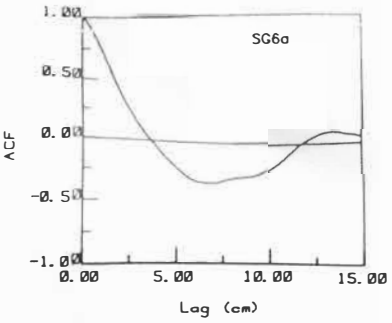
SG6a
ACF
Lag (cm)

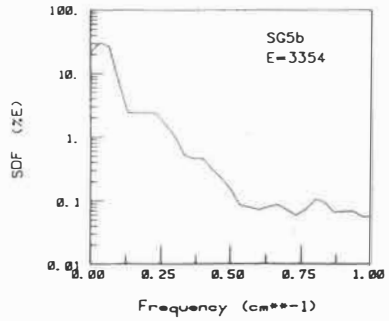
SG5b
E=3354
SDF (%E)
Frequency (cm**-1)

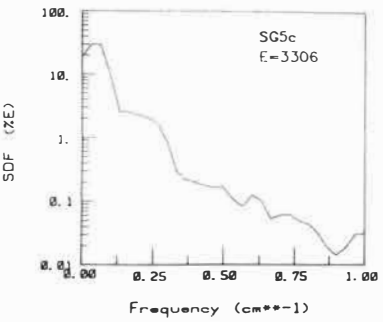
SG5c
E=3306
SDF (%E)
Frequency (cm**-1)

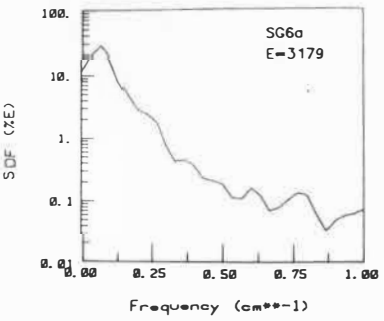
SG6a
E=3179
SDF (%E)
Frequency (cm**-1)

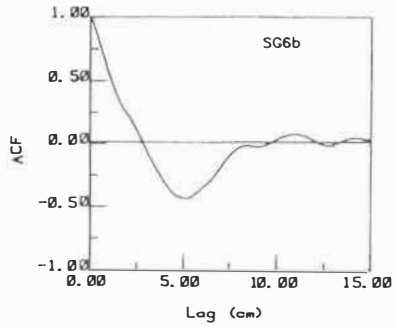
SG6b
ACF
Lag (cm)

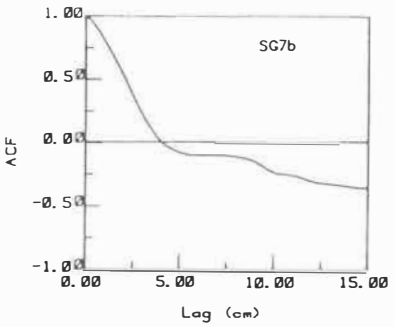
SG7b
ACF
Lag (cm)

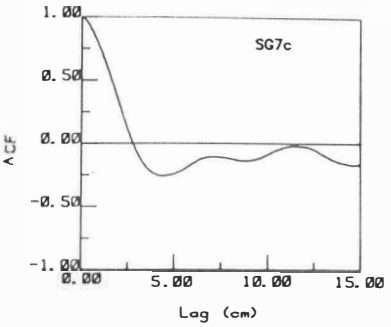
SG7c
ACF
Lag (cm)

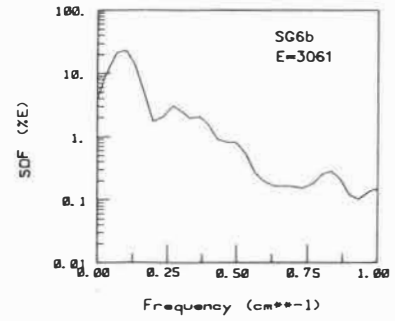
SG6b
E=3061
SDF (%E)
Frequency (cm**-1)

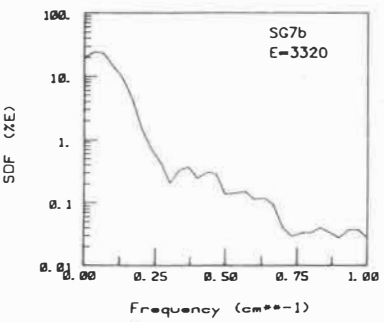
SG7b
E=3320
SDF (%E)
Frequency (cm**-1)

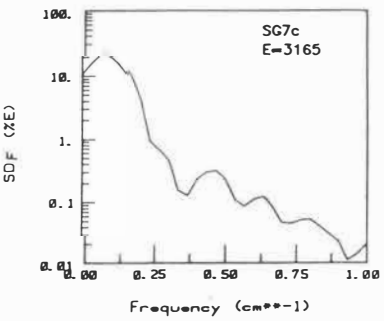
SG7c
E=3165
SDF (%E)
Frequency (cm**-1)

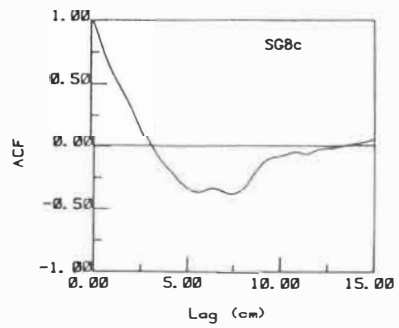
SG8c
ACF
Lag (cm)

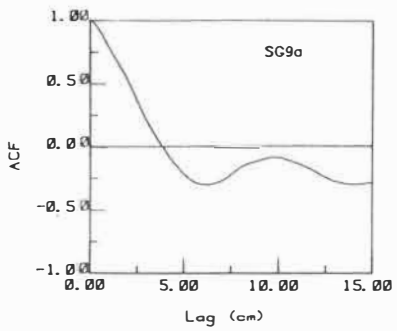
SG9a
ACF
Lag (cm)

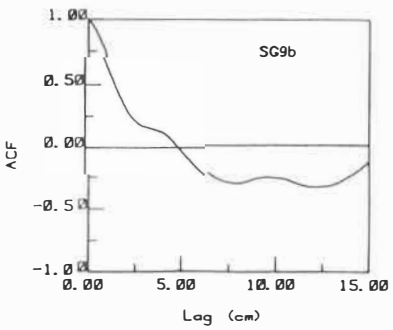
SG9b
ACF
Lag (cm)

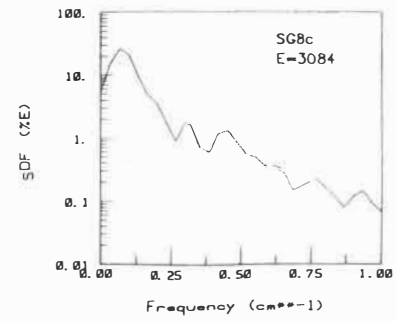
SG8c
E=3084
SDF (%E)
Frequency (cm**-1)

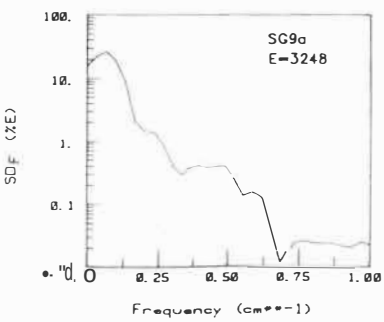
SG9a
E=3248
SDF (%E)
Frequency (cm**-1)

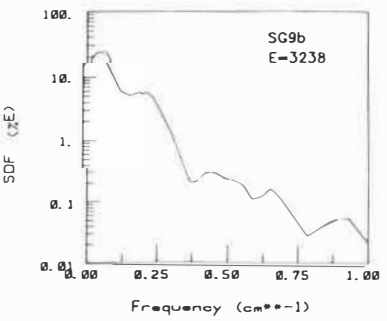
SG9b
E=3238
SDF (%E)
Frequency (cm**-1)

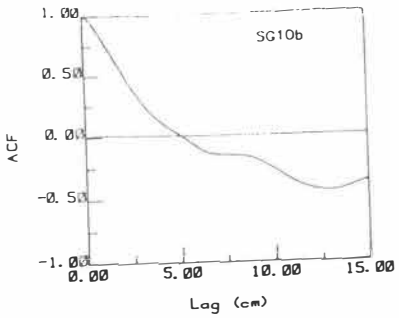
SG10b
ACF
Lag (cm)

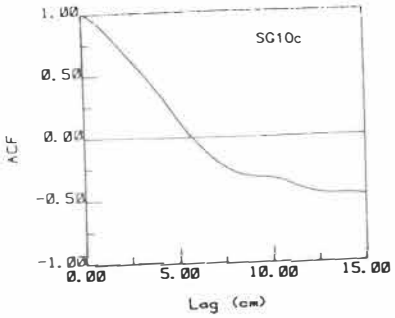
SG10c
ACF
Lag (cm)

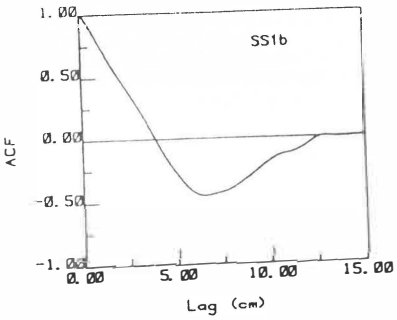
SS1b
ACF
Lag (cm)

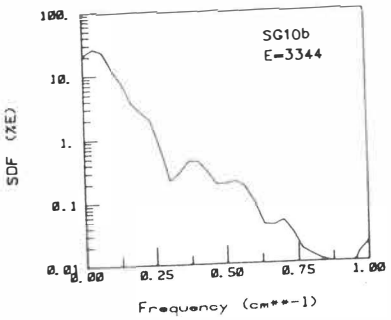
SG10b
E=3344
SDF (%E)
Frequency (cm**-1)

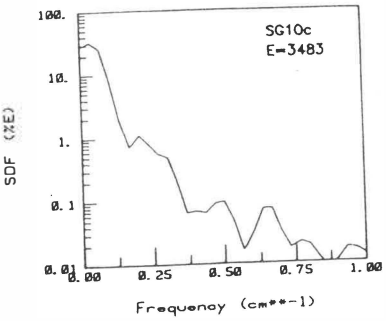
SG10c
E=3483
SDF (%E)
Frequency (cm**-1)

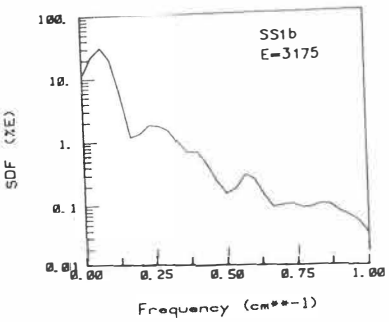
SS1b
E=3175
SDF (%E)
Frequency (cm**-1)

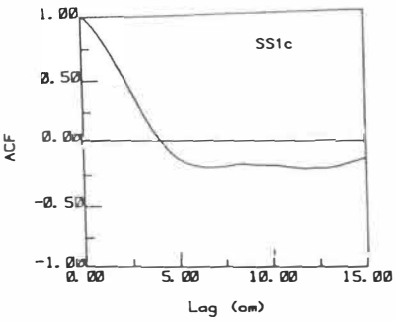
SS1c
ACF
Lag (cm)

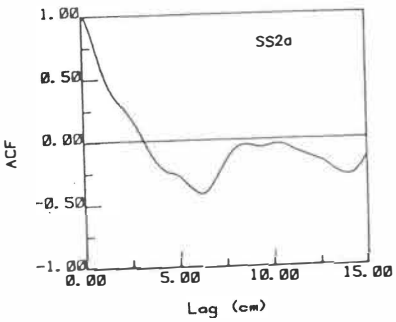
SS2a
ACF
Lag (cm)

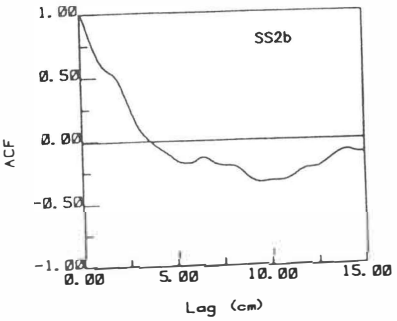
SS2b
ACF
Lag (cm)

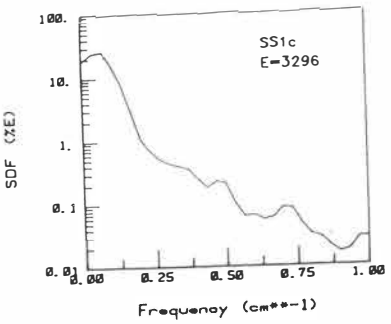
SS1c
E=3296
SDF (%E)
Frequency (cm**-1)

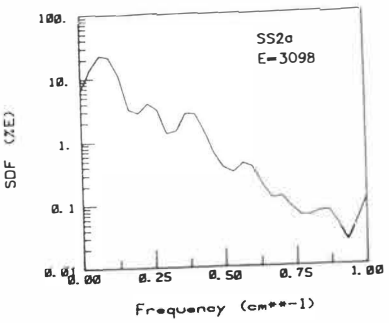
SS2a
E=3098
SDF (%E)
Frequency (cm**-1)

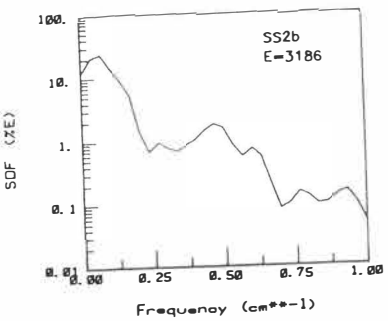
SS2b
E=3186
SDF (%E)
Frequency (cm**-1)

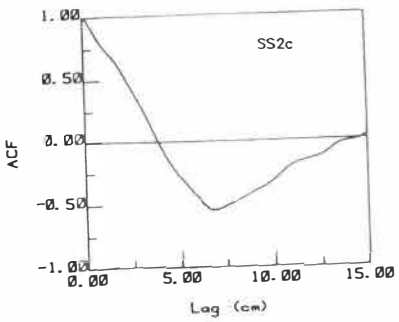
SS2c
ACF
Lag (cm)

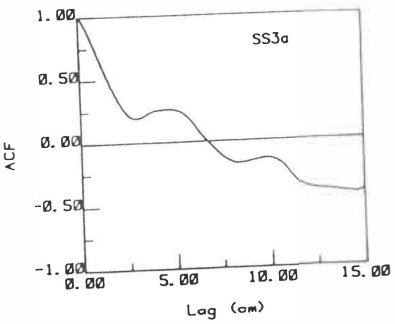
SS3a
ACF
Lag (cm)

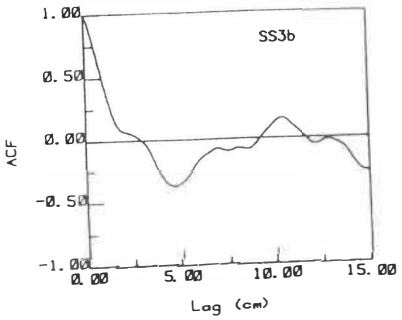
SS3b
ACF
Lag (cm)

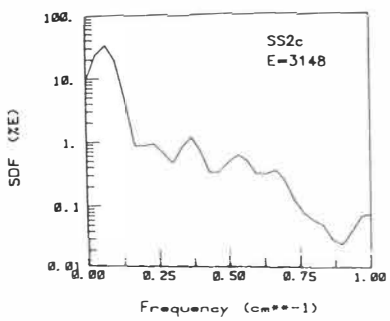
SS2c
E=3148
SDF (%E)
Frequency (cm**-1)

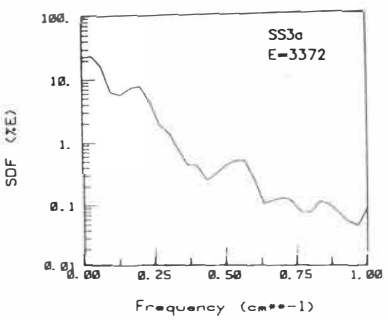
SS3a
E=3372
SDF (%E)
Frequency (cm**-1)

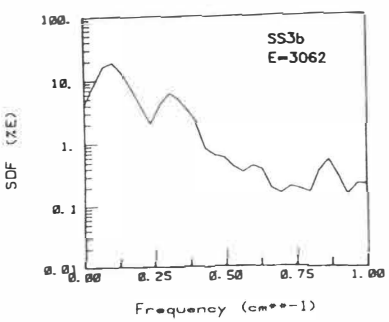
SS3b
E=3062
SDF (%E)
Frequency (cm**-1)

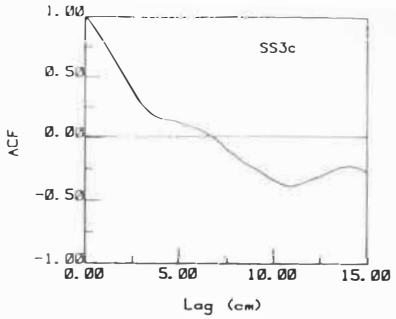
SS3c
ACF
Lag (cm)

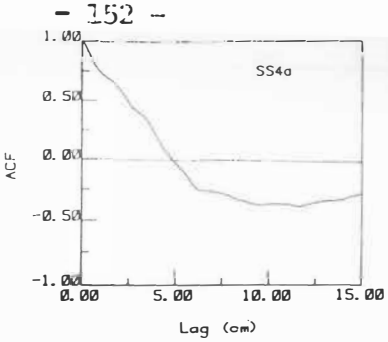
SS4a
ACF
Lag (cm)

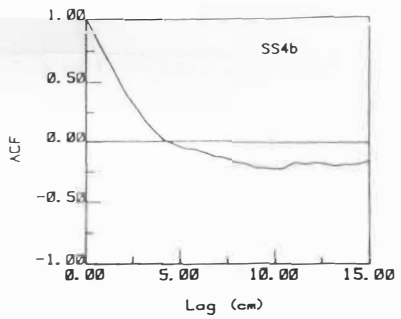
SS4b
ACF
Lag (cm)

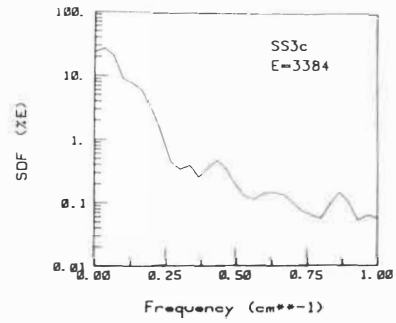
SS3c
E=3384
SDF (%E)
Frequency (cm**-1)

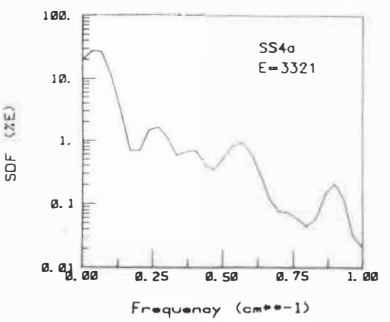
SS4a
E=3321
SDF (%E)
Frequency (cm**-1)

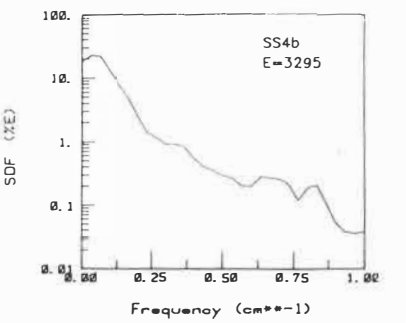
SS4b
E=3295
SDF (%E)
Frequency (cm**-1)

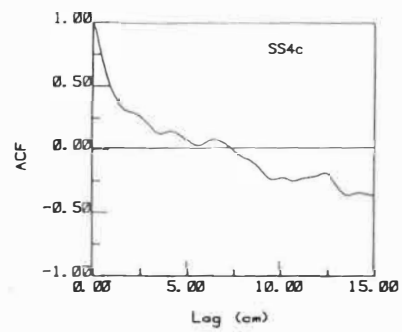
SS4c
ACF
Lag (cm)

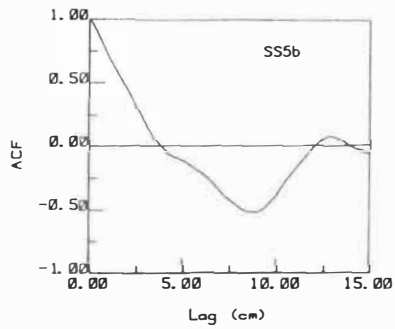
SS5b
ACF
Lag (cm)

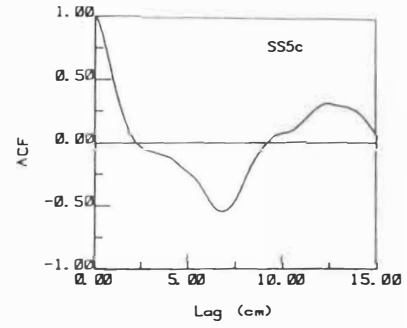
SS5c
ACF
Lag (cm)

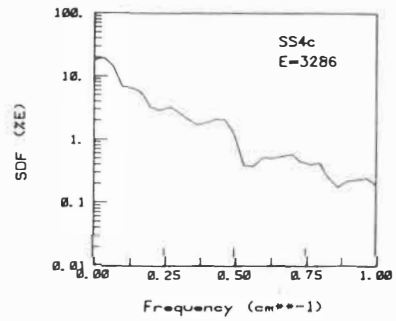
SS4c
E=3286
SDF (%E)
Frequency (cm**-1)

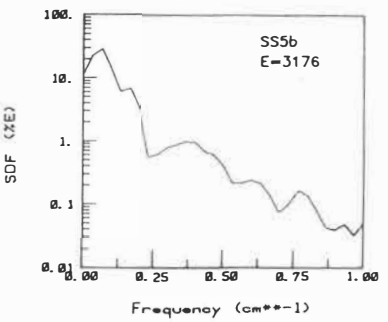
SS5b
E=3176
SDF (%E)
Frequency (cm**-1)

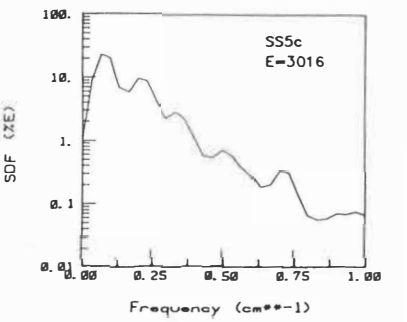
SS5c
E=3016
SDF (%E)
Frequency (cm**-1)

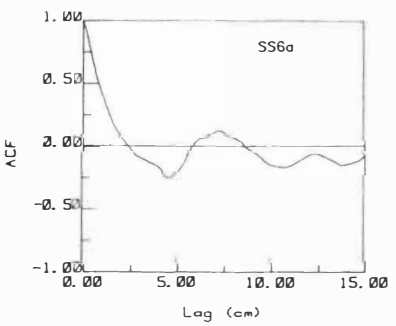
SS6a
ACF
Lag (cm)

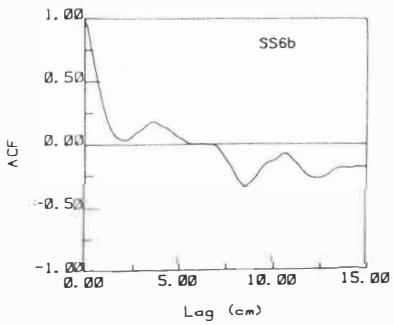
SS6b
ACF
Lag (cm)

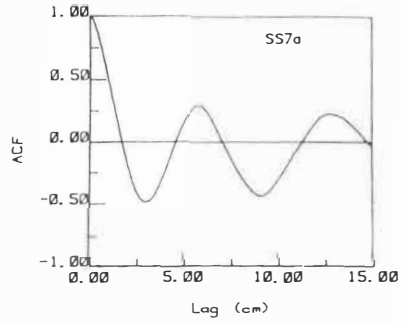
SS7a
ACF
Lag (cm)

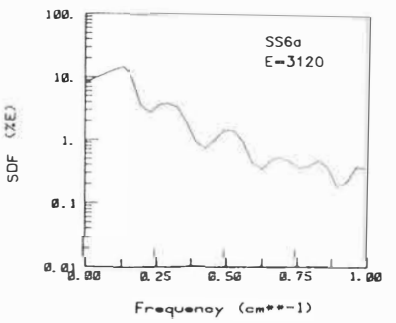
SS6a
E=3120
SDF (%E)
Frequency (cm**-1)

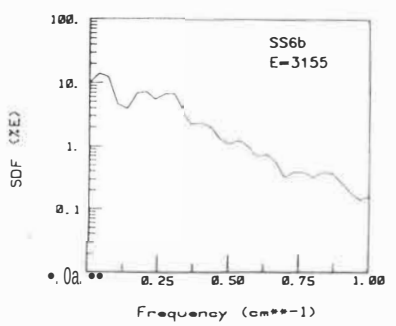
SS6b
E=3155
SDF (%E)
Frequency (cm**-1)

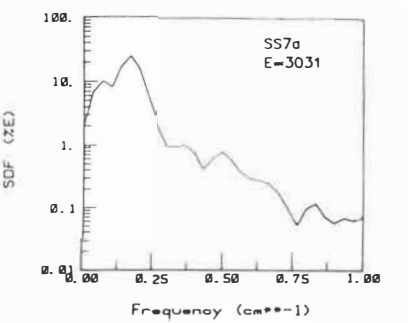
SS7a
E=3031
SDF (%E)
Frequency (cm**-1)

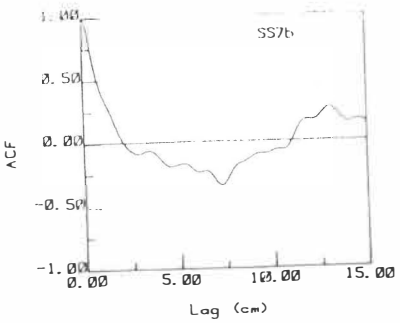
SS7b
ACF
Lag (cm)

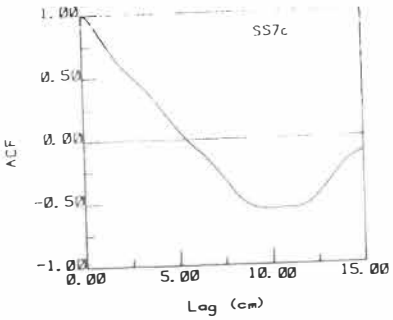
SS7c
ACF
Lag (cm)

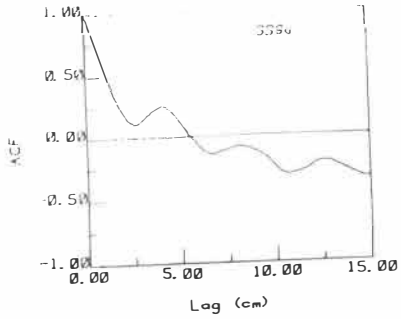
ACF
Lag (cm)

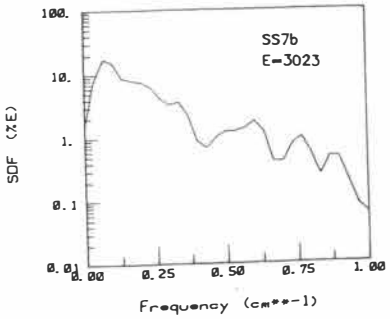
SS7b
E=3023
SDF (%E)
Frequency (cm**-1)

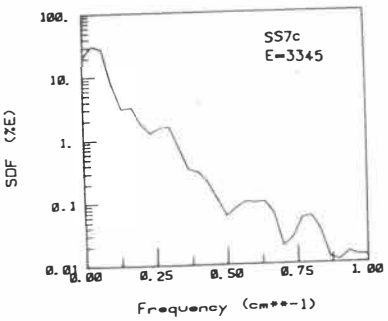
SS7c
E=3345
SDF (%E)
Frequency (cm**-1)

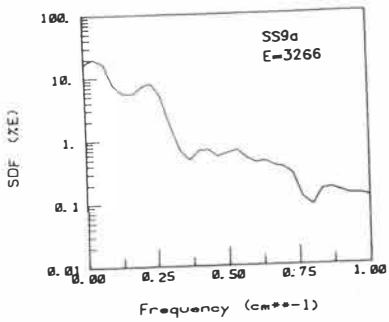
SS9a
E=3266
SDF (%E)
Frequency (cm**-1)

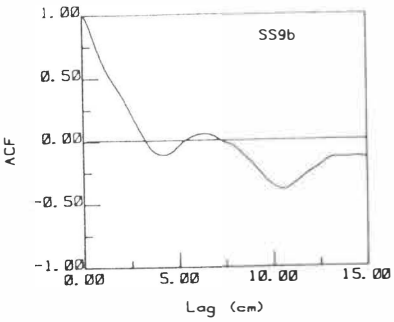
SS9b
ACF
Lag (cm)

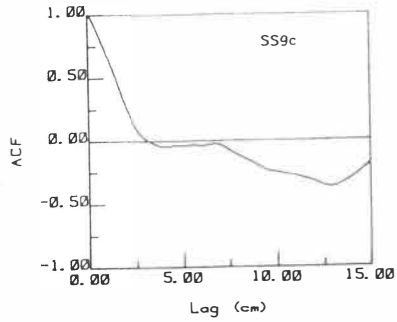
SS9c
ACF
Lag (cm)

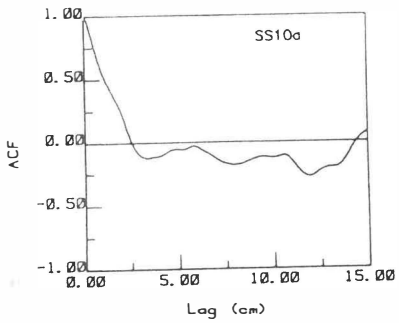
SS10a
ACF
Lag (cm)

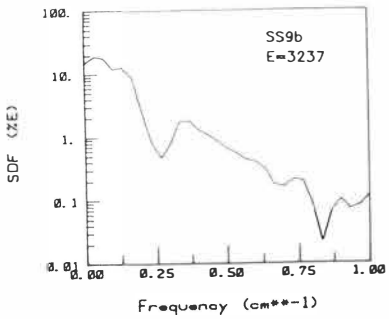
SS9b
E=3237
SDF (%E)
Frequency (cm**-1)

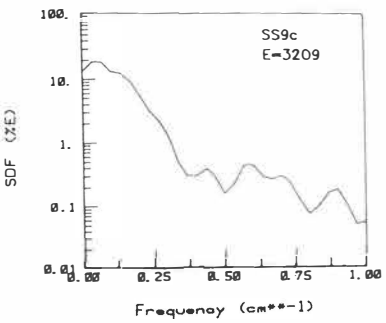
SS9c
E=3209
SDF (%E)
Frequency (cm**-1)

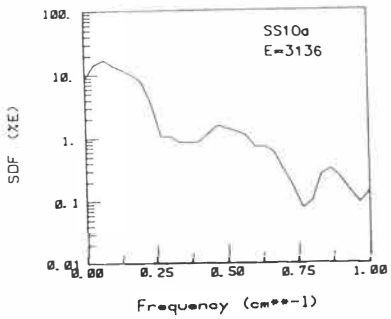
SS10a
E=3136
SDF (%E)
Frequency (cm**-1)

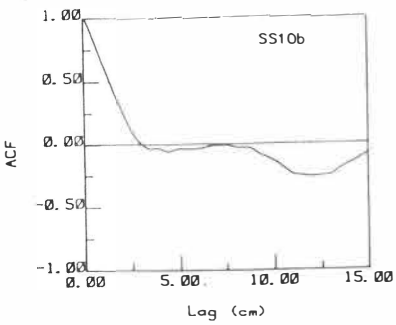
SS10b
ACF
Lag (cm)

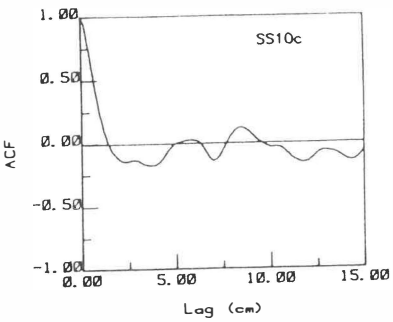
SS10c
ACF
Lag (cm)

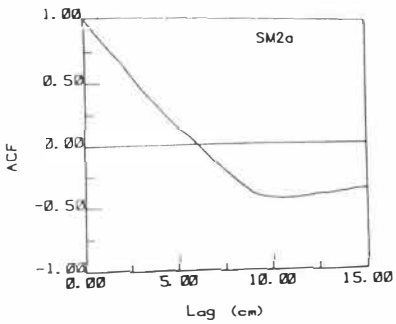
SM2a
ACF
Lag (cm)

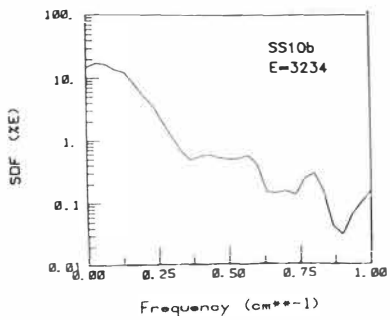
SS10b
E=3234
SDF (%E)
Frequency (cm**-1)

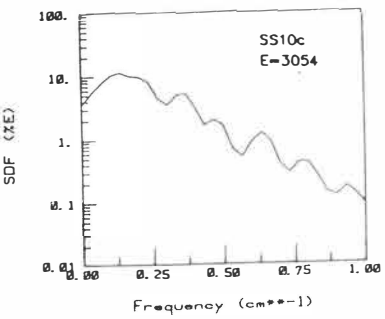
SS10c
E=3054
SDF (%E)
Frequency (cm**-1)

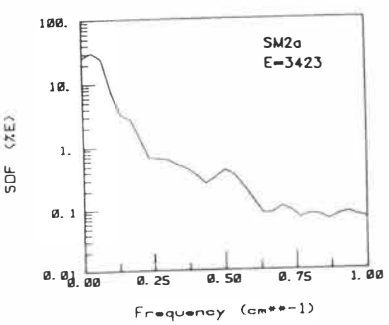
SM2a
E=3423
SDF (%E)
Frequency (cm**-1)

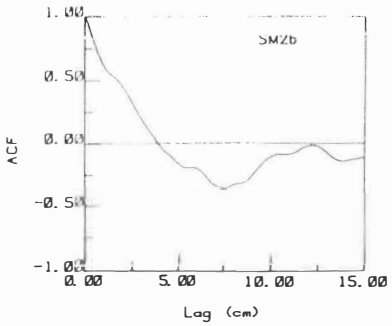
SM2b
ACF
Lag (cm)

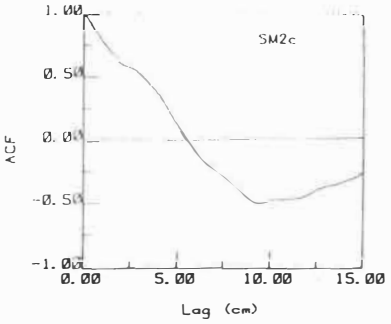
SM2c
ACF
Lag (cm)

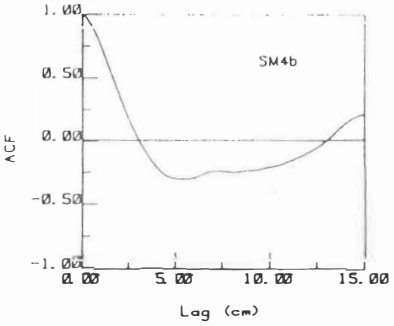
SM4b
ACF
Lag (cm)

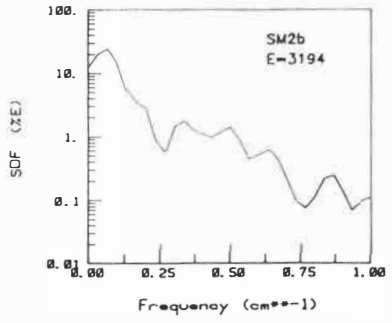
SM2b
E=3194
SDF (%E)
Frequency (cm**-1)

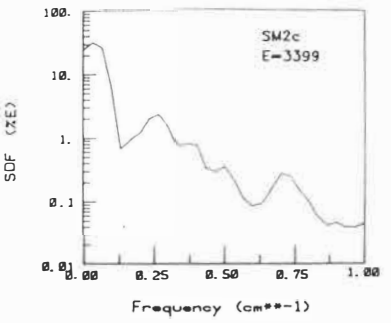
SM2c
E=3399
SDF (%E)
Frequency (cm**-1)

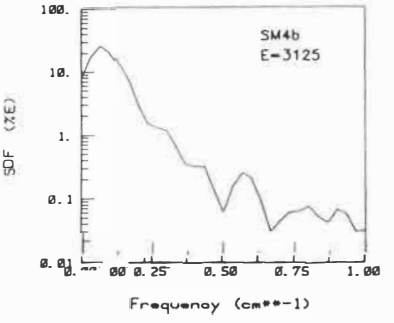
SM4b
E=3125
SDF (%E)
Frequency (cm**-1)

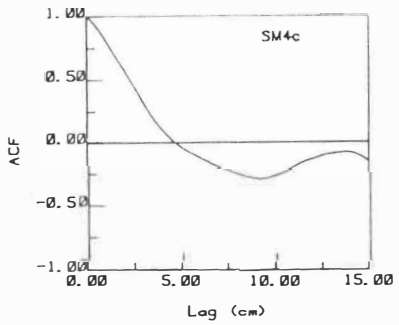
SM4c
ACF
Lag (cm)

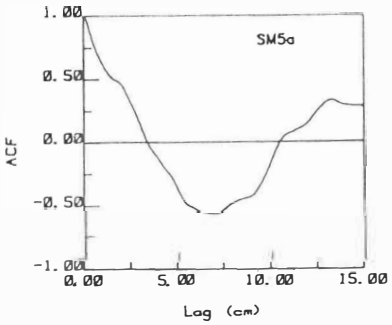
SM5a
ACF
Lag (cm)

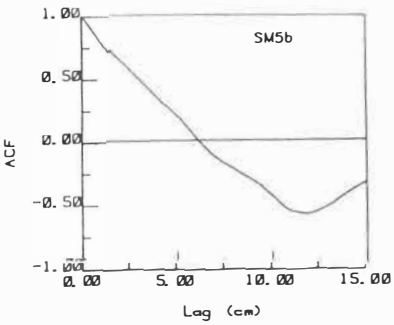
SM5b
ACF
Lag (cm)

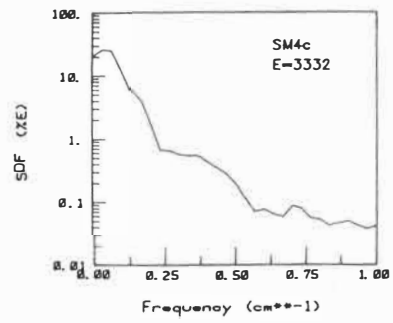
SM4c
E=3332
SDF (%E)
Frequency (cm**-1)

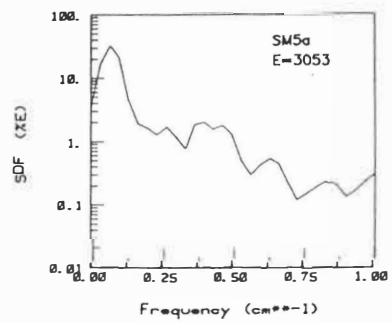
SM5a
E=3053
SDF (%E)
Frequency (cm**-1)

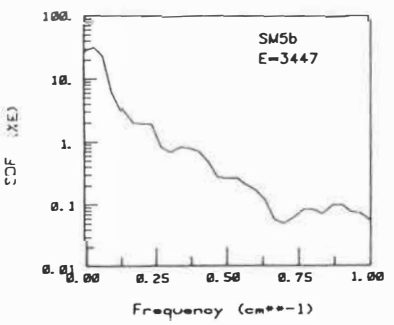
SM5b
E=3447
SDF (%E)
Frequency (cm**-1)

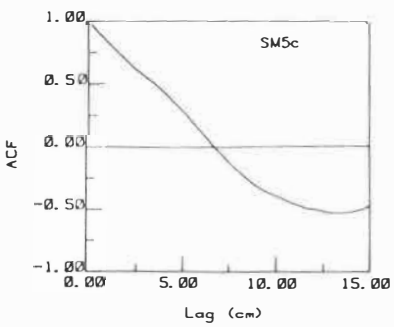
SM5c
ACF
Lag (cm)

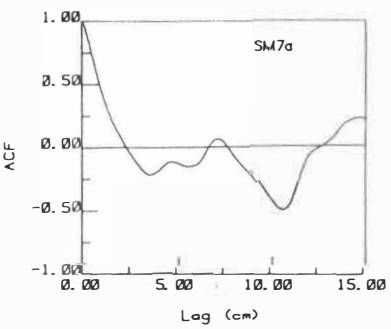
SM7a
ACF
Lag (cm)

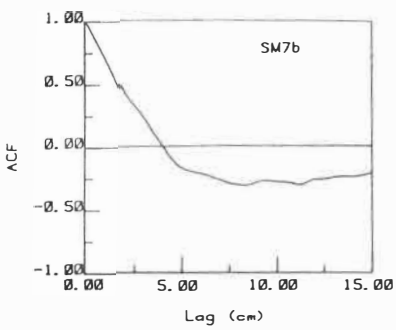
SM7b
ACF
Lag (cm)

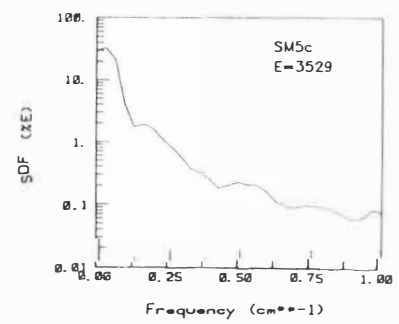
SM5c
E=3529
SDF (%E)
Frequency (cm**-1)

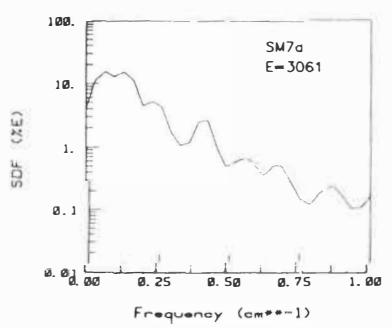
SM7a
E=3061
SDF (%E)
Frequency (cm**-1)

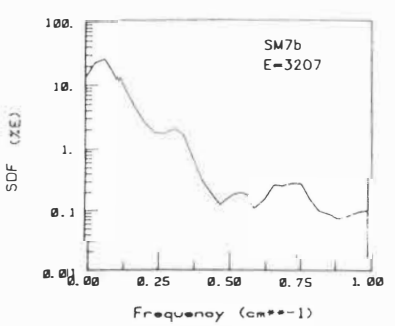
SM7b
E=3207
SDF (%E)
Frequency (cm**-1)

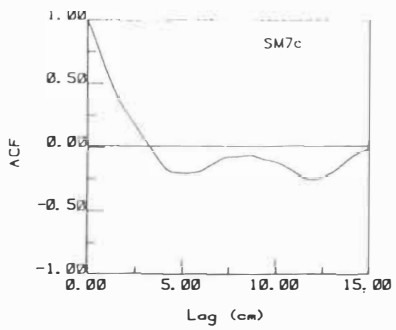
SM7c
ACF
Lag (cm)

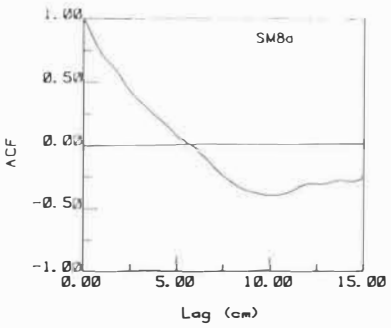
SM8a
ACF
Lag (cm)

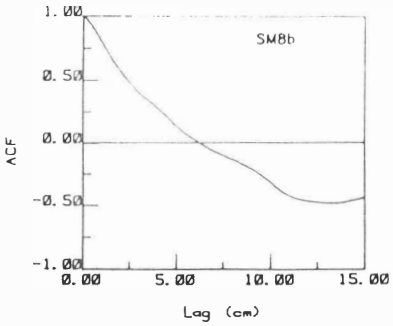
SM8b
ACF
Lag (cm)

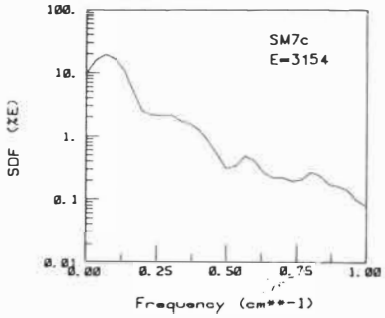
SM7c
E-3154
SDF (%E)
Frequency (cm**-1)

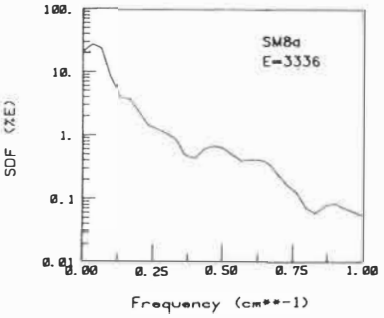
SM8a
E-3336
SDF (%E)
Frequency (cm**-1)

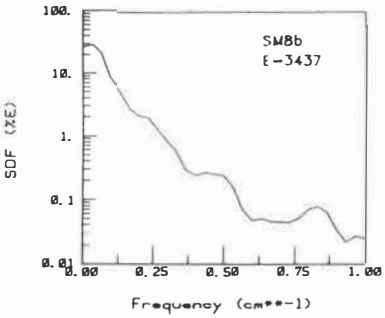
SM8b
E-3437
SDF (%E)
Frequency (cm**-1)

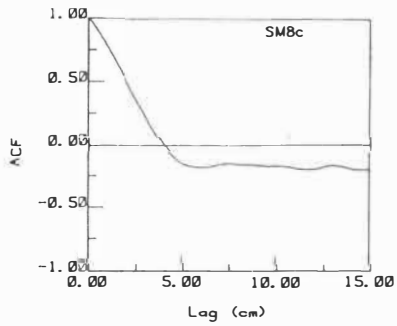
SM8c
ACF
Lag (cm)

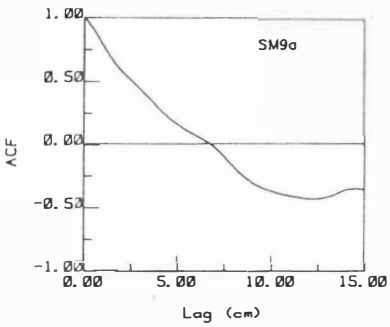
SM9a
ACF
Lag (cm)

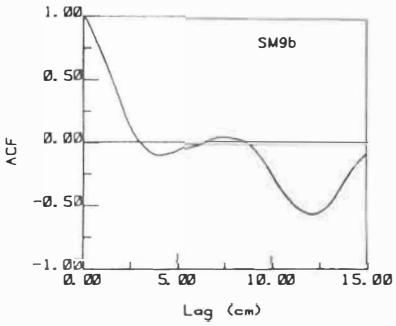
SM9b
ACF
Lag (cm)

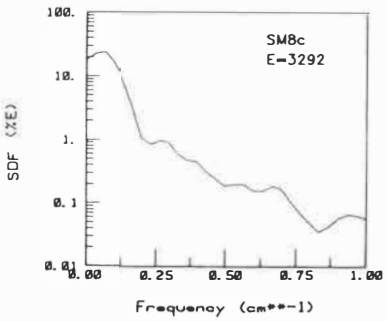
SM8c
E-3292
SDF (%E)
Frequency (cm**-1)

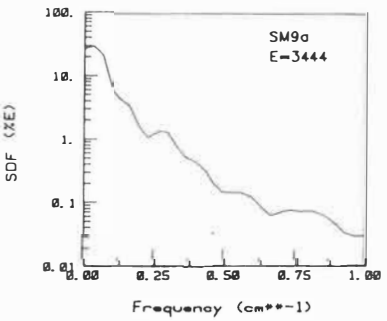
SM9a
E-3444
SDF (%E)
Frequency (cm**-1)

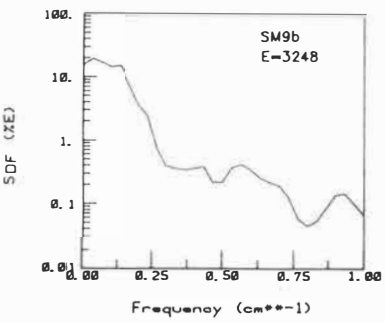
SM9b
E-3248
SDF (%E)
Frequency (cm**-1)

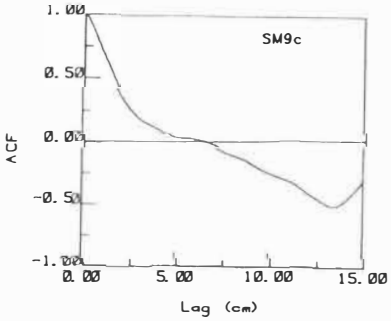
SM9c
ACF
Lag (cm)

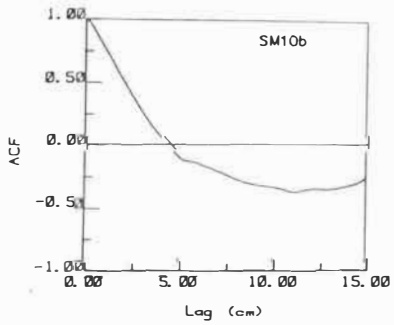
SM10b
ACF
Lag (cm)

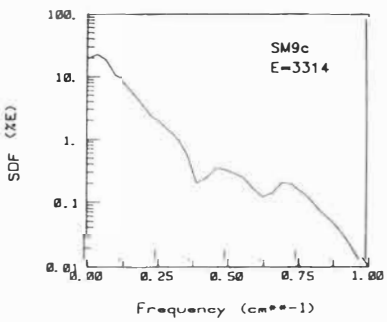
SM9c
E-3314
SDF (%E)
Frequency (cm**-1)

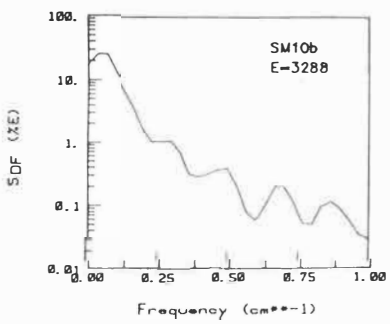
SM10b
E-3288
SDF (%E)
Frequency (cm**-1)

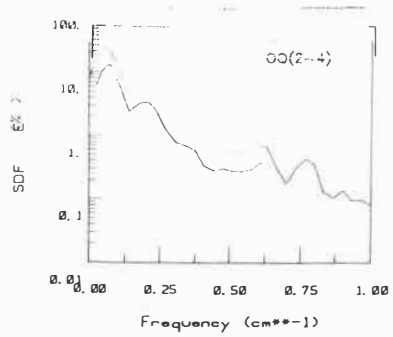
OQ(2-4)
SDF (%E)
100.
10.
1.
0.1
0.01
0.00
0.25
0.50
0.75
1.00
Frequency (cm**-1)

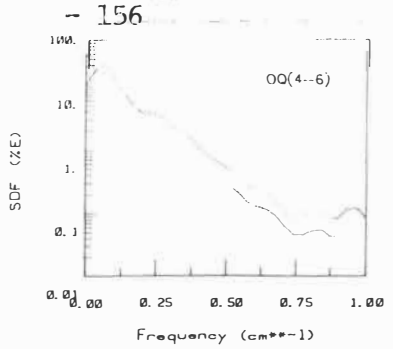
OQ(4-6)
SDF (%E)
100.
10.
1.
0.1
0.01
0.00
0.25
0.50
0.75
1.00
Frequency (cm**-1)

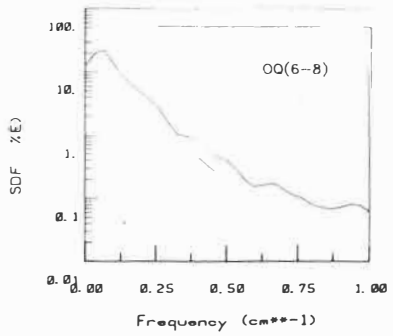
OQ(6-8)
SDF (%E)
100.
10.
1.
0.1
0.01
0.00
0.25
0.50
0.75
1.00
Frequency (cm**-1)

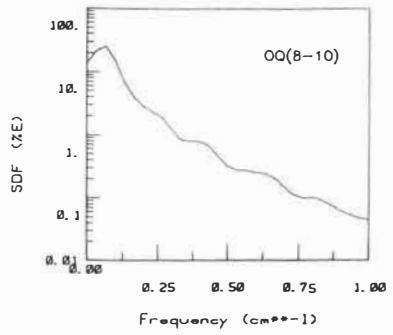
OQ(8-10)
SDF (%E)
100.
10.
1.
0.1
0.01
0.00
0.25
0.50
0.75
1.00
Frequency (cm**-1)

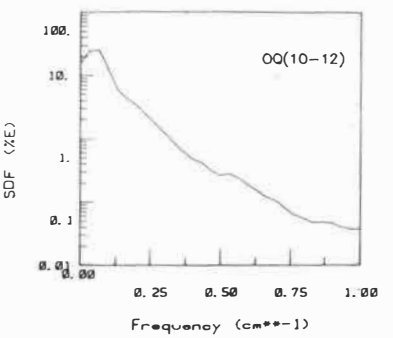
OQ(10-12)
SDF (%E)
100.
10.
1.
0.1
0.01
0.00
0.25
0.50
0.75
1.00
Frequency (cm**-1)

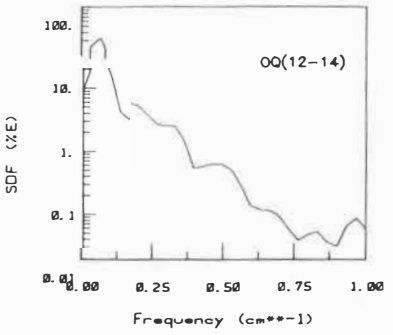
OQ(12-14)
SDF (%E)
100.
10.
1.
0.1
0.01
0.00
0.25
0.50
0.75
1.00
Frequency (cm**-1)

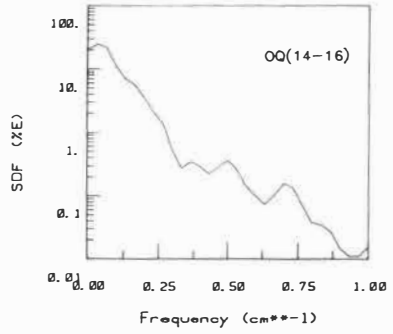
OQ(14-16)
SDF (%E)
100.
10.
1.
0.1
0.01
0.00
0.25
0.50
0.75
1.00
Frequency (cm**-1)

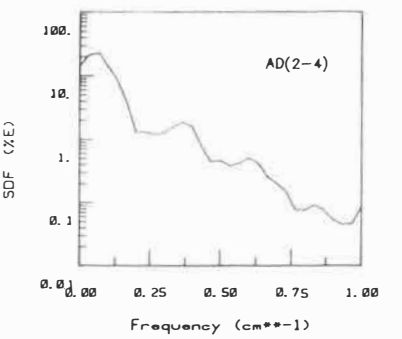
AD(2-4)
SDF (%E)
100.
10.
1.
0.1
0.01
0.00
0.25
0.50
0.75
1.00
Frequency (cm**-1)

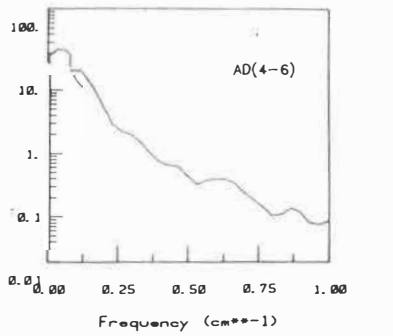
AD(4-6)
SDF
100.
10.
1.
0.1
0.01
0.00
0.25
0.50
0.75
1.00
Frequency (cm**-1)

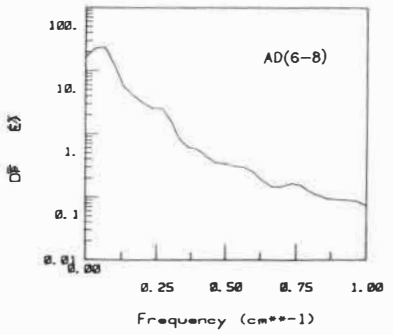
AD(6-8)
100.
10.
1.
0.1
0.01
0.00
0.25
0.50
0.75
1.00
Frequency (cm**-1)

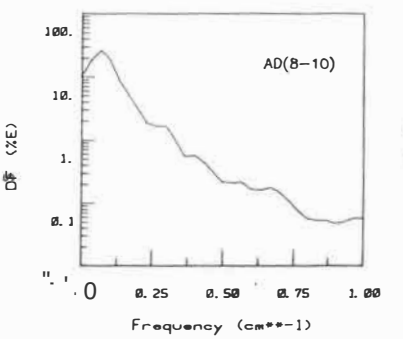
AD(8-10)
100.
10.
1.
0.1
0.25
0.50
0.75
1.00
Frequency (cm**-1)

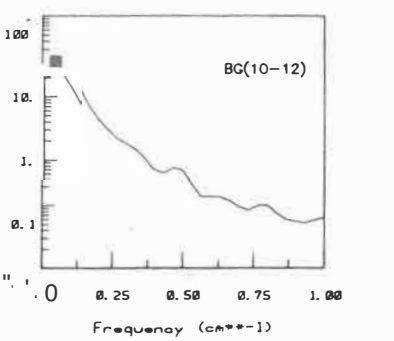
BG(10-12)
100
10.
1.
0.1
0.25
0.50
0.75
1.00
Frequency (cm**-1)

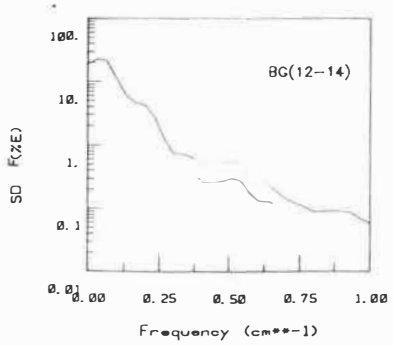
BG(12-14)
100.
10.
1.
0.1
0.01
0.00
0.25
0.50
0.75
1.00
Frequency (cm**-1)

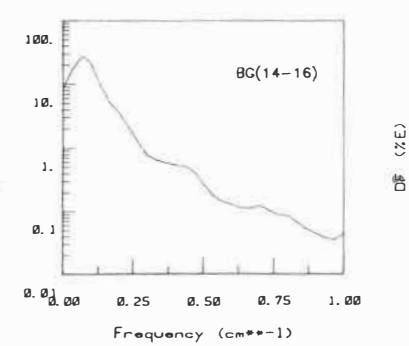
BG(14-16)
100.
10.
1.
0.1
0.01
0.00
0.25
0.50
0.75
1.00
Frequency (cm**-1)

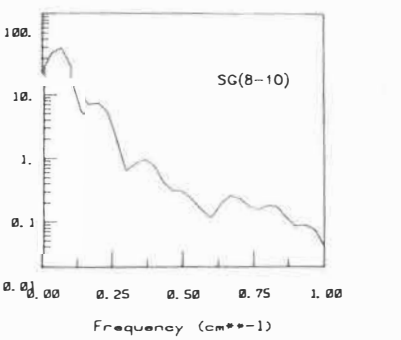
SG(8-10)
100.
10.
1.
0.1
0.01
0.00
0.25
0.50
0.75
1.00
Frequency (cm**-1)

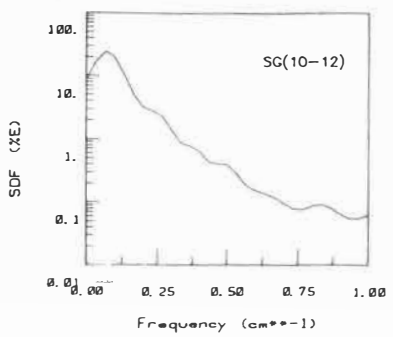
SG(10-12)
SDF (%E)
100.
10.
1.
0.1
0.01
0.00
0.25
0.50
0.75
1.00
Frequency (cm**-1)

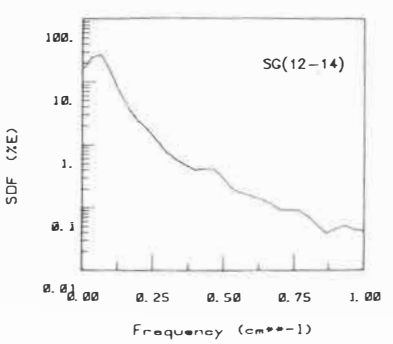
SG(12-14)
SDF (%E)
100.
10.
1.
0.1
0.01
0.00
0.25
0.50
0.75
1.00
Frequency (cm**-1)

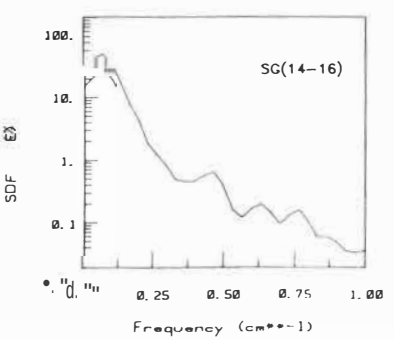
SG(14-16)
SDF
100.
10.
1.
0.1
0.25
0.50
0.75
1.00
Frequency (cm**-1)

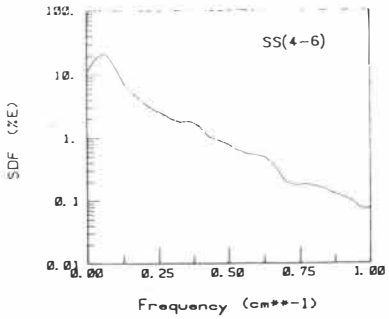
SS(4-6)
SDF (%E)
100.
10.
1.
0.1
0.01
0.00
0.25
0.50
0.75
1.00
Frequency (cm**-1)

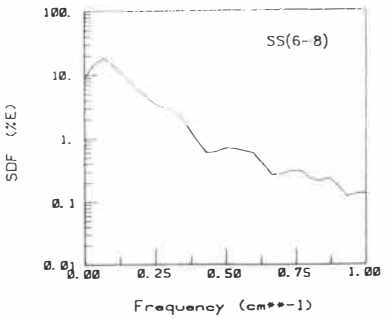
SS(6-8)
SDF (%E)
100.
10.
1.
0.1
0.01
0.00
0.25
0.50
0.75
1.00
Frequency (cm**-1)

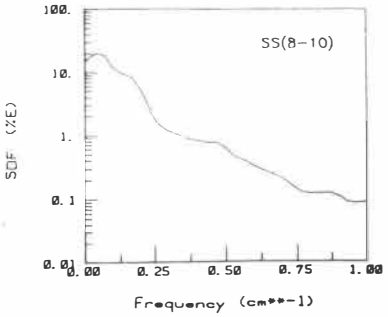
SS(8-10)
SDF (%E)
100.
10.
1.
0.1
0.01
0.00
0.25
0.50
0.75
1.00
Frequency (cm**-1)

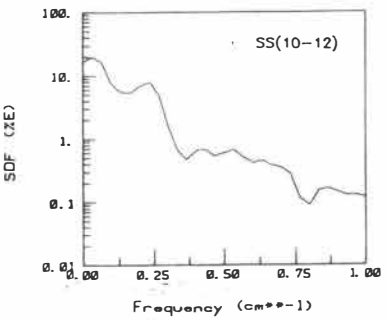
SS(10-12)
SDF (%E)
100.
10.
1.
0.1
0.01
0.00
0.25
0.50
0.75
1.00
Frequency (cm**-1)

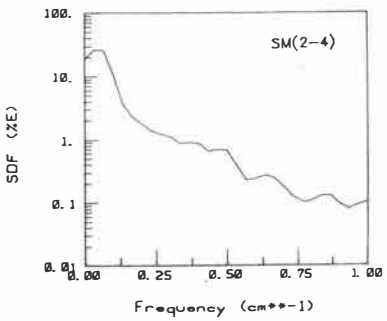
SM(2-4)
SDF (%E)
100.
10.
1.
0.1
0.01
0.00
0.25
0.50
0.75
1.00
Frequency (cm**-1)

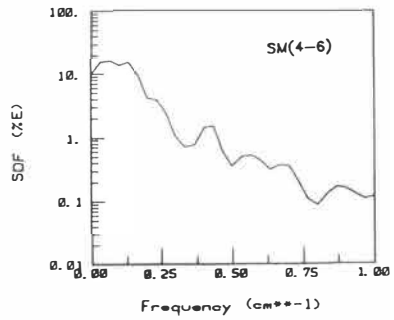
SM(4-6)
SDF (%E)
100.
10.
1.
0.1
0.01
0.00
0.25
0.50
0.75
1.00
Frequency (cm**-1)

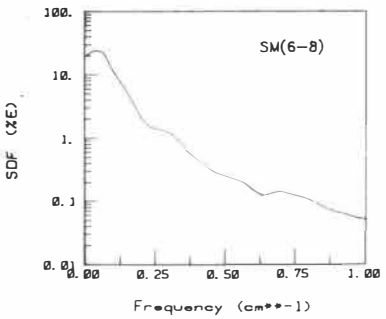
SM(6-8)
SDF (%E)
100.
10.
1.
0.1
0.01
0.00
0.25
0.50
0.75
1.00
Frequency (cm**-1)

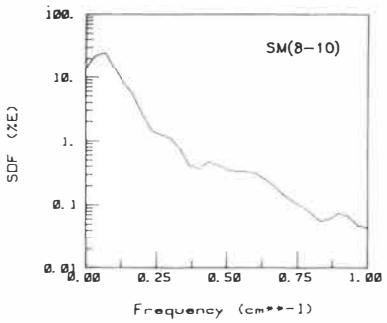
SM(8-10)
SDF (%E)
100.
10.
1.
0.1
0.01
0.00
0.25
0.50
0.75
1.00
Frequency (cm**-1)

BIBLIOGRAPHY

BIBLIOGRAPHY

Armstrong, R.L. 1978: K-Ar dating : late Cenozoic McMurdo Volcanic Group and dry valley glacial history, Victoria Land, Antarctica. *New Zealand journal of geology and geophysics 21(6)*: 685-698.

Bandis, S.; Lumsden, A.C.; Barton, N.R. 1981: Experimental studies of scale effects on the shear behaviour of rock joints. *International journal of rock mechanics and mining science and geomechanics abstracts 18*: 1-21.

Barrett, P.J. 1981: History of the Ross Sea region during the deposition of the Beacon Supergroup 400-180 million years ago. *Journal of the Royal Society of New Zealand 11(4)*: 447-458.

Barton, N. 1973: Review of a new shear-strength criterion for rock joints. *Engineering geology 7(4)*: 287-332.

Barton, N. 1976: The shear strength of rock and rock joints. *International journal of rock mechanics and mining science and geomechanics abstracts 13*: 255-279.

Barton, N.; Bandis, S. 1980: Some effects of scale on the shear strength of joints. *International journal of rock mechanics and mining science and geomechanics abstracts 17*: 69-73.

Barton, N.; Choubey, V. 1977: The shear strength of rock joints in theory and practice. *Rock mechanics 10*: 1-54.

Battey, M.H. 1975: Mineralogy for students. Longman. 323 p.

Bendat, J.S.; Piersol, A.G. 1971: Random data : analysis and measurement procedures. Wiley-Interscience. 407 p.

Bienawski, Z.T. 1975: The point load test in geotechnical practice. *Engineering geology 9*: 1-11.

Bradshaw, M.A. 1981: Paleoenvironmental interpretations and systematics of Devonian trace fossils from the Taylor Group (lower Beacon Supergroup), Antarctica. *New Zealand journal of geology and geophysics 24(5)*: 615-652.

Broch, E.; Franklin, J.A. 1972: The point load strength test. *International journal of rock mechanics and mining science and geomechanics abstracts 9*: 669-697.

Brook, N. 1985: The equivalent core diameter method of size and shape correction in point load testing. *International journal of rock mechanics and mining science and geomechanics abstracts 22(2)*: 61-70.

Brown, E.T. *ed.* 1981: Rock characterisation testing and monitoring : International Society Rock Mechanics suggested methods. Pergamon Press. 211 p.

Bryan, J.; Whitby, K.; Edbrooke, S. 1983: Upper Wright Valley. Unpublished geological map 1:25 000. Antarctic Coal Measures Study Group (New South Wales) and New Zealand Geological Survey.

Bull, C.; McKelvey, B.C.; Webb, P.N. 1962: Quaternary glaciations in Southern Victoria Land, Antarctica. *Journal of glaciology 4(31)*: 63-78.

Burgess, C.J.; Palmer, A.; Anderson, J.M. 1981: The geology of the Fry Glacier area, South Victoria Land, Antarctica, with particular reference to the Taylor Group. *New Zealand journal of geology and geophysics 24(3)*: 373-388.

Coulson, J.H. 1972: Shear strength of flat surfaces in rock. Pp. 77-105 *in* Cording, E.J. *ed.* Stability of rock slopes. American Society of Civil Engineers.

Davis, J.C. 1973: Statistics and data analysis in geology. John Wiley and Sons. 550 p.

Day, M.J.; Goudie, A.S. 1977: Field assessment of rock hardness using the Schmidt test hammer. Pp. 19-29 *in* Finlayson, B.L. *et al. British Geomorphological Research Group technical bulletin 18.*

Deere, D.U.; Miller, R.P. 1966: Engineering classification and index properties for intact rock. *Air Force Weapons Laboratory technical report AFWL-TR-65-116.*

Dight, P.M.; Chiu, H.K. 1981: Prediction of shear behaviour of joints using profiles. *International journal of rock mechanics and mining science and geomechanics abstracts 18*: 369-386.

Doolin, B.; Selby, M.J. 1984: The frictional resistance of rock joints : evaluation and comparison of field techniques for the determination of joint frictional strength. Pp. 11-20 *in Waikato University Antarctic Research Unit report 13.*

Findlay, R.H.; Skinner, D.N.B.; Craw, D. 1984: Lithostratigraphy and structure of the Koettlitz Group, McMurdo Sound, Antarctica. *New Zealand journal of geology and geophysics 27*: 513-536.

Greminger, M. 1982: Experimental studies of the influence of rock anisotropy on size and shape effects in point-load testing. *International journal of rock mechanics and mining science and geomechanics abstracts 19*: 241-246.

Gunn, B.M.; Warren, G. 1962: Geology of Victoria Land between the Mawson and Mulock Glaciers, Antarctica. *New Zealand Geological Survey bulletin 71.*

Haskell, T.R.; Kennett, J.P.; Prebble, W.M.; Smith, G.; Willis, I.A.G. 1965: The geology of the middle and lower Taylor Valley of South Victoria Land, Antarctica. *Transactions of the Royal Society of New Zealand, geology 2(12)*: 169-186.

ISRM Commission on Testing Methods 1985: Suggested method for determining point load strength. *International journal of rock mechanics and mining science and geomechanics abstracts 22(2)*: 51-60.

Jones, L.M.; Faure, G. 1967: Age of the Vanda porphyry dikes in Wright Valley, Southern Victoria Land, Antarctica. *Earth and planetary science letters 3*: 321-324.

Krahn, J.; Morgenstern, N.R. 1979: The ultimate frictional resistance of rock discontinuities. *International journal of rock mechanics and mining science and geomechanics abstracts 16*: 127-133.

Kyle, P.R.; Cole, J.W. 1974: Structural control of volcanism in the McMurdo Volcanic Group, Antarctica. *Bulletin volcanologique 38*: 16-25.

Louden, T.V.; Wheeler, J.F.; Andrew, K.P. 1980: A computer system for handling digitised line data from geological maps. *Computers and geosciences 6(3)*: 299-308.

McKelvey, B.C.; Webb, P.N. 1962: Geological investigations in Southern Victoria Land, Antarctica. Part 3 - geology of the Wright Valley. *New Zealand journal of geology and geophysics 5(1)*: 143-162.

McKelvey, B.C.; Webb, P.N.; Gorton, M.P.; Kohn, B.P. 1970: Stratigraphy of the Beacon Supergroup between the Olympus and Boomerang Ranges, Victoria Land, Antarctica. *Nature 227*: 1126-1128.

McKelvey, B.C.; Webb, P.N.; Kohn, B.P. 1977: Stratigraphy of the Taylor and lower Victoria Groups (Beacon Supergroup) between the Mackay Glacier and Boomerang Range, Antarctica. *New Zealand journal of geology and geophysics 20(5)*: 813-863.

Myers, N.O. 1962: Characterisation of surface roughness. *Wear 5*: 182-189.

Palmer, D.F.; Bradley, J.; Prebble, W.M. 1967: Orbicular granodiorite from Taylor Valley, South Victoria Land, Antarctica. *Geological Society of America bulletin 78*: 1423-1428.

Patton, F.D. 1966: Multiple modes of shear failure in rock. *Proceedings 1st congress, International Society Rock Mechanics, Lisbon, 1*: 509-513.

Pearson, C. 1981: The relationship between microseismicity and high pore pressures during hydraulic stimulation experiments in low permeability granitic rocks. *Journal of geophysical research 86(B9)*: 7855-7864.

Peek, R. 1981: Roughness - shear strength relationship. *Journal of the Geotechnical Engineering Division, American Society of Civil Engineers 107(GT5)*: 672-677.

Plume, R.W. 1978: A revision of the existing stratigraphy of the New Mountain Sandstone (Beacon Supergroup), South Victoria Land, Antarctica. *New Zealand journal of geology and geophysics 21(2)*: 167-173.

Poole, R.W.; Farmer, I.W. 1980: Consistency and repeatability of Schmidt hammer rebound data during field testing. *International journal of rock mechanics and mining science and geomechanics abstracts 17(3)*: 167-171.

Proceq S.A. 1977: Operating instructions - concrete test hammer types N and NR. Proceq S.A., Zurich. 16 p.

Quinn, K.J.D. 1974: Eton four-figure mathematical and statistical tables. Eton Press. 64p.

Ryan, T.A.; Joiner, B.L.; Ryan, B.F. 1982: Minitab reference manual. Pennsylvania State University. 154p.

SAS Institute Inc. 1982: SAS users guide: statistics. SAS Institute Inc. 584p.

Sayles, R.S.; Thomas, T.R. 1977: The spatial representation of surface roughness by means of the structure function : a practical alternative to correlation. *Wear 42*: 263-276.

Selby, M.J. 1982: Controls on the stability and inclinations of hillslopes formed on hard rock. *Earth surface processes and landforms 7*: 449-467.

Stimpson, B. 1981: A suggested technique for determining the basic friction angle of rock surfaces using core. *International journal of rock mechanics and mining science and geomechanics abstracts 18(1)*: 63-65.

Streckeisen, A. 1976: To each plutonic rock its proper name. *Earth science reviews 12*: 1-33.

Sugden, D.E.; John, B.S. 1976: Glaciers and landscape, a geomorphological approach. Edward Arnold. 376 p.

Tse, R.; Cruden, D.M. 1979: Estimating joint roughness coefficients. *International journal of rock mechanics and mining science and geomechanics abstracts 16(5)*: 303-307.

United States Geological Survey 1962: Taylor Glacier. Antarctica reconnaissance series map 1:250 000.

United States Geological Survey 1970: Ross Island. Antarctica reconnaissance series map 1:250 000.

Weissbach, G. 1978: A new method for the determination of the roughness of rock joints in the laboratory. *International journal of rock mechanics and mining science and geomechanics abstracts 15*: 131-133.

Williams, P.F.; Hobbs, B.E.; Vernon, R.H.; Anderson, D.E. 1971: The structural and metamorphic geology of basement rocks in the McMurdo Sound area, Antarctica. *Journal of the Geological Society of Australia 18(2)*: 127-142.

Wu, T.H.; Ali, E.M. 1978: Statistical representation of joint roughness. *International journal of rock mechanics and mining science and geomechanics abstracts 15*: 259-262.

Yaalon, D.H.; Singer, S. 1974: Vertical variation in strength and porosity of calcrete (nari) on chalk, Shefela, Israel, and interpretation of its origin. *Journal of sedimentary petrology 44(4)*: 1016-1023.